Polymers, catalysts and nanostructures: A hybrid approach to biomolecule detection

Submitted in fulfilment of the requirements for the degree of

Master of Science

in

Biotechnology

at

Rhodes University

by

KELLY-ANNE FRITH

Supervisor: Dr. Janice L. Limson

February 2009

Abstract

The main goals in electroanalytical sensing are towards improved sensitivity and selectivity, or specificity, of an analyte. There are several approaches to achieving these goals with the main approach being modification of an electrode surface with synthetic or natural catalysts (enzymes), polymers and also utilisation of nanostructured materials. At present, there is a strong movement towards hybrid sensing which couple different properties of two or more surface modification approaches. In this thesis, a range of these surface modifications were explored for analysis and detection of two main analytes: the amino acid, tryptophan (Trp); and, the neurotransmitter, dopamine (DA). Specifically, this thesis aimed to utilise these methods to enhance the sensitivity and selectivity for Trp over an interferent, the indoleamine, melatonin (Mel); and, DA over the vitamin, ascorbic acid (AA).

For Trp detection, immobilisation of an enzyme, Tryptophanase (Trpase) resulted in poor selectivity for the analyte. However, enhanced sensitivity and selectivity was achieved through pH manipulation of the electrolyte medium at a Nafion®-modified electrode surface for both Trp and Mel. At pH 3.0, the Mel and Trp anodic peak potentials were sufficiently resolved allowing for an LOD of 1.60 and 1.62 nM, respectively, and permitting the accurate analysis of Trp in a dietary supplement containing Mel. Multi-walled carbon nanotubes (MWCNTs) suspended in Nafion® exhibited further increases in the signal responses of these analytes at pH 3.0 and 7.4 with minimal change in the resolution of the anodic peaks. A lower sensitivity was, therefore, observed at the Nafion® and MWCNT modified electrode compared to the Nafion®-modified electrode at pH 3.0 with LODs of 0.59 and 0.80 nM exhibited for Trp and Mel, respectively. Enhanced selectivity for Trp in the presence of Mel can be achieved with MWCNTs in the presence of metallotetrasulphonated phthalocyanines (MTSPcs) particularly at pH 3.0, owing to cation exchange effects. However, the lack of sensitivity towards Trp, and even Mel, at this CoTSPc and MWCNT modified electrode remains a drawback.

For DA, detection at the MWCNT and Nafion® surface resulted in improved sensitivity over that of both the bare electrode (613.0 nM) and the Nafion® modified

electrode (1045.1 nM) with a calculated LOD of 133.9 nM at this layer. Furthermore, improvements in the selectivity of DA were achieved at the Nafion® and MWCNT modified electrode as exclusion of AA (150 µM) was achieved. At the MWCNT and CoTSPc surface, AA was excluded up to 130 µM with sensitivity for DA extending as low as 14.3 nM, far greater than observed for Trp and Mel. These concentrations are well within physiological concentration ranges and represent the most significant solution yet in terms of AA exclusion and enhanced sensitivity for DA.

An examination of the surface layering by impedance spectroscopy and atomic force microscopy indicates that the success of the hybrid sensor utilising CoTSPc and MWCNTs lay in improved dispersion of MWCNTs and improved electron transfer kinetics, facilitated by the net charge of the materials present.

This thesis, thus, showed the utility of a judicious selection of synthetic and biological catalysts, polymers and carbon nanomaterials towards a hybrid approach to the electrochemical sensing of Trp, Mel, DA and AA with focus on sensitivity and selectivity of these analytes.

Acknowledgements

I would sincerely like to thank my supervisor, Dr. Janice Limson, for her patience, enthusiasm, encouragement and endless hours perusing the intricacies of this work.

Further thanks are extended to the members of the Biosensor Research Group for their valuable input and understanding; as well as Dr. C.A. Togo for the hours spent imaging the layers under the Atomic Force Microscope.

A special and loving thanks go to my father, Mr. Ian M. Frith, whose support, encouragement, insight and guidance has helped me in reaching my aims and ambitions.

A loving thanks is further extended to my fiancée, Dr. Roman Tandlich, for his endless support and encouragement; and, the daunting task of proof-reading this thesis.

A warm thank you to the rest of my family and friends for believing in me and helping me through the emotionally trying times.

And, finally, I would like to thank the Medical Research Council (MRC) and MINTEK/Department of Science and Technology Nanotechnology Innovation Centre for funding; and, Rhodes University for giving me the opportunity to conduct this research.

Index

CHAPTER 5

The voltammetric analysis of dopamine, tryptophan and melatonin using a CoTSPc/fMWCNT nanocomposite layer

.

CHAPTER 6

Exclusion of ascorbic acid at the CoTSPc/fMWCNT nanocomposite sensors

List of Abbreviations

AA..... Ascorbic acid
AdSV..... Adsorptive stripping voltammetry
AFM..... Atomic force microscopy
$AlPcS_4$..... Aluminium tetrasulphonated phthalocyanine
BGCE..... Bare glassy carbon electrode
BSA..... Bovine serum albumin
CNT..... Carbon nanotube
CoPc..... Cobalt phthalocyanine
CoTSPc..... Cobalt tetrasulphonated phthalocyanine
CuTSPc..... Copper tetrasulphonated phthalocyanine
CV..... Cyclic voltammetry
DA..... Dopamine
DNA..... Deoxyribose nucleic acid
DPV..... Differential pulse voltammetry
fMWCNTs..... Functionalised multi-walled carbon nanotubes
GA..... Glutaraldehyde
GC..... Gas chromatography
GCE..... Glassy carbon electrode
HPLC..... High performance liquid chromatography
L-DOPA..... L-3,4-dihyroxy phenylalanine
LSV..... Linear sweep voltammetry
LOD..... Limit of detection
LOQ..... Limit of quantification
Mel..... Melatonin
MPc..... Metallophthalocyanine
MS..... Mass spectrophotometry
MWCNT..... Multi-walled carbon nanotube
MTSPc..... Metallotetrasulphonated phthalocyanine
Pc..... Phthalocyanine
pH..... Potential hydrogen
PLP..... Pyridoxal 5-phosphate
pKa..... Dissociation constant of acid
SWCNT..... Single-walled carbon nanotubes
SWV..... Squarewave voltammetry
TLC..... Thin layer chromatography
TMO..... Tryptophan monooxygenase
Trp..... Tryptophan
Trpase..... Tryptophanase
UV-Vis..... Ultraviolet-visible spectroscopy
ZnPc..... Zinc phthalocyanine

List of Electrode Surface Modification Designations

BGCE.....	Bare GCE
BSA-GCE.....	Adsorbed BSA
BSA/GA-GCE.....	BSA with GA cross-linking (control)
CoPc-GCE.....	Adsorbed CoPc
CoPc/fMWCNT-GCE.....	Adsorbed mixture of CoPc and fMWCNTs
CoTSPc-GCE.....	Adsorbed CoTSPc
CoTSPc/fMWCNT-GCE.....	Adsorbed mixture of CoTSPc and fMWCNTs
CuTSPc/fMWCNT-GCE.....	Adsorbed mixture of CuTSPc and fMWCNTs
fMWCNT-GCE.....	Adsorbed fMWCNTs
Nafion®-GCE.....	Nafion® coating
Nafion®/fMWCNT-GCE.....	fMWCNTs dispersed in Nafion® resin
Trpase-GCE.....	Adsorbed Trpase
Trpase/BSA/GA-GCE.....	Trpase and BSA with GA cross-linking
Trpase/fMWCNT/GA-GCE.....	Trpase and fMWCNTs with GA cross-linking

Figure legends

Table legends

Equations

Chapter 1

General Introduction

1.1. Background

One of the greatest challenges in electroanalytical sensing technology is the simultaneous achievement of enhanced selectivity, or specificity, and sensitivity. In order to overcome this challenge and achieve these goals, modification of electrode surfaces through a range of modifiers has been the approach of choice. Recently, construction of hybrid sensors which couple different modifiers (be they biological or synthetic) has opened a new paradigm in electroanalytical sensing, with nanosensing (use/incorporation of nanostructures) as the particular focus of the contemporary electroanalyst. Indeed, there exists a continuous need for greater selectivity and sensitivity for detection of biomolecules as indicators of disease as these biomolecules have a lasting impact on human health.

This thesis explores the selective and sensitive detection of two biomolecules of importance, namely tryptophan (Trp) and dopamine (DA), in the presence of their interferents, melatonin (Mel) and ascorbic acid (AA), respectively. This will be achieved through examination of the possible benefits afforded by various electrode modifications using synthetic and biological molecules either alone or coupled in a hybrid sensor. Such modifiers include polymers; biocatalysts, such as enzymes; electrocatalysts, such as metallophthalocyanines; and, nanostructures, such as carbon nanotubes.

1.2. Indoleamines: Tryptophan and Melatonin

1.2.1. Introduction

Tryptophan (Trp) was isolated from casein in milk in 1901 and is an essential amino acid as it cannot be synthesised in the body and must be obtained in the diet (Hopkins & Cole, 1901). Trp can exist as a monomer in the primary structure of proteins and enzymes; or, can exist independently in biological fluids where it can adsorb to inert proteins or exist freely (McMenamy & Oncley, 1958; Annesini *et al.,*

2007). As an independent molecule, Trp can fulfil its physiological function in nutrition, health and well-being. The structure of Trp, shown in Figure 1.1, includes a hydrophobic indole ring (Gogoleva *et al*., 2003), the functional group that gives Trp some of its specific properties, and carboxyl and amine groups commonly associated with all amino acids.

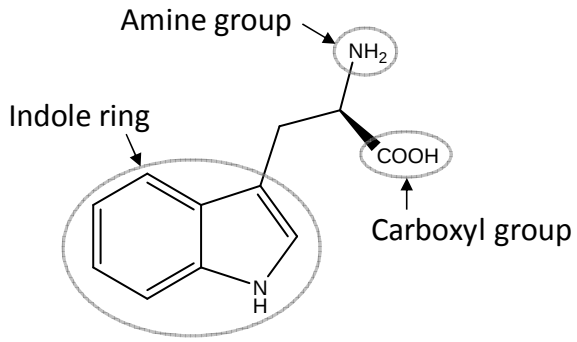

Figure 1.1: The chemical structure of tryptophan (Trp)

Trp metabolism involves numerous, complex metabolic pathways. However, the metabolic pathway of interest for the purpose of this research catalyses the formation of serotonin and Mel (Reiter, 1991). Figure 1.2 shows the synthetic pathway of Mel in humans (Macchi & Bruce, 2004). The synthesis of Mel in humans begins with the uptake of Trp from the blood into the cells of the target tissues (Reiter, 1991). Trp is hydroxylated to 5-hydroxytryptophan by tryptophan hydroxylase, which is then decarboxylated to serotonin, also known as 5-hydroxytrypamine by 5-hydroxytryptophan decarboxylase (Ferry *et al*., 2005). Tryptophan hydroxylase is responsible for the regulation of serotonin synthesis from Trp. The *N*-acetylation of serotonin by *N*-acetyl transferase produces *N*-acetylserotonin, which is *o*-methylated at the 5-hydroxyl position to form Mel (Ferry *et al*., 2005). *N*-acetyl transferase exhibits a higher activity in the dark or at night (Klein *et al*., 1997; Malpaux *et al*., 2001), resulting in higher levels of Mel and is, therefore, responsible for the circadian (or daily) rhythms in the body (Reiter, 1991).

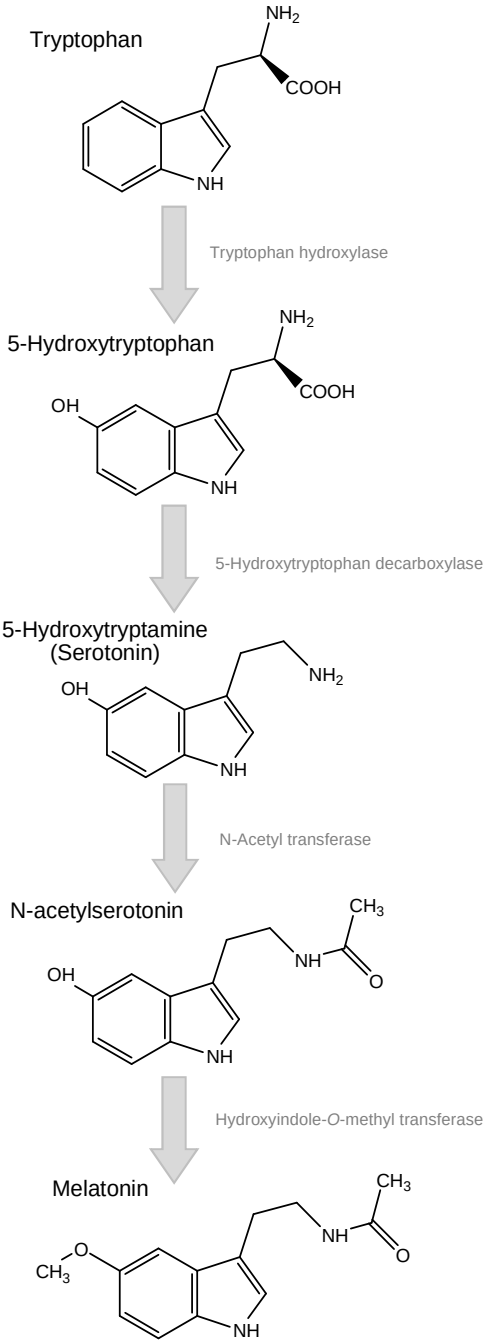

Figure 1.2: Chemical structures and biosynthesis of Mel from Trp including the enzymes involved at each step (adapted from Macchi & Bruce, 2004)

Mel, discovered in 1958 by Aaron Lerner at Yale University (Skene, 1996), is produced in the pineal gland and in lower quantities by the retina (Reiter, 1991). Mel has various physiological functions including control of circadian and circannual biological rhythms (Reiter, 1993); control of immune function (Guerrero & Reiter, 2002); retinal physiology (Dubocovich *et al*., 1999); tumour inhibition (Blask *et al*., 2002); antioxidant and free radical scavenging properties (Reiter, 1997); and, the

recently discovered metal binding properties (Limson *et al*., 1998; Parmar *et al*., 2002).

1.2.2. Physiological significance of tryptophan and melatonin

There are many deficiencies involving Trp and its metabolites, 5-hydroxytryptophan and serotonin, as previously shown by Fernstrom and co-workers (1990) and Tagliamonte and co-workers (1971). Vitamin B_3 (Niacin) is one such important molecule of which Trp is the precursor (Horwitt *et al*., 1965). A deficiency in Niacin and Trp leads to dermatitis, diarrhoea and dementia, which are symptoms commonly associated with pellagra (Hegyi *et al*., 2004). Due to the fact that Trp is one of the twenty proteinaceous amino acids, a lack or lowered level of Trp in the body may be associated with conditions related to a lack or lowered protein intake, such as carbohydrate craving and kwashiorkor (Williams, 1935). A low physiological level of Trp, or complete lack thereof, may be accompanied by depression (Mendels *et al.*, 1975).

Since Mel is synthesised in the brain and is easily accessible to the brain, there is a greater possibility of a localised antioxidant effect taking place by Mel (Poeggeler *et al*., 1993; Reiter, 1995). The brain has a high oxygen consumption relative to the rest of the body which leads to neuronal degradation caused by oxidative stress, autoxidation and free radical damage. It is this oxidation and free radical damage that is believed to be one of the leading causes for the progression of Alzheimer's and Parkinson's disease (Fahn & Cohen, 1992; Frolich & Rierder, 1995). The levels of Mel in the body decrease with age and this reduction may be a contributing factor to the onset of these age-related diseases (Reiter, 1995).

There exists a correlation between an increased Trp intake and lowered depression (Fernstrom & Wurtman, 1971; Biggio, *et al*., 1974; Smith *et al*., 1987; Young *et al*., 1987; Young, *et al*., 1989, Smith *et al*., 1997). This is due to the fact that Trp is a precursor to serotonin biosynthesis (Figure 1.2). Moreover, serotonin has been shown to be indirectly involved in the diseases, Alzheimer's and Parkinson's disease, as there is a link between dementia and depression, particularly in the elderly (Fischer *et al*., 1990, Meltzer et al., 1998). Researchers have shown a

correlation between depression in the elderly and the onset of neurodegenerative diseases over time (Alexopolous *et al.*, 1993; Devanand *et al*., 1996). Lowered Mel biosynthesis, and the resulting physiological levels in the brain tissue, is regulated by *N*-acetyl transferase activity on serotonin in the pineal gland (Klein *et al*., 1997). Therefore, a link exists between depleted Trp and serotonin levels and the onset of the neurodegenerative diseases associated with lowered Mel levels (Reiter, 1991).

1.2.3. Methods of tryptophan and melatonin detection

Previous methods utilized in the detection of Trp in blood serum, pharmaceutical formulations and dietary supplements include high performance liquid chromatography (HPLC) (Krstulovic *et al*., 1984), thin-layer chromatography (TLC) (Tonelli *et al*., 1982), gas-liquid chromatography (GC) (Wegmann *et al*., 1978) and capillary electrophoresis (Shen *et al*., 2002). Methods of detection of Mel in biological samples include HPLC, mass spectrophotometry (MS), UV-visible spectrometry (UV-Vis) and fluorimetry (Tan *et al*., 1999; Skinner & Malpaux, 1999; Martin *et al*., 2000). The electrochemical methods of detecting Trp and Mel in solution include amperometry, differential pulse voltammetry (Moreno *et al.,* 2004), cyclic voltammetry (Moreno *et al.,* 2004), linear sweep voltammetry (Brabec, 1980; Nguyen et al., 1985) and stripping voltammetry (Chen *et al.*, 2002, Ensafi & Hajian, 2006). The electrochemical detection of Trp has previously been attempted, with varying degrees of success, using assorted modifications to a GCE surface. These modifications include hemin (Chen *et al.*, 2002a); butyrylcholine (Jin & Lin, 2004); single-walled carbon nanotubes alone (Huang *et al*., 2004) and with copper microparticles (Luque et al., 2007); multi-walled carbon nanotubes in cerium hexacyanoferrate (Fang *et al*., 2007); and, multi-walled carbon nanotubes in 4-aminobenzenesulphonic acid (Huang *et al.*, 2008). The sensitivities achieved for Trp detection at these modifications ranged between 0.25 nM and 0.6 µM.

Trp and Mel exhibit electrochemical oxidation peak potentials at 0.63 and 0.61 V, respectively, versus Ag/AgCl reference electrode at physiological pH (Frith & Limson, 2009). Due to the proximity of the peak potentials of Trp and Mel, no clear separation of these analytes has been achieved using basic electrochemical means. Therefore, various methods of modification of an electrode are required in order to

obtain separation of the oxidation peaks of these analytes or elimination of the interfering analyte peak and, simultaneously, offering a sensitive response to the desired analyte. This separation of the oxidation peaks, or elimination of the interfering peak aids in the selectivity, or specificity, of an analyte whist achieving a sensitive response towards that analyte.

1.3. Catecholamine: Dopamine, and its interferent: Ascorbic acid

1.3.1. Introduction

Dopamine (DA, Figure 1.3) was first discovered in 1952, by Arvid Carlsson, at the Laboratory for Chemical Pharmacology in Sweden. However, in 1957, he demonstrated that DA exhibited properties as a neurotransmitter (Carlsson & Lindqvist, 1957). Furthermore, DA functions as a neurohormone as it is produced in many areas of the brain and released by the hypothalamus (Alex & Pehek, 2007). DA is the immediate precursor for norepinephrine and epinephrine in the biosynthetic pathways of these neurotransmitters (Gilman *et al*., 1980).

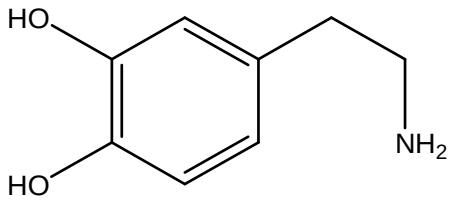

Figure 1.3: The chemical structure of dopamine (DA)

Ascorbic acid (AA, Figure 1.4) was first discovered in the 1920's when it was identified as the biomolecule that prevented scurvy, the disease from which the name, "ascorbic acid", is derived. In 1937, Walter Hayworth elucidated the structure of AA and Albert Szent-Györgyi discovered the biological functions of AA. The essential biomolecule, AA or Vitamin C, has antioxidant properties and, thus, has the ability to prevent the oxidation of other macromolecules (Martin & Frei, 1997).

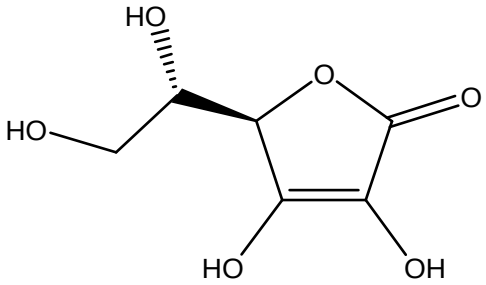

Figure 1.4: The chemical structure of ascorbic acid (AA)

1.3.2. Physiological significance of dopamine and ascorbic acid

Abnormal levels of the biologically significant biomolecule, DA, have been found in patients suffering from schizophrenia (Carlsson & Lindqvist, 1963) and Parkinson's disease (Wightman *et al*., 1988). Carlsson & Lindqvist (1963) propose that schizophrenia is due to a hyperactivity of DA transmission. Parkinson's disease is caused by the loss of dopaminergic neurons with age which induces motor and cognitive disorders later in life (McGeer *et al*., 1977; Bramford *et al*., 2004). Therefore, the absence of DA in the body affects the neuronal membrane properties and the firing patterns of these neurons. However, the effects of DA consumption as a drug are limited as it does not have the ability to cross the blood brain barrier (Gilman *et al*., 1980). Hence, to prevent the onset of Parkinson's disease, the precursor for DA, L-3,4-dihydroxyphenylalanine (L-DOPA), is administered as it has the ability to cross the blood brain barrier where it is converted to DA (Cotzias *et al*., 1967).

As a vitamin, AA (Vitamin C) prevents and cures the ailment, scurvy, which presents itself when AA is deficient in the diet. AA is a physiologically relevant molecule as it is an antioxidant and, therefore, has the ability to act as a reducing agent (Martin & Frei, 1997). AA fulfils this role by reducing and, thereby, neutralising the reactive oxygen species, such as hydroxyl and superoxide radicals, which would otherwise damage macromolecules such as proteins and deoxyribose nucleic acids (DNA) (Padayatty *et al*., 2003).

1.3.3. Methods of dopamine and ascorbic acid detection

Methods of DA detection include fluorescence, spectrophotometry (Salem, 1987), HPLC (Sarre *et al*., 1992) using ion exchange chromatography (Guan *et al*., 2000) and the various waveforms of electrochemical detection. The methods utilised for the detection of AA are colorimetry/spectrophotometry (Szepesi, 1947), titrimetry (Hughes, 1982), fluorimetry (Wu *et al*., 2002), HPLC with an anion exclusion column (Kim & Kim, 2006), chemiluminescence (Alwarthan, 1993), capillary zone electrophoresis (Lin Ling *et al.*, 1992) and electrochemistry. The electrochemical methods of DA and AA detection include cyclic voltammetry (Millar *et al.*, 1985), differential pulse voltammetry (Zhao *et al*., 2007), squarewave voltammetry (Giz *et al*., 1999), adsorptive stripping voltammetry (Zen *et al*., 1998) and amperometry (Jin *et al.*, 2005). The sensitivities achieved for DA and AA detection using these techniques ranged between 2.2 nM and 5.0 µM.

Although electrochemical methods offer advantages, such as sensitivities in the picomolar range, a major drawback of this technique as stated before is that it may, at times, lack specificity or selectivity. This pertains, in particular, to the detection of DA in biological samples which often contain AA in a concentration that is far greater than that of DA (Capella *et al*., 1990). During the electrochemical analysis of DA, the oxidation peak indicative of the DA concentration is often overlapped/overshadowed by that of AA, as discovered by Schenk and co-workers (1983); causing a high degree of interference in detection. In order to combat this problem, modifications to the electrode, which include electrode pretreatment (Gonon *et al*., 1981), polymers (Rubianes & Rivas, 2001) and ion-exchange membranes (Sun *et al*., 1998), have previously been employed. Modification of various electrodes surfaces for DA detection and AA exclusion include Nafion® (Nagy *et al*., 1985); nanoclusters with overoxidised-polypyrrole on a glassy carbon electrode (GCE) (Li & Lin, 2007); poly(*p*-aminobenzene sulphonic acid) on GCE (Jin *et al.*, 2005); self-assembled gold nanoparticles on GCE (Hu *et al*., 2008); self-assembled monolayers on a gold electrode (Zhang *et al.*, 2000); choline and acetylcholine on GCE (Jin *et al*., 2004); and, poly(phenosafranine) on GCE (Selvaraju & Ramaraj, 2003). Furthermore, DA analysis with multi-walled carbon nanotubes (MWCNTs) (Wu *et al.*, 2003) with various composite-forming materials, including thionine/Nafion® (Shahrokhian &

Zare-Mehrjardi, 2007), poly(methylene blue) (Yogeswaran & Chen, 2008) and ionic liquid gel (Zhao *et al*., 2005), have also been studied.

The use of the cation-exchange, perfluorinated ion-exchange polymer, Nafion®, for the exclusion of AA is the most widely known method of obtaining DA selectivity (Nagy *et al*., 1985). At physiological pH and in biological samples, Nafion® functions by accumulating the protonated and positively charged DA at the surface of the polymer whilst excluding the negatively charged, anionic ascorbic acid or ascorbate, resulting in the improved sensitivity and selectivity of DA (Nagy *et al*., 1985).

1.4. Methods of detection and sensing techniques

1.4.1. Introduction to electrochemical techniques

The use of electrochemistry as an analytical tool is becoming increasingly popular with many advances in the utilisation and application of this tool. Increasing popularity is owed to the portability of these analytical devices; ability to monitor samples in real time; rapid response; sensitivity; cost-effectiveness; and, ease of operation (Rasooly & Rasooly, 1999; Bilitewski & Turner, 2000). Moreover, little sample pretreatment is required for samples that are analysed using electrochemistry, allowing direct analysis of analytes in complex matrices, such as pharmaceutical formulations, dietary supplements and blood serum.

Certain electrochemical waveforms offer advantages over others in terms of sensitivity. The electrochemical waveforms that predominate in this study include cyclic voltammetry (CV) and squarewave voltammetry (SWV). CV is the ideal waveform with which to study the electrochemical mechanism and characterise the oxidation and reduction of a particular analyte (Wang, 1994), such as Trp. For CV, the potential is scanned from an initial potential to an end potential (forward scan), which is beyond the oxidation or reduction peak potential of the analyte but within range of the potential of the working electrode, and returned to the initial potential (return scan) (Wang, 1994). Oxidation/reduction, and resulting reversibility where present, of the analyte of interest will result during the forward and reverse scans. SWV yields a rapid, well-resolved, sensitive catalytic response due to the applied

symmetrical square-wave pulse and step potential (Kounaves, 1997). The net current (the difference between the forward and reverse current) is centred at the redox potential, which is where the symmetrical oxidation/reduction peak forms. In SWV, the background currents are removed as they are cancelled out during the applied square-wave (Kounaves, 1997). Averaging of the background current and speed of this technique facilitates repetitive, consecutive scanning and an increased signal-to-noise ratio, leading to lower detection limits and facilitating the determination of trace analytes (Kounaves, 1997).

1.4.2. Electrode modifications

When developing an electrochemical sensing technique, the appropriate electrode modification must be taken into consideration. Ideally, these modifications should be applicable to the sensitive and specific detection of an analyte, whilst utilising properties that eliminate interferents in complex matrices; however, achieving both sensitivity and selectivity is not always possible. Commercial polymers commonly used include Nafion® (Chapter 1.4.2.), Teflon and poly (vinyl alcohol) (Ren *et al.*, 2006). A broad range of synthetic electrocatalysts have been utilised. In particular, the metallophthalocyanines represent a rich class of versatile molecules with catalytic properties towards a range of analytes. Biosensors that have been modified with enzymes, antibodies (immunosensors) or DNA fragments (DNA probes) provide specific detection of an analyte. There are various immobilisation strategies for these biological macromolecules. One form of immobilisation that has increasing popularity is that of carbon nanostructures, such as carbon nanotubes (CNTs, Chapter 1.4.4.), which may be coupled to the biorecognition entity of interest. Examples of such modifications include immobilisation of acetylcholinesterase using CNTs (Joshi *et al.*, 2005), DNA-hydridisation sensors (Jung *et al*., 2004), DNA probes (Cai *et al*., 2003) and immunosensors in which the antibody is immobilised on the CNT wall (Wohlstadter et al., 2003). CNTs have also be incorporated into polymer membranes and coupled directly to metallophthalocyanine complexes (Oni & Nyokong, 2001). Sensors modified with CNTs, Nafion®, metallophthalocyanine complexes and an enzyme specific for Trp, will be discussed further in the sections below.

1.4.3. Commercial polymers

The specificity and sensitivity of a biosensor, or chemosensor, can be further improved by the addition of a polymer film to the electrode surface. Figure 1.5 shows an example of a polymer, Nafion® (Heitner-Wirguin, 1996). Nafion® is part of the class of polymers known as the ionomers as it has a tetrafluorethylene, or Teflon®, backbone with perfluorovinyl ether groups terminated with sulphonate groups (Heitner-Wirguin, 1996). Nafion® (pK_a = -6.0) is a cation exchanger and is, therefore, negatively charged at physiological pH (pH 7.4) allowing positively charged molecules or cations to pass through the pores in the film (Nagy *et al*., 1985; Kreuer *et al*., 2000) with any interfering, negatively charged species, such as urate and ascorbate (both present in blood sera) being excluded (Zhang *et al*., 2005). Thus, the positively charged analyte approaches the electrode surface and may result in an increase in sensitivity and relative specificity of the biosensor for the analyte.

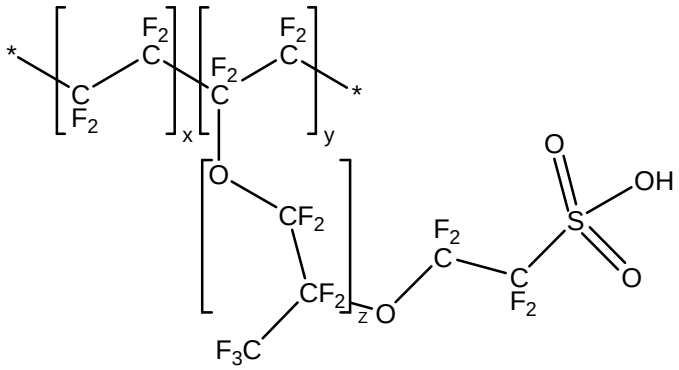

Figure 1.5: Chemical structure of Nafion® (adapted from Heitner-Wirguin, 1996)

Nafion® has many properties which makes it highly versatile (Perma Pure LLC, 1994). Nafion®, in particular the tetrafluoroethylene backbone, can act as a polymeric binder thereby binding enzymes or other polymers, such as carbon nanotubes (Tsai & Chui, 2007). The property of Nafion® as a cation exchanger is the property of interest concerning its role in biosensors. Although there have been no experiments concerning the detection of Mel with Nafion®, it has been demonstrated that Nafion® has the ability to increase sensitivity at the electrode surface to other neurotransmitters, such as serotonin, which is a precursor in Mel synthesis (Brazell *et al*., 1987; Rivot *et al*., 1995; Zhang *et al*., 2005), and dopamine (Gerhardt *et al*., 1984).

The pH of the electrolyte solution, in which the Nafion®-coated electrode is placed, alters the charge of the analyte in the solution. This change in charge is dependent on the pKa value/s of the analyte. Thus, detection of that particular analyte at the Nafion®-modified GCE is affected as negatively charged molecules would be repelled resulting in the lowering or absence of a signal. This was shown with the amino acids alanine, aspartic acid, phenylalanine and lysine (Lee & Hong, 1992).

1.4.4. Electrocatalytic complexes

The phthalocyanines (Pcs) are large macrocyclic compounds and have a structure similar to that of a porphyrin ring (biological analogue) except that the phthalocyanines have four identical isoindole subunits (Dent *et al*., 1934). The metallophthalocyanines (MPcs) include a transition metal cation at the centre of the ring (Figure 1.6a). The MPcs act as mediators or catalysts and can catalyse homogenous and heterogenous reactions that involve the transfer of electrons (Zagal, 1992). The catalytic effect of the MPcs can be seen when the Pc has been immobilised onto the electrode surface and the oxidation and reduction analysed electrochemically. The oxidation and reduction can occur either at the central metal cation or the Pc ring (Lever *et al*., 1981). However, it is the central metal in the Pc that is involved in reactions such as metal-ligand interactions, electronic structure and the majority of the redox reactions (Zagel *et al*., 1992). These properties differ according to the identity of the central transition metal used (Zagel *et al*., 1992). However, the physical and chemical properties of the MPcs may be enhanced by substituting functional groups into the Pc ring (de la Torre *et al.*, 1998), such as amino or sulphonate groups (Figure 1.6b).

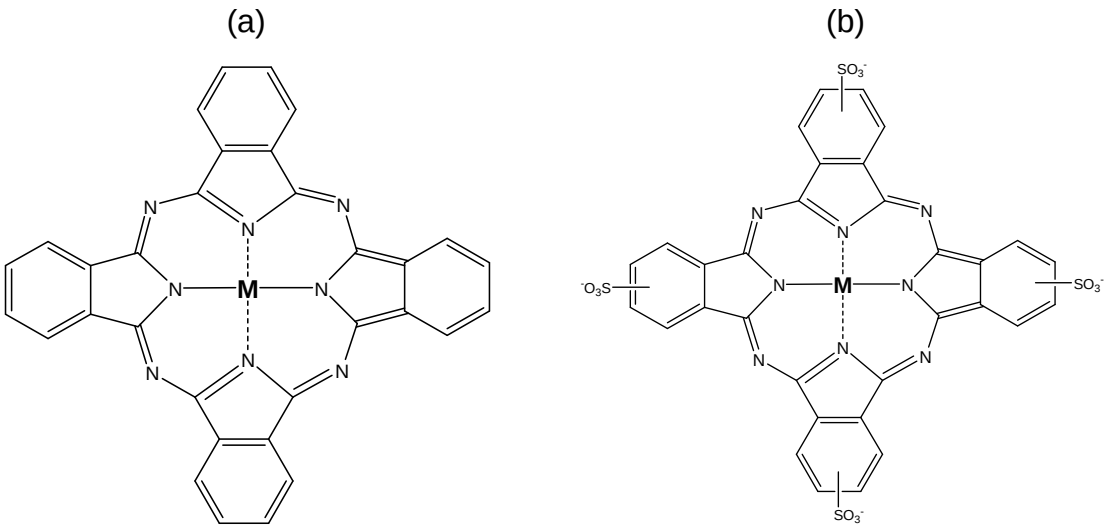

Figure 1.6: The chemical structure of (a) metallophthalocyanine and (b) metallotetrasulphonated phthalocyanine (adapted from Oni and Nyokong, 2001). M represents the divalent metal cation.

According to Langlois and co-workers (1986), phthalocyanines of interest in Trp detection include zinc phthalocyanine (ZnPc) and aluminium tetrasulphonated phthalocyanine ($AlPcS_4$). However, MPcs utilised in the detection of indoleamines and their derivatives include cobalt phthalocyanine (CoPc) or cobalt tetrasulphonated phthalocyanine ($CoPcS_4$ or CoTSPc) (Zagal *et al.*, 1992). Therefore a number of possible MPcs exist which could result in the sensitive detection of an analyte with functional groups that may aid in selectivity.

Recently, Mashazi and coworkers (2006) and Fogel and co-workers (2007) developed a biocomposite sensor in which the enzyme, glucose oxidase, was covalently coupled to functionalised MPc complexes. A biocomposite sensor consists of a biological entity that is intimately associated with a chemical agent (Fogel *et al*., 2007), in which both agents allow for increased sensitivity and specificity. Tsai and Chui (2007) have demonstrated that by developing the biocomposite in advance, the efficiency of the production of the sensor is increased as only addition of the biocomposite is required.

1.4.5. Nanomaterials

Nanomaterials such as carbon nanotubes, fullerenes and quantum dots, are novel materials in electrochemical sensing (Merkoçi *et al.*, 2005). These nanomaterials can

be used to sensitively detect particular analytes owing to their specific properties. Furthermore, they have the ability to be directly coupled to biological and synthetic molecules, thereby promoting the electrochemical reactions and amplify the (bio)recognition event (Pumera *et al.*, 2007). Indeed, nanostructured materials such as carbon nanotubes (CNTs) have been coupled to both MPcs (hybrid sensors) (Ozoemena *et al*., 2006) and to enzymes (biocomposite sensors) (Withey *et al*., 2006), as previously stated. CNTs have gained increasing popularity in electrochemical sensing due to their electronic and thermal transport abilities (Ebbesen *et al*., 1996), mechanical strength (Treacy *et al*., 1996), chemical properties (Guo *et al.*, 2002) and ability to increase the area of the detecting surface (Peigney *et al.*, 2001). These properties far exceed those of their common, macroscale counterparts, such as steel (tensile strength), diamond (thermal conductivity) and copper (electrical conductivity) (Merkoçi *et al.*, 2005). These properties can be utilised in electrochemistry for an improved electrochemical response thereby allowing the detection of trace amounts of an analyte in such areas as cancer diagnostics and detection of infectious organisms (Pumera *et al.*, 2007).

There are many theories as to how the CNTs are able to elicit the effects that they have on current response at the electrode. One such popular theory is that of electrocatalysis (Wang *et al*., 2003a) in which the observed increase in the analyte's current response and decrease in peak-to-peak separation is due to the CNT. However, Compton and co-workers (2004) demonstrated how graphite powder at the electrode surface was able to elicit similar results to that of the CNTs. Compton and co-workers later describe that the observed effects at the CNT-modified electrode may be attributed to edge plane-like sites at the open ends of the CNTs similar to those at an edge plane pyrolytic graphite electrode (Banks *et al*., 2004). Therefore, through addition of additional edge plane sites through modification with CNTs, thereby enhancing the surface area, further increases in response may be observed. Other research suggests, however, that any observed catalysis may be due to metal impurities, such as platinum, in the CNT structure.

Observed increases in current responses for certain analytes may be attributed to the conducting, or semi-conducting, properties of nanostructured materials. The electrical conducting/ semi-conducting property arise from the quantum-mechanical

effect exerted by the small internal diameter (Guo *et al.*, 2002). The quantum-mechanical effects give the CNTs their electronic structure, which allows conducting energy to move along the perimeter of the CNTs. These semiconducting properties are utilised and applied in the field of nanoelectronics (Merkoçi *et al.*, 2005).

CNTs exist as single- and multi-walled structures (Merkoçi *et al.*, 2005), as illustrated in Figure 1.7, designated SWCNTs and MWCNTs, respectively. SWCNTs exist as cylindrical sheets of graphite with hemispherical ends. SWCNTs typically have a diameter of 0.4 to 1.0 nm. MWCNTs comprise of several concentric graphite cylinders with diameters that range from 2.0 to 100.0 nm and a distance of 0.3 to 0.4 nm between the concentric layers.

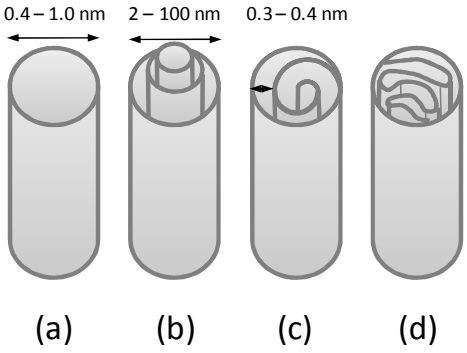

Figure 1.7: The structures of SWCNTs (a) and MWCNTs in the form of concentric tubes (b) and rolled (c) and rippled (d) graphite sheets.

Both SWCNTs and MWCNTs are commercially available as a black or dark grey powder from suppliers such as Sigma Aldrich. The commercially supplied CNT powder commonly has many impurities such as amorphous carbon, graphite nanoparticles and carbon-encapsulated metal nanoparticles that are produced during the production of the CNTs. Pretreatment is required prior to application in order to remove the impurities that may negatively affect the properties exhibited by CNTs (Giles, 2004). Pretreatment commonly occurs in the steps preceding the solubilisation of the CNTs as solubilisation is required prior to application for optimal functioning. A number of solubilisation strategies have been studied, including water, dimethyl sulphoxide and amylose (Kim *et al.*, 2003) and water with anionic surfactants, such as sodium dodecyl sulphate or Triton X-100 (Liu *et al*., 1998). These solubilisation strategies require modification of the CNTs. Such modifications

include addition of functional groups at the ends and on the walls of the CNTs (Chen *et al*., 1998, Tasis *et al.*, 2003); enveloping the CNTs with a polymer (Wang *et al.*, 2003); and, protonation using concentrated acids (Ramesh *et al*., 2004). The addition of functional groups, particularly carboxyl groups, as a means of CNT solubilisation, occurs through the chemical pretreatment and oxidation of the CNTs with concentrated nitric acid (Merkoçi *et al.*, 2005). Pretreatment with nitric acid has a tendency to alter the electronic properties of the CNTs; resulting in a change in the purported electrocatalytic behaviour exhibited by the CNTs. However, anodic pretreatment of capped MWCNTs resulted in an increase in electrocatalytic activity exhibited by the MWCNTs (Moore *et al*., 2004). This is due to the formation of open ends in the CNT as a result of the removal of the caps (Musemah *et al*., 2002). The modifications often include fragmentation of CNTs through the use of sonication (Liu *et al*., 1998). Further sonication may be required in order to disaggregate and disperse the CNTs in the solvent (Kim *et al.*, 2003). Disaggregation and dispersion of CNTs is required for correct orientation of individual CNTs at the electrode surface.

CNTs exhibit two orientation forms when applied and dried at the GCE surface. These include orientated and non-orientated (Merkoçi *et al.*, 2005). Orientated MWCNT modifications exhibit faster electron transfer rates and higher specific capacitance compared to orientated SWCNT modifications due to the existence of an open end (McCreery, 1991). Non-orientated modifications are more commonly used in the modification of GCEs (Musemah *et al*., 2002).

1.4.6. Enzyme-modified biosensors

A biosensor consists of a catalytically active biological entity, such as an enzyme or a whole cell, which has been immobilised onto the surface of a transducer, such as an electrode (Sangur, 2004). Enzymes are commonly used in biosensors as they are vital components in biorecognition events. They are highly specific and their catalytic properties result in a transduction signal (Mulchandani *et al*., 1998). Enzymes of interest are required to selectively bind the analyte of interest and catalyse an anabolic or catabolic reaction. The oxidation or reduction of this reaction would then be analysed electrochemically, as in the case of electrochemical biosensors, the

products or reactants thereof serving as a sensitive measure of the concentration of the analyte of interest.

When developing a biosensor, the method of immobilisation is of importance as this may alter the native conformation of the enzyme, thus affecting the activity of the enzyme (Chaubey & Malhotra, 2002; Brosseau *et al*., 2005). The conditions under which the enzyme is immobilised must be sufficiently stable so as to prevent the enzyme from leaching from the surface of the electrode; to improve the electron transfer between the enzyme-substrate complex and the electrode surface; and, prevent damage to the enzyme and/or loss of function (Chaubey & Malhotra, 2002). There are a number of immobilisation strategies, including adsorption, covalent binding and cross-linking (Anzai *et al.*, 1987; Anzai *et al*., 1992; Wolowacz *et al.*, 1992). Adsorption involves the enzyme being deposited directly onto the surface of the electrode and being immobilised via weak van der Waals forces (Achtnich *et al*., 1992). Covalent binding involves the enzyme binding, via covalent bonds, to carboxyl or hydroxyl groups on the surface of the electrode (Achtnich *et al*., 1992). Finally, cross-linking involves the immobilization of the enzyme using cross-linking agents, such as glutaraldehyde and hydrogels (Achtnich *et al*., 1992).

Selection of the biorecognition agent is a critical component. The specific electrochemical detection of Trp, for example, would exploit an immobilised enzyme that is specific for Trp. Briefly, some examples of such enzymes with low specificity towards Trp include indoleamine 2,3-dioxygenase, tryptophan hydroxylase and aromatic L-amino acid decarboxylase. Tryptophanase (EC 4.1.99.1), abbreviated as Trpase, exhibits significant specificity towards Trp (Gogoleva *et al*., 2003) with a dissociation constant of 11.6 mM; however, specificity towards other molecules has been shown, such as serine and cysteine (Newton & Snell, 1964; Newton *et al.*, 1965). The binding affinities for cysteine and serine are, however, lower than that for Trp with dissociation constants of 10.9 mM and 103.0 mM, respectively (Gogoleva *et al*., 2003). Due to the activity that Trpase exhibits on Trp, ease of availability and cost, it is ideally suited for a Trp-selective, electrochemical biosensor. However, Zoulis *et al.* (1990) reported that Trpase has a 20.0 % loss of activity over a period of 5 months regardless of storage conditions.

Trpase (Figure 1.8) is a homotetramer consisting of four identical subunits with each subunit having the ability to bind one unit of pyridoxal 5-phosphate (PLP; Isupov *et al*., 1998).

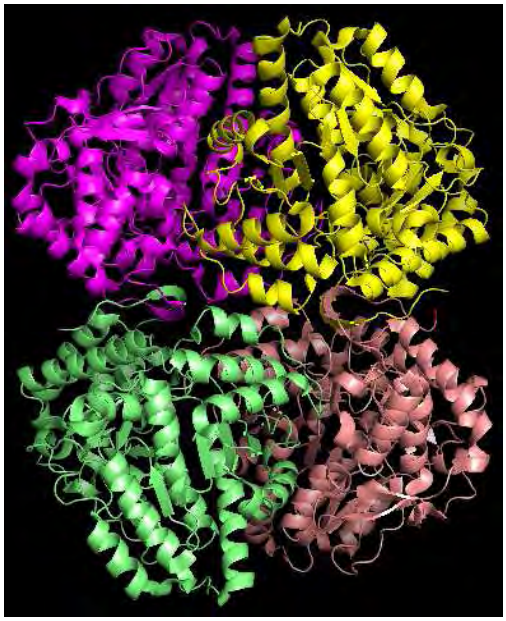

Figure 1.8: The crystal structure of Trpase

Trpase catalyses the hydrolytic decomposition of Trp by means of an α,β-elimination reaction (Gogoleva *et al*., 2003), as given by Reaction 1.1:

$$\text{Trp} + H_2O \xrightarrow{\text{Trpase}} \text{Indole} + \text{Pyruvate} + NH_3 \quad \text{..... Reaction 1.1}$$

The enzyme mechanism involves the formation of a Schiff base between the aldehyde group of the coenzyme, PLP, to the ε-amino group of the lysine_{266} residue at the active site of the holoenzyme (Morino & Snell, 1967; Ikeda *et al*., 1975; Kulikova *et al*., 2006). Subsequent to the addition of the substrate, the covalent bond of the Schiff base is broken, forming the apoenzyme-sustrate-coenzyme complex (Ikeda *et al*., 1975). This is in part due to the affinity of apotryptophanase for PLP being relatively low (2 μM). Moreover, the rate of this dissociation is slower than that of the apoenzyme and Trp substrate (Newton *et al*., 1965). The Trp substrate, anchored with an arginine_{414} residue in the active site, binds to PLP (Kulikova *et al.*,

2006). The products, indole, pyruvate and ammonia, are subsequently hydrolysed and released from the complex, thereby regenerating the holoenzyme (Kulikova *et al*., 2006).

The reaction is reversible, thereby catalysing the β-replacement reaction of indole to produce Trp (Snell, 1975). The reaction is, however, only reversible in the presence of high concentrations of its indole metabolite. Therefore, inhibition of the forward reaction may occur through the accumulative production of the indole (Snell, 1975).

Previous methods of Trpase immobilisation have been reported by Ikeda and Fukui (1973). They demonstrated that coupling of apotryptophanase to Sepharose-bound PLP resulted in high activity of the immobilised holoenzyme towards Trp. This was due to only one subunit of Trpase being utilised for the immobilisation whilst the other three remained free to carry out the Trp catalysis. However, a lowered optimum activity was the end result. In order to retain full Trpase activity, all four active sites are required to remain open and active (Ikeda *et al*., 1975). This is achieved by means of cyanobromide-activated Sepharose which couples the holoenzyme, Trpase, directly to the Sepharose. Trpase immobilisation in a carbon paste electrode (with Nujol and graphite) was previously used to preconcentrate Trp and indole for the indirect determination of Trp using voltammetry (Zoulis *et al*., 1990). They reported limitations in the analysed concentration range; non-specificity towards protein-bound and free Trp; and, real sample analyses that require pretreatment. Immobilisation of Trpase onto an electrode has been studied by Vincke *et al*. (1986) for the potentiometric detection of Trp in solution. Therefore, Sepharose-bound Trpase exhibited a decrease in activity; and, limitations in the movement of substrate towards the entrapped Trpase exist at the carbon paste electrode.

An amperometric biosensor for detection of Trp in nutrient broth was developed by Simonian and coworkers (1999). This biosensor comprises of the flavoprotein enzyme, tryptophan monooxygenase (TMO), and functions by quantifying the oxygen concentration throughout the oxidative decarboxylation reaction of the enzyme. However, to obtain TMO, the over-expression and purification of this

enzyme is required (Emanuele *et al*., 1995). This leads to an increase in the development costs of the biosensor and lack of availability.

1.5. General and Specific Aims

In this study, the feasibility of various electrochemical sensing techniques and GCE modifications in the electrochemical detection of Trp and its interferent, Mel, and of DA and its interferent, AA, was addressed. By utilising these analytes, we examine and demonstrate the feasibility of utilising or manipulating different electrode modifications (enzyme, polymer, nanostructures and electrocatalysts) separately and in hybrid sensors towards achieving enhanced sensitivity or selectivity in electrochemical sensor technology.

Specifically, this includes:

- Assessment of Trp detection and catalysis with immobilised Trpase at the GCE surface (Chapter 2);
- Determination of the effect of fMWCNTs on the localised detection and catalysis of Trp by Trpase (Chapter 2);
- Analysis of Trp and Mel detection at a Nafion®-modified GCE and the effect of pH manipulation on Trp selectivity in presence of interfering compounds found in formulations and supplements (Chapter 3);
- Assessment of fMWCNTs on the detection of Trp, Mel, DA and AA in the presence of Nafion® (Chapter 4);
- Analysis of the utility of fMWCNTs to facilitate the immobilisation of MPc complexes at the GCE surface and enhance the signal response for detection of:
    - DA, Trp and Mel (Chapter 5); and,
    - Exclusion of AA (Chapter 6);
- Chapter 7 concludes with an examination of surface topographies using atomic force microscopy and analysis of GCE surface coverage of and electron flow kinetics through the film using impedance spectroscopy (Chapter 7).

Each chapter comprises of a separate introduction, results and discussion section and conclusion (Chapter 2 to 7), while Chapter 8 provides general conclusions to this study and recommendations for future prospects for this study.

Chapter 2

Catalysis and detection of tryptophan with the biocatalyst, tryptophanase

2.1. Introduction

Enzyme-modified electrodes utilise the reaction and/or mechanism that an enzyme has towards a specific substrate. The reaction, most suitably a catabolic reaction, exhibits a transduction signal, the oxidation or reduction of which can be monitored electrochemically (Mulchandani *et al*., 1998). The enzyme-modified sensor acts by initially accumulating the substrate at the modified surface due to the biorecognition event between the enzyme and substrate and is followed by the rapid catalysis of the substrate by the enzyme, thereby eliciting the desired reaction. This catalysis of the specific substrate at the electrode surface facilitates the rapid transfer of electrons from the enzyme active site towards the surface (Merkoçi *et al*., 2005), resulting in an enhanced electrochemical response for the desired analyte. Therefore, enzyme-modified electrochemical sensors may act by measuring the change in the concentrations of the electrochemically active substrate; or, alternatively, measuring the formation of an electrochemically active product. However, a common drawback in biosensor development is the stability of the enzymatic activity during biosensor preparation. It is, therefore, important to constantly monitor enzyme activity towards its substrate throughout the development process through spectrophotometric, or electrochemical, means.

The specificity and relative low cost of the enzyme, tryptophanase, compared to others utilised for tryptophan (Trp) detection (such as tryptophan monooxygenase) represent ideal properties for sensor development. Tryptophanase (Trpase), as described earlier in Chapter 1.4.6., catalyses the α,β-elimination reaction of Trp to form indole, pyruvate and ammonia, as given in the Reaction 1 (Gogoleva *et al*., 2003):

$$\text{Trp} + H_2O \xleftrightarrow{\text{Trpase}} \text{Indole} + \text{Pyruvate} + NH_3 \quad \text{..... Reaction (2.1)}$$

Trp catalysis by Trpase can be monitored by either monitoring the decrease in the

Trp concentrations, given as a decrease in the oxidation peak amplitude; or, as the formation of a peak representing an electrochemically active product.

Briefly, as described in Chapter 1.4.6., previous methods of Trpase immobilisation for the electrochemical detection of Trp was achieved through the mechanical entrapment of Trpase in a carbon paste slurry (using Nujol and graphite) with preconcentration of Trp prior to analysis (Zoulis *et al.*, 1990). They were able to retain optimal activity at the carbon paste electrode and measure Trp concentrations indirectly through detection of the indole product. However, preconcentration of Trp requires time and, therefore, does not produce results immediately. Therefore, other more immediate methods of detection are required.

Adsorption of the enzyme occurs through the weak van der Waal's interactions between the carboxyl and hydroxyl groups on the glassy carbon electrode (GCE) surface and amine groups on the enzyme surface (Achtnich *et al*., 1992). Although this method is unstable, adsorption does allow for rapid assessment of the success of the biorecognition element. As a result, a more stable method of enzyme immobilisation would be required, such as glutaraldehyde (GA) cross-linking. GA (Figure 2.1) cross-linking, through covalent attachment with the functional groups of surface amino acids (Achtnich *et al*., 1992), offers many advantages. These include stability (so as to prevent the enzyme from leaching from the GCE surface); proximity to the detecting surface (to ensure that electron transfer can occur efficiently between the enzyme-substrate complex and the electrode surface); and, the ability to retain the enzymatic activity (Chaubey & Malhotra, 2002).

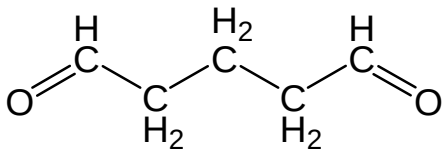

Figure 2.1: The chemical structure of glutaraldehyde (GA).

Use of CNTs as an immobilisation strategy has only recently been utilised for immobilisation of enzymes, such as acetylcholinesterase (Joshi *et al.*, 2005); DNA (Jung *et al*., 2004); and, antibodies (Wohlstadter et al., 2003). CNTs offer certain advantages during the electrochemical detection of analytes (Merkoçi *et al.*, 2005),

most notably improved electrical conductivity (Ebbesen *et al*., 1996); increased surface area of the detecting surface; and, increased mechanical strength (Treacy *et al*., 1996). Therefore, CNTs allow for the enhanced detection or electrochemical response of an analyte during electrochemical analysis. Methods of immobilisation that are studied in the following chapter include adsorption, cross-linking by means of glutaraldehyde and cross-linking with carbon nanotubes (CNTs), thereby forming a hybrid sensor. As discussed in Chapter 1.4.6., immobilisation is one of the key elements in successful biosensor design.

2.2. Aim

The specific aims of this study were to:

1) Determine Trpase activity for Trp in solution using spectrophotometric methods;
2) Monitor Trpase activity for Trp in solution using electrochemical methods;
3) Assess the effects that different Trpase immobilisation strategies have on Trp detection/catalysis at the Trpase-modified GCE;
4) Determine the catalytic effects of immobilised Trpase for Trp, and;
5) Assess the effects that functionalised multi-walled carbon nanotubes (fMWCNTs) exert on Trp analysis at the Trpase modified GCEs.

2.3. Experimental Procedure

2.3.1. Spectrophotometric activity assay for tryptophanase

The endpoint spectrophotometric activity assay for Trpase (Sigma, Johannesburg, South Africa) was carried out as per the supplier's protocol. All reagents and chemicals were, therefore, purchased from Sigma (Johannesburg, South Africa). Solutions of Trp (50.0 mM), melatonin (Mel; 50.0 mM), PLP (Trpase cofactor; 0.81 mM) and indole (0.43 mM) were prepared in Milli-Q water (Millipore, UK) and the Trpase solution (2.0 mg/ml) was prepared in 1.0 M potassium phosphate buffer, pH 8.3 at 37.0 ^{o}C (assay buffer). An assay mixture prepared in a test tube contained, in sequential order, 1.3 ml of Milli-Q water, 200.0 µl of 1.0 M potassium phosphate buffer, pH 8.3 (assay buffer; 0.1 M), 100.0 µl PLP (cofactor; 40.5 µM) and 200.0 µl of a freshly prepared Trpase solution (0.2 mg/ml). This Trpase-containing solution was

thoroughly mixed and temperated to 37.0 ^{o}C. Thereafter, 200.0 µl of 50.0 mM Trp (or 50.0 mM Mel) solution (5.0 mM) was added and the solution incubated for 10 min at 37.0 ^{o}C to allow the reaction to occur. A volume (2.0 ml) of analytical grade toluene was added and vigorously shaken in order to extract the indole from the aqueous solution. Upon phase separation, 200.0 µl of the organic (top) phase was removed and added to 2.0 ml Kovac's reagent (Sigma Aldrich, South Africa) in a clean test tube. The indole reacts with the benzaldehyde in the Kovac's reagent (yellow) resulting in the formation of a bright purple colour, which is read spectrophotometrically. Absorbance readings (540 nm) were taken at room temperature using a DU® 530 Life Science UV/Vis Spectrophotometer (Beckman). Substrate and enzyme controls were performed, as described above, with the exclusion of Trp and Trpase, respectively, from the reaction mixture. According to the suppliers, one unit of activity is defined by 1.0 mg of Trpase releasing 15.0 to 40.0 µg of indole from Trp in 10 min at pH 8.3 and 37.0 ^{o}C.

A linear calibration curve for the assay was produced by uniformly increasing the indole concentration (µM) in the assay buffer solution. The assays were carried out as described above using varying concentrations of indole. Indole was used in the assay standard curves as the measured concentration of indole that results from reaction of Trpase on Trp is indicative of the concentration of Trp present in the solution during Trpase activity analysis according to the stoichiometry of the reaction. The indole concentrations ranged from 21.5 to 107.5 µM. The calibration curve was blanked against the Kovac's reagent.

All control and assay samples were prepared in triplicate with the results expressed as the mean. Trpase specific activity was calculated from the calibration curve and expressed as µg of indole released per mg enzyme. All samples and controls were blanked against analytical grade methanol.

2.3.2. Electrochemical analysis of tryptophanase activity

2.3.2.1. Electrochemical apparatus and electrode pretreatment

The three electrode system was used for all electrochemical analyses conducted on the Potentiostat/Galvanostat 30 (PGSTAT 30) from Autolab using General Purpose Electrochemical software (GPES) Version 4.9 (Eco Chemie, Netherlands). The

reference electrode consisted of silver-silver chloride (Ag/AgCl) (BioAnalytical Systems (BAS)), stored in 3.0 M KCl, and the auxiliary, or reference, electrode consisted of a platinum wire. The working electrode was a glassy carbon electrode (GCE), 3.0 mm in diameter (BAS). The three electrodes were then placed in an electrochemical cell, with the working aqueous solution, taking care as to ensure that the electrodes were equidistant. The aqueous solution of the electrochemical cell consisted of a 5.0 ml working solution of 0.1 M potassium phosphate buffer (Merck), pH 8.3, unless otherwise specified. The cyclic voltammetry (CV) scans were conducted from a start potential (V) of 0.0 V to an end potential of 1.0 V, with a step potential of 1.8 mV and a scan rate of 50 mV/s.

2.3.2.2. Cleaning of electrodes and electrochemical cell

The GCE was initially rinsed with Milli-Q water, dipped into a solution of ~5.0 % (v/v) nitric acid and thoroughly rinsed with Milli-Q water. The surface was polished prior to all electrochemical analyses by means of a Buëhler felt pad (BAS) with an alumina oxide (Sigma Aldrich) powder paste. The electrode was thereafter thoroughly rinsed with Milli-Q water. Thereafter, the GCE was placed in an ultrasonic waterbath for 2.0 min in order to remove any alumina oxide still attached to the GCE surface. The electrode was cleaned after each set of scans, unless otherwise stipulated. The reference and auxiliary electrodes were washed thoroughly with Milli-Q water prior to use in the electrochemical cell. When the auxiliary electrode was not in use, it was placed in a ~5.0 % (v/v) nitric acid solution and, thereafter, thoroughly rinsed with Milli-Q. The electrochemical cell itself was washed thoroughly subsequent to the analyses sequentially using Milli-Q water, ~5.0 % nitric acid and, thereafter, rinsed in Milli-Q water.

2.3.2.3. Solution phase electrochemical monitoring of Tryptophanase activity

The electrochemical cell was set up as described above. The working solution consisted of 1.5 ml of the Trpase assay buffer (0.1 M potassium phosphate buffer, pH 8.3, at 37.0 ^{o}C) and PLP (100.0 µl; 40.5 µM). A substrate blank was produced by analysing the buffer and PLP solution using CV. Thereafter, Trp (200.0 µl; 5.0 mM) was added and the solution was calibrated to 37.0 ^{o}C using a thermometer and heating plate. Trpase (200 µl; 0.2 mg/ml) was then added to the working solution and catalysis of Trp was monitored over 12 mins.

2.3.2.4. Tryptophanase-modified GCE for tryptophan

Two methods of Trpase immobilisation onto the GCE surface were examined: adsorption and crosslinking with glutaraldehyde (GA; Sigma Aldrich, South Africa).

Adsorption

Electrode modification was accomplished by carefully applying 10.0 µl of Trpase (2.0 mg/ml) to a cleanly polished GCE surface. The modified GCE was allowed to dry under ambient temperatures and laminar air flow for 45 to 60 mins or until solvent evaporation. This Trpase modification will be designated Trpase-GCE.

Optimisation of the Trpase concentration, determined by an increased current response, was carried out using various concentrations of Trpase at the GCE surface. The concentrations of Trpase used in solution were 0.5, 1.0, 1.5 and 2.0 mg/ml. The adsorbed Trpase control consisted of the bare GCE with no Trpase and an equal concentration of BSA (designated BSA-GCE).

Glutaraldehyde Crosslinking

The method of GA crosslinking was adapted from Narasaiah (1994). A 7.5 µl solution of Trpase (2.0 mg/ml) and 2.0 µl of bovine serum albumin (BSA; 5.0 mg/ml; Sigma, South Africa) were carefully applied to a cleanly polished GCE surface. BSA was used as a co-linker in order to prevent the over-crosslinking, and subsequent inactivation, of Trpase (Li *et al*., 1999). Thereafter, 0.5 µl of GA (10 %) was carefully mixed in with the enzyme solution on the GCE surface prior to use. This Trpase/BSA/GA mixture was applied using the “drip-dry” method in such a way so as to cover the entire GCE surface. The Trpase modified GCE was allowed to dry at ambient temperature for 1 hour (or completion) under laminar air flow. This Trpase modified GCE is designated Trpase/BSA/GA-GCE.

The control for this modified GCE was prepared in a similar fashion with the exception that the Trpase was replaced with BSA in equal concentration. Briefly, 5.0 µl of BSA (5.0 mg/ml) was carefully applied to the GCE surface after which 0.5 µl of GA (5.0 %) was carefully mixed in on the GCE surface. The BSA/GA mixture was applied in such a way so as to completely cover the GCE surface. This modification of the GCE surface will be designated BSA/GA-GCE.

2.3.2.5. Limits of Detection and Quantification (LOD and LOQ)

The LOD and LOQ were calculated as the concentration that corresponds to, respectively, 3.3 and 10.0 times the quotient of the standard deviation of the noise (δ) by slope (S) or, alternatively, by the quotient of the current response (I_p) by the corresponding concentration (C), as outlined below (FDA Guidelines, 2005):

LOD = 3.3 X (δ / S).....Equation (2.1)

OR

LOD = 3.3 X (δ / (Ip/C)).....Equation (2.2)

LOQ = 10.0 X (δ / S).....Equation (2.3)

OR

LOQ = 10.0 X (δ / (Ip/C)).....Equation (2.4)

2.3.2.6. Variability and reproducibility

Variability, given as a percentage of the standard deviation (SD) over the mean of three replicates, was calculated as outlined in Equation 2.5:

Variability (%) = (SD / mean) X 100.....Equation (2.5)

Reproducibility, calculated as the difference between variability and total percentage, as outlined in Equation 2.6:

Reproducibility (%) = 100 – Variability (%).....Equation (2.6)

2.3.3. The influence of functionalised multi-walled carbon nanotubes (fMWCNT) on tryptophan detection and catalysis

2.3.3.1. Functionalisation of MWCNTs

Multiwalled carbon nanotubes (MWCNTs; OD: 10-15 nm; ID: 2-6 nm; length: 0.1-10.0 μm) were purchased from Sigma Aldrich (South Africa) and functionalised according to a method adapted from Liu *et al.* (1998) and Francisco Silva *et al*., (2007).The MWCNTs were functionalised and washed in 60.0 ml of a 3:1 concentrated nitric (55.0 %) to concentrated sulphuric acid (95.0 %) mixture with

sonication for 8 hrs. Thereafter, the funtionalised MWCNTs (fMWCNTs) were further washed in 200.0 ml of 0.02 M NaOH. This step was repeated with the concentration of NaOH decreasing by a factor of two until the fourth and final wash consisted of Milli-Q water or a pH of ~7.0 was obtained for the suspended fMWCNTs. The fMWCNTs were allowed to dry at ambient temperature under laminar air flow. Thereafter, a fMWCNT suspension of 1.3 mg/ml was prepared in distilled dimethylformamide (dDMF), unless stipulated otherwise.

2.3.3.2. Electrode Modification

Trpase immobilisation using adsorption and GA crosslinking was conducted as described in Chapter 2.3.2.4. Trpase immobilisation using adsorption incorporated fMWCNTs (1.3 mg/ml in Milli-Q water) into the Trpase solution. Trpase immobilisation via GA crosslinking encompassed the replacement of 2.0 µl of BSA with 2.0 µl of fMWCNTs (1.3 mg/ml in Milli-Q water). FMWCNTs were used as a co-linker due to the ability of the terminal carboxyl groups (COO^-) to form covalent bonds with amine groups on the Trpase surface.

2.3.4. Statistics

All studies were conducted in triplicate. Results are presented as the mean of the three replicates ±standard deviation.

3. Results and Discussion

2.4.1. Spectrophotometric assay for tryptophanase activity

The linear calibration curve of absorbance versus indole concentration for the Trpase reaction is demonstrated in Figure 2.2. The calibration curve for Trpase exhibited an R^2 value of 0.999 demonstrating excellent linearity with an average of 99.3 % reproducibility.

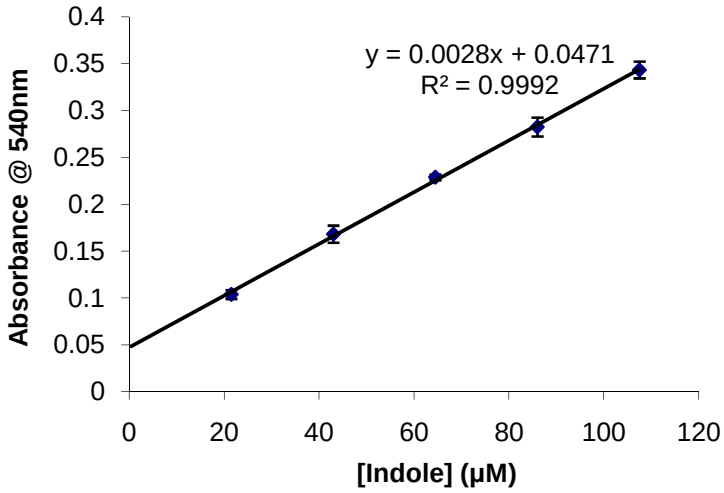

Figure 2.2: The Trpase calibration curve with absorbance (at 540 nm) versus indole concentration in µM in 0.1 M potassium phosphate buffer at pH 8.3. (*n* = 3; Error bars represent standard deviation)

The specific Trpase activity on Trp produced 27.71 ±0.94 µg of indole from 1.0 mg of Trpase. Therefore, the Trpase activity remained within the window of activity provided by the suppliers. Trpase exhibited no activity towards Mel.

2.4.2. Electroanalysis of tryptophan at the BGCE

The irreversible anodic oxidation peak for Trp at the BGCE is demonstrated in the CV illustrated in Figure 2.3.

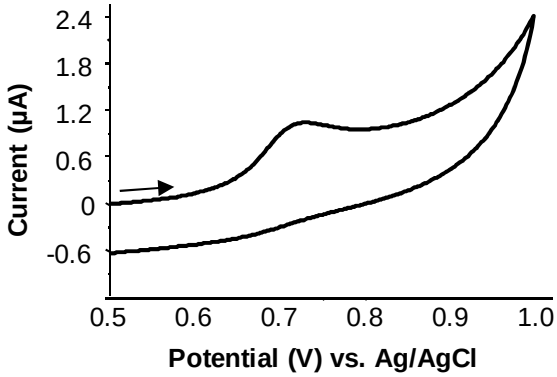

Figure 2.3: CV of Trp oxidation at the BGCE in 0.1 M potassium phosphate buffer (pH 8.3). [Trp] = 19.6 µM; Scan rate = 50 mV/s.

This result concurs with that found in literature as many extensive electrochemical studies have been conducted on Trp due to its relevance as an important biological molecule and amino acid. The electrochemical oxidation of Trp yields one single, irreversible oxidation peak in its two electron reaction (Nguyen et al., 1985). The electrochemical oxidation of Trp leads to the formation of a highly electroactive

intermediate, methylene-imine (Nguyen et al., 1985). Further oxidation of this species leads to the formation of isomeric degradation products, including kynurenine (Nguyen et al., 1985). Trp exhibited one oxidation peak which had a potential of 0.71 ±0.002 V (vs. Ag/AgCl) in 0.1 M potassium phosphate buffer, pH 8.3. This potential concurs with literature (Morino *et al*., 2004). The shallow peak shape for Trp demonstrates that the movement of electrons away from the GCE surface was a slow process (Babaei *et al*., 2008). The LOD and LOQ obtained for CV analysis of Trp at the BGCE were 14.4 & 43.7 nM, respectively

2.4.3. Solution phase electrochemical monitoring of tryptophanase activity

The depletion of Trp by Trpase in the assay mixture at the BGCE was measured using CV analysis (Figure 2.4) in order to assess the viability of an electrochemical approach for monitoring Trpase activity on Trp. Trp consumption, measured under Trpase assay conditions (Chapter 2.3.1), was measured over a period of 12 min with the first measurement (0 mins) taken immediately after addition of Trpase.

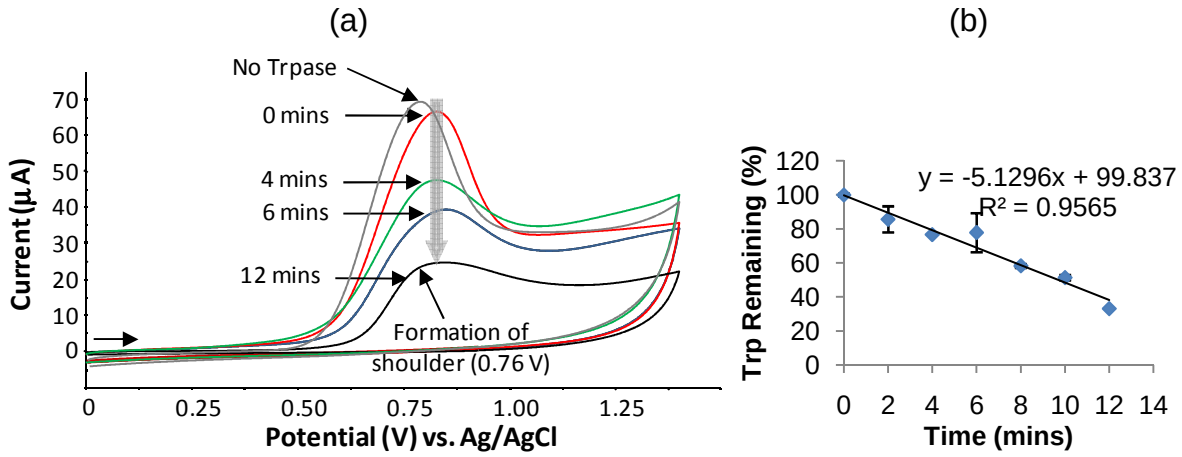

Figure 2.4: (a) Trp consumption at the BGCE during the electrochemical monitoring of Trpase activity in 0.1 M potassium phosphate buffer, pH 8.3, in the presence of PLP (40.5 µM) over 12 min. (b) Plot of Trp consumption at the electrode surface measured as a percentage of the initial Trp current response over time (*n* = 3). [$Trp_{initial}$] = 5 mM; Scan rate = 50 mV/s.

An electrochemical potential shift of +0.09 V was observed for the Trp anodic oxidation peak in 0.1 M potassium phosphate buffer, pH 8.3, in the presence of Trpase and PLP at 0 mins, when compared to the Trp oxidation peak potential in phosphate buffer without Trpase (No Trpase), as illustrated in Figure 2.4a. This shift in peak potential is indicative of a change in the oxidation kinetics of Trp at the GCE surface as Trp oxidation increases in difficulty (Heineman & Kissinger, 1996). The

increase in difficulty of Trp oxidation can be attributed to accumulation of Trp at the active site of Trpase in solution; binding of the Trp molecules in the active sites of the solvent-bound Trpase, facilitated by the presence of PLP in the active site; and, consequent, catalysis of Trp by this Trpase to form indole, pyruvate and ammonia.

As evident in Figure 2.4(a), a decrease in the Trp current response was observed at the BGCE when monitored in the assay mixture. This is due to catalysis of Trp by Trpase in the presence of PLP. Therefore, as observed in Figure 2.4a, Trp catalysis with Trpase can be monitored electrochemically by measuring the Trp peak height or amplitude. The formation of a shoulder was observed on the Trp peak, as observed at 6 mins in Figure 2.4(a). Further decrease in the Trp peak amplitude and the concomitant presence of the shoulder results in the formation of a broad peak in the Trp potential window as observed at 12 mins (Figure 2.4a). The simultaneous decrease in the Trp peak amplitude and broadening of this peak is indicative of the formation of an oxidisable product with a potential similar to that of Trp. Further studies were conducted in order to identify which oxidisable Trpase product was responsible for the observed peak formation.

The anodic peaks for the Trpase assay cofactor and products: (a) PLP; (b) indole; and, (c) pyruvate (Sigma, South Africa), are illustrated in the CVs in Figure 2.5. The concentrations of the assay components used in the electrochemical analyses, demonstrated in Figure 2.5 (a) and (b), were identical to those outlined in Chapter 2.3.1.

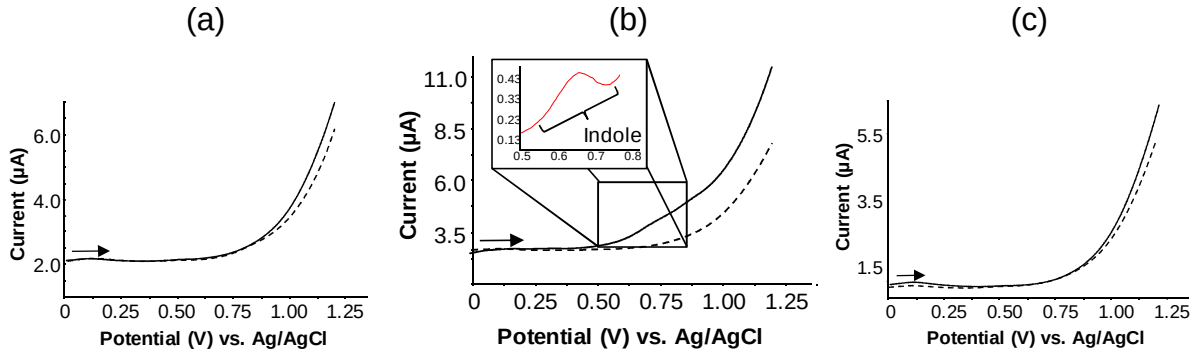

Figure 2.5: The forward CV scans of (a) 40.5 µM PLP, (b) 43.0 µM indole and (c) 47.6 µM pyruvate (solid) in 2 ml potassium phosphate buffer, pH 8.3 (dashed) at the BGCE under assay conditions. Insert in (b): The anodic oxidation peak for indole. Scan rate = 50 mV/s

As observed in Figure 2.5, no anodic waves were observed for PLP (a) and pyruvate (c) at the GCE in the potential window examined. The product, indole, produced from the Trpase reaction can be measured electrochemically. The irreversible anodic oxidation peak for indole (Figure 2.5b) was found at 0.65 ±0.03 V (vs. Ag/AgCl), which is within close proximity to that of Trp (Figure 2.3). The oxidisable assay component responsible for the broadening of the Trp peak was thus attributed to indole. The proximity of the indole and Trp peak potentials excludes indole as a means of analysing Trpase activity. Due to the slight difference in potential between the Trp and indole oxidation peaks, it is not likely that indole formation would directly affect the Trp peak amplitude but would result in the observed oxidation peak plateaux. Furthermore, the lack of electrochemical responses for PLP and pyruvate exclude them as a means of Trpase activity analysis.

2.4.4. Tryptophan catalysis at the electrode

The two immobilisation strategies employed were adsorption of the Trpase onto the GCE and crosslinking of Trpase using GA and BSA as a co-linker. The controls for this study incorporated the use of an inert protein in order to determine the effect of Trp adsorption to a protein. This was carried out in order to ascertain whether or not any observed effect in the Trp current response was due to catalytic effects of Trpase or rather of protein adsorption. Therefore, the control set up for both immobilisation strategies involved the replacement of Trpase with an equal concentration of the inert protein, BSA.

The anodic oxidation peak of Trp at the adsorbed Trpase-GCE, BSA-GCE and BGCE obtained during CV analysis is illustrated in Figure 2.6.

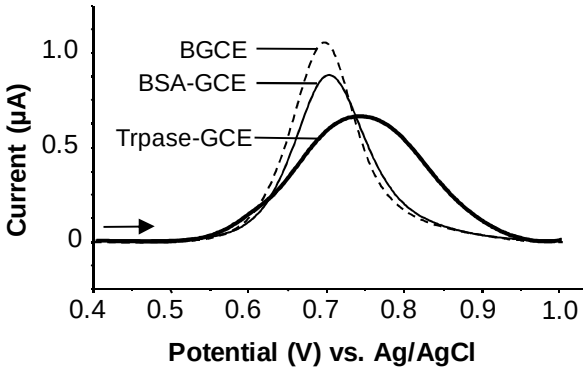

Figure 2.6: Anodic peaks obtained during CV analysis of Trp at the BGCE (dashed), adsorbed BSA-GCE (thin solid) and adsorbed Trpase-GCE (thick solid) in 0.1 M potassium phosphate buffer, pH 8.3, in the presence of PLP (only forward scans are shown with baseline correction). [Trp] = 19.6 µM; Scan rate = 50 mV/s.

The anodic oxidation peak of Trp at the crosslinked Trpase/BSA/GA-GCE, BSA/GA-GCE and BGCE obtained during CV analysis is illustrated in Figure 2.7.

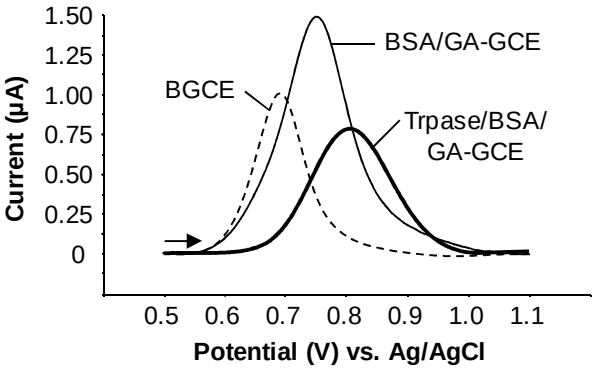

Figure 2.7: Anodic peaks obtained during CV analysis of Trp at the BGCE (dashed), crosslinked BSA/GA-GCE (thin solid) and crosslinked Trpase/GA/BSA-GCE (thick solid) in 0.1 M potassium phosphate buffer, pH 8.3, in the presence of PLP (only forward scans are shown with baseline correction). [Trp] = 19.6 µM; Scan rate = 50 mV/s.

As evident in Figure 2.8, which compares the results obtained for Trp at the Trpase-modified GCEs (Figure 2.6 and Figure 2.7), inclusion of Trpase at the GCE surface resulted in the decrease in the peak amplitude for Trp regardless of the method of immobilisation when compared to the BGCE.

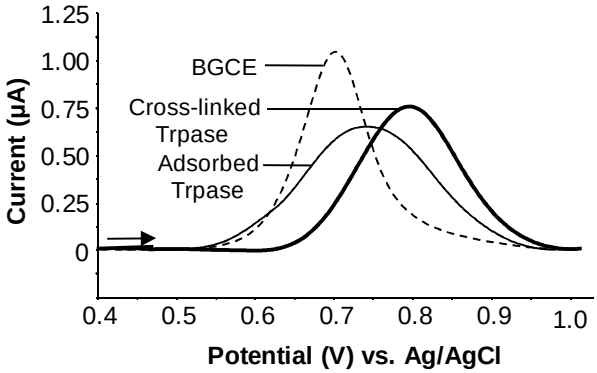

Figure 2.8: Anodic peaks obtained during CV analysis of Trp at the BGCE (dashed), adsorbed Trpase-GCE (thin solid) and crosslinked Trpase/BSA/GA-GCE (thick solid) in 0.1 M potassium phosphate buffer, pH 8.3, in the presence of PLP (only forward scans are shown with baseline correction). [Trp] = 19.6 µM; Scan rate = 50 mV/s.

A comparison of the respective mean current responses for the two Trpase immobilisation strategies and the unmodified GCE is shown in Figure 2.9.

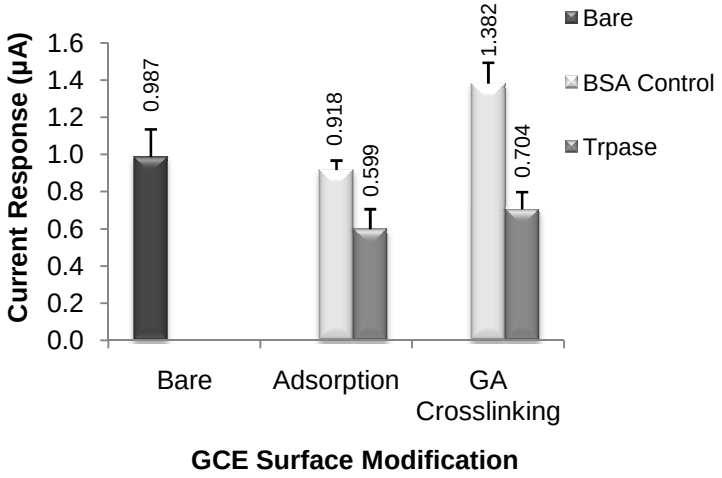

Figure 2.9: Comparative responses for Trpase immobilisation strategies, namely adsorption and GA crosslinking, and an unmodified GCE (n = 3)

As observed in Figure 2.7 and Figure 2.9, an increase in the current response for Trp was observed at the BSA/GA-GCE over the BGCE and Trpase/BSA/GA-GCE, demonstrating adsorption of Trp to the inert protein, BSA. Evidence of this phenomenon was also observed by McMenamy and Oncley (1958) and Annesini and co-workers (2007). They attribute this phenomenon to low affinity and non-specific interactions between Trp molecules and blood proteins, such as albumin. Therefore, Trp is able to exist freely in blood serum whilst having the potential to adsorb to proteins. This observed increase in current response at the BSA/GA-GCE was not observed at the BSA-GCE as a decrease in current response was observed

when compared to the BGCE. This decrease can be attributed to the inability of the BSA to remain at the GCE surface as the presence of GA would stabilise the immobilised BSA.

The cross-linked BSA control (BSA/GA-GCE) exhibited a current response that was 0.264 ±0.024 μA greater than that observed for the adsorbed BSA control (BSA-GCE). This increase in current response demonstrates that the adsorbed BSA was leached resulting in solution phase Trp-BSA adsorption; or, Trp molecules were cross-linked with free glutaraldehyde sites at the BSA/GA-GCE surface. Thus, retention or accumulation of Trp was enhanced at the GCE surface, resulting in the observed increase. A decrease in the current response for Trp was observed at the Trpase modified GCEs over the BGCE and BSA-modified control GCEs. This demonstrates that a large degree of rapid Trp catalysis by Trpase occurred at the GCE surface in the time that it took to initiate and run the CV analysis. In this unstirred solution, this indicates a localised depletion of Trp.

As observed in Figure 2.6 and Figure 2.7, a shift in the Trp peak potential towards a more positive potential (vs. Ag/AgCl) from that of the BGCE was observed when Trpase was present at the GCE surface, as previously shown in Figure 2.4. The observed shift towards a more positive potential demonstrates that oxidation of Trp increased in difficulty. This can be attributed to the binding of Trp to the Trpase active site. An increase towards a more positive potential was observed for Trp at the BSA/GA-GCE over the BGCE with a further increase towards a more positive potential observed at the Trpase/BSA/GA-GCE over the BSA/GA-GCE (Figure 2.7). This may be linked to the lowering of electron transfer at the GCE surface as a result of the layer thickness. However, the greater increase in potential observed for the Trpase-modified GCEs over the BSA control GCEs suggests that binding of Trp to the Trpase strongly influences the peak potentials, indirectly providing further evidence for the specific recognition of Trp by Trpase.

The localised catalysis of Trp at the GCE surface results in the progressive and rapid decrease in the concentration of accumulated Trp at the GCE surface. Therefore, the accumulation of Trp at the GCE surface, as observed for the BSA controls, results in an increase in current response; however, localised Trp catalysis at the GCE surface

by the immobilised Trpase results in a lowered oxidation peak. Therefore, the current response exhibited for Trp at the Trpase-modified GCEs was as a result of the effects of accumulation or adsorption of Trp to Trpase which was counteracted, to a greater extent, by catalysis of Trp by Trpase.

As observed in Figure 2.8, an increased current response was observed at the Trpase/BSA/GA-GCE over that of the Trpase-GCE. This demonstrates the possibility of a low degree of solution phase catalysis occurring at the Trpase-GCE in which binding of Trp to the active sites of the leached Trpase away from the electrode would occur. Therefore, a more stable catalytic process occurred at the Trpase/BSA/GA-GCE compared to the Trpase-GCE providing strong evidence towards the beneficial effects that GA exhibits on current response. Due to the fact that GA crosslinking is known to exhibit increased stability during enzyme immobilisation over that of adsorption (Betancor *et al*., 2006), GA crosslinking was used in further studies. The table below shows the LODs and LOQs that were obtained for Trp at the BGCE and Trpase/BSA/GA-GCE after the first scan, indicating little change in sensitivity between the BGCE and Trpase/BSA/GA-GCE.

Table 2.1: The LOD and LOQ for Trp at the BGCE and Trpase/BSA/GA-GCE during CV analysis

Modification	LOD (nM)	LOQ (nM)
BGCE	14.41	43.65
Trpase/BSA/GA-GCE	18.45	55.90

Therefore, this study provides strong evidence for a selective recognition event and detection of Trp. However, as a product cannot be measured, the question remains whether this method can reliably be used to measure the Trp concentration in an unknown sample.

Tryptophanase catalysis with increasing tryptophan concentration

CV scans of increasing Trp concentration at the Trpase/BSA/GA-GCE (Figure 2.10a) were conducted in order to determine linearity at the Trpase/BSA/GA-GCE.

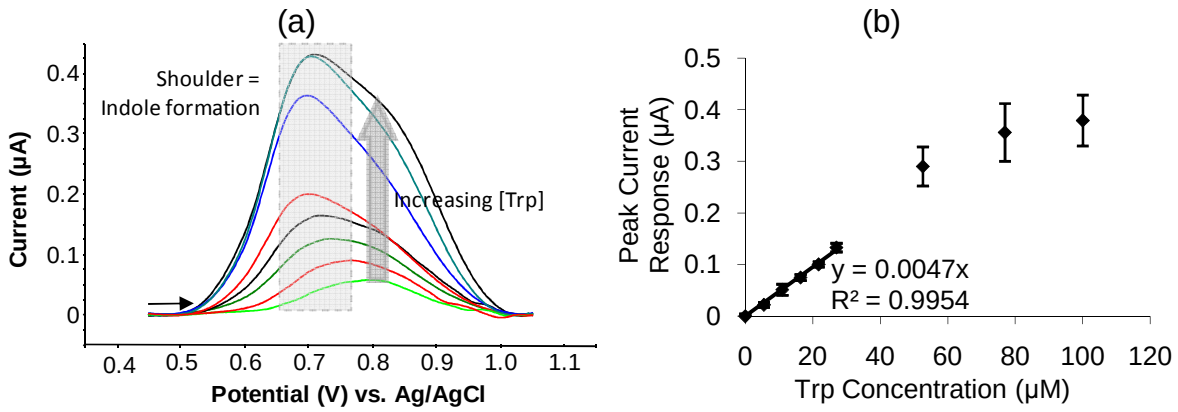

Figure 2.10: (a) CVs of Trp from 5.53 to 100.0 µM with the Trpase/BSA/GA-GCE in 0.1 M potassium phosphate buffer, pH 8.3, in the presence of PLP (Shaded block shows the position of the peak shoulder indicative of indole formation with only the forward scans shown with baseline correction). (b) Linear curve of current response versus Trp concentration at the Trpase/BSA/GA-GCE. Scan rate = 50 mV/s.

The catalytic effects exhibited by Trpase on Trp current at the Trpase/BSA/GA-GCE are evident in Figure 2.10(a) and (b). Over time and upon increasing Trp concentration, a shoulder at less the potential than the expected 0.8 V (shaded block) vs. Ag/AgCl, for the Trp oxidation peak began to form demonstrating interfering bioelectrochemical behaviour (Figure 2.10a). As previously observed (Figure 2.4a & Figure 2.5b), this shoulder is indicative of the formation of an indole product formed as a result of Trp catalysis by Trpase. The indole oxidation peak proceeded to gain in amplitude and exceeded that of the Trp peak as the Trp concentration increased (Figure 2.10a). This is indicative of the fact that as catalysis proceeds, Trp is increasingly catalysed to indole, resulting in the simultaneous decrease in Trp concentration and increase in indole concentration. This process accounts for the concentration dependant formation of a broad peak over time. The increasing Trp concentration would theoretically favour the forward reaction as described in Chapter 1.4.5.; hence, favouring indole formation due to the constant excess of substrate or Trp. Therefore, Trp catalysis or breakdown would occur continually as more Trp is added to the solution. Due to this constant increase in Trp concentration and based on the thermodynamics of the reaction, the reverse reaction (Trp production from indole as described in Chapter 1.4.5.) would not take place to a significant extent. Therefore, an increasing concentration of indole is observed.

Upon increasing Trp concentration (0 to 27.03 µM), a linear response was obtained

with an R^2 value of 0.995 and an average reproducibility of 99.3 % (Figure 2.10b). However, upon further increase in Trp concentration (52.6 to 100.0 µM) deviation from the linear trend occurred as current response started to plateau. The formation of this plateau in the curve can be attributed, firstly, to current response dampening exhibited by an excess of analyte as the upper limits of a detectable concentration of an analyte would be reached. Secondly, formation of the plateau can be attributed to analyte interference due to co-adsorption of the two analytes, Trp and indole. Alternatively, the observed peak formation can be attributed to the concentration of Trpase at the GCE surface, resulting in increased catalysis of Trp and formation of indole.

In order to confirm that the observed deviation in the current response was indeed due to Trp catalysis, a study of Trp catalysis at the Trpase/BSA/GA-GCE was conducted over time using consecutive scans. Figure 2.11 illustrates the exhibited effect of consecutive scans, with stirring in between scans, at the Trpase/BSA/GA-GCE. Figure 2.11(a) shows the CVs that were obtained during this study with the insert illustrating the difference in peak shape between the initial and final scan against the buffer.

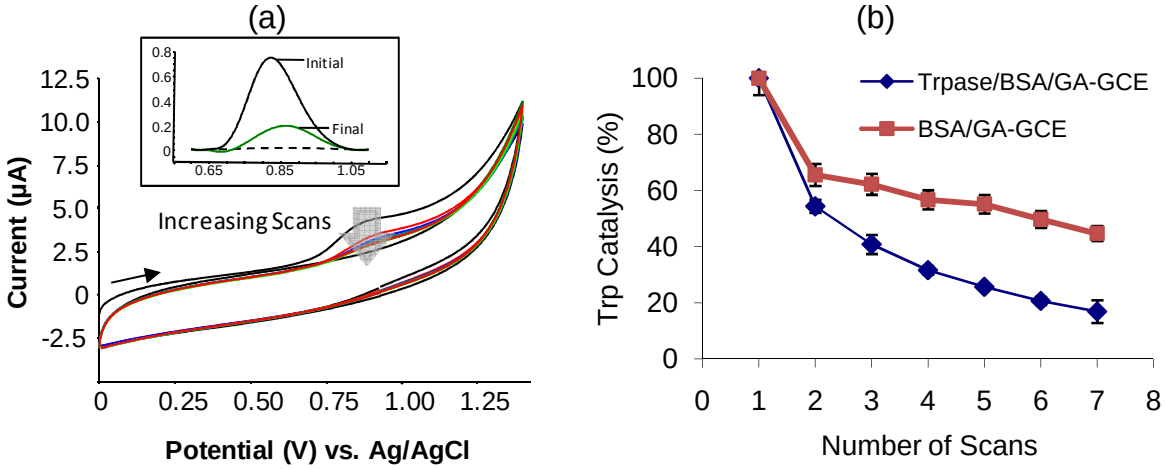

Figure 2.11: (a) CVs of the time study of Trp catalysis at the Trpase/BSA/GA-GCE using consecutive scans in 0.1 M potassium phosphate buffer, pH 8.3, in the presence of PLP. Insert: The differences in current and peak shape between the initial and final scan compared to the assay buffer (dashed). (b) Plot of the percentage Trp catalysis at the Trpase/BSA/GA-GCE versus time (mins). [Trp] = 19.6 µM; Scan rate = 50 mV/s.

A decrease of 80.25 ±2.36 % was obtained for Trp at the Trpase/BSA/GA-GCE after seven consecutive scans with a 55.61 ±2.41% loss in signal at the BSA/GA-GCE.

The observed decrease in current response at the BSA/GA-GCE can be attributed to the effects of fouling. This demonstrates that there was a 24.65 % loss in Trp due to catalysis by Trpase. The effects of fouling at the Trpase/BSA/GA-GCE are limited owing to the stirring that takes place between scans. Therefore, a general decrease in current response was observed for Trp analysis at the Trpase/BSA/GA-GCE with the formation of indole causing the observed peak broadening.

2.4.5. The influence of fMWCNTs on tryptophan detection and catalysis

The effect of fMWCNTs on Trp detection at the BGCE is demonstrated in Figure 2.12.

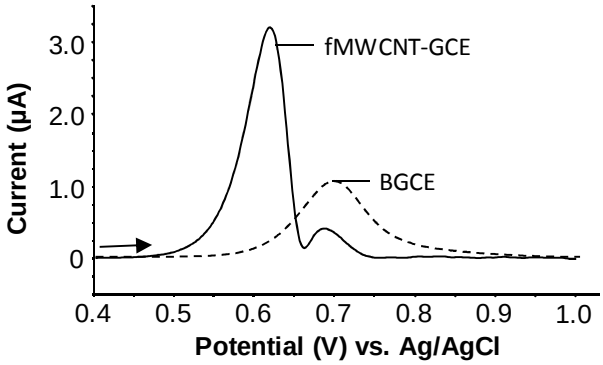

Figure 2.12: Anodic oxidation peaks during CV analysis of Trp at the BGCE (dashed) and fMWCNT-GCE (solid) (only baseline-corrected forwards scans are shown). [Trp] = 19.6 µM; Scan rate = 50 mV/s

As observed in Figure 2.12, an increase in the Trp current response was observed at the fMWCNT-GCE over the BGCE. The increase in Trp current response exerted by carbon nanotubes was previously noted at an MWCNT/cobalt salophen carbon paste electrode (Shahrokhian & Fotouhi, 2007) and for single-walled CNTs at a GCE (Huang *et al*., 2004). The observed increase in response is attributed to properties that the fMWCNTs exert on electron flow during oxidation as well as an increase in the oxidising surface area at the GCE surface. The fMWCNTs act to enhance the movement of electrons towards the GCE surface, thereby enhancing the response during analysis (Ebbesen *et al.*, 1996; Tans *et al*., 1997). Due to the oxidative acid functionalisation of the CNTs, a greater number of open ended fMWCNTs are produced (Rao *et al.*, 2001; Day *et al.*, 2004). These fMWCNTs have a number of functionalised sidewall defects caused by the harsh pretreatment, resulting in a greater number of negatively charged carboxyl groups. Moreover, the open areas on the fMWCNTs are responsible for the electrocatalytic properties of fMWCNTs (Moore

et al., 2004). Therefore, end opening and sidewall perforation of fMWCNTs results in a larger number of open catalytic sites and accommodating the detection of a greater number of Trp molecules. The fMWCNTs, therefore, provide a greater catalytically active surface area for Trp oxidation over that provided by the BGCE. A shift in the anodic peak potential of -0.085 V (vs. Ag/AgCl) for Trp was observed at the fMWCNT-GCE from that of the BGCE (Figure 2.12). The observed potential shift towards a more negative potential, as observed for Trp in Figure 2.12, is indicative of an increased ease of oxidation. This can be attributed to an increased surface area, improved electrical conductivity and potential catalytic effects.

A study was conducted in order to determine the effect of fMWCNTs on Trp detection at the Trpase modified GCE. A spectrophotometric assay was conducted on the Trpase/fMWCNT mixture in order to determine Trpase activity on Trp when the enzyme is cross-linked with the fMWCNTs. The specific activity of the cross-linked Trpase and fMWCNTs yielded 24.95 ±1.62 µg of indole. This value is lower than that obtained for the solvent-bound Trpase (27.71 ±0.94 µg). Therefore, the specific activity of Trpase was lowered when cross-linked with fMWCNTs; however, it remains within the range of activity stipulated by the supplier (15.0 – 40.0 µg of indole).

The electrochemical analysis of Trpase activity on Trp in the presence of fMWCNTs was demonstrated. When the Trpase/fMWCNT mixture was adsorbed to the GCE surface, an unstable layer formed and, as a result, cross-linked Trpase and fMWCNTs were tested. The incorporation of fMWCNTs into the Trpase modified GCEs (Trpase/fMWCNTs/GA-GCE) showed no discernible effect on Trp current response compared to the Trpase/BSA/GA-GCE (Figure 2.13), demonstrating that fMWCNTs have little effect on the current response for Trp in presence of Trpase.

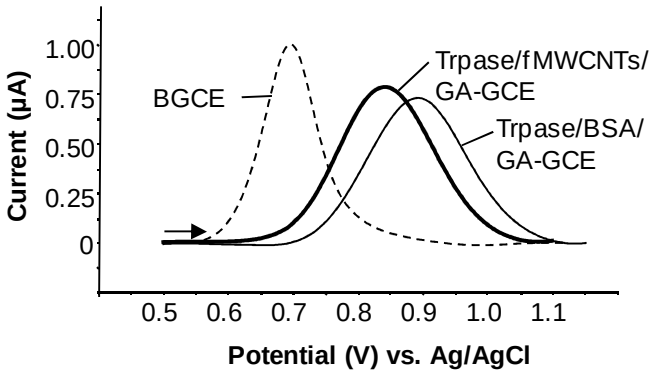

Figure 2.13: Anodic peaks obtained during CV analysis of Trp at the BGCE (dashed), Trpase/BSA/GA-GCE (thin solid) and Trpase/fMWCNT/GA-GCE (thick solid) in 0.1 M potassium phosphate buffer, pH 8.3, in the presence of PLP (only baseline-corrected forwards scans are shown). [Trp] = 19.6 µM; Scan rate = 50 mV/s.

However, the current responses for Trp obtained at both the Trpase/fMWCNT/GA-GCE and the Trpase/BSA/GA-GCE are lower than the BGCE (Figure 2.13), demonstrating catalysis of Trp by Trpase. A peak potential shift towards a more positive potential was observed at the Trpase/BSA/GA-GCE (0.89 ±0.015 V vs. Ag/AgCl) when compared to this BGCE (0.69 ±0.002V vs. Ag/AgCl). This demonstrates an increasing difficulty in oxidation upon modification with Trpase/BSA/GA for reasons previously discussed (Chapter 2.4.4.). A lowering of the Trp oxidation peak potential towards a less positive potential was observed at the Trpase/fMWCNT/GA-GCE (0.84 ±0.008 V vs. Ag/AgCl) compared to the Trpase/fMWCNT/GA-GCE. This demonstrates an increase in the ease of Trp oxidation at the Trpase/fMWCNT/GA-GCE as the electron transfer properties, exhibited by the fMWCNTs, are enhanced with the current responses remaining the same.

4. Conclusions

In summary, the Trpase/BSA/GA-GCE can be used to monitor a localised decrease in the Trp current response. Lower sensitivity towards Trp was obtained at the Trpase/BSA/GA-GCE (LOD and LOQ were 18.45 and 55.90 nM, respectively) over the BGCE (LOD and LOQ were 14.41 and 43.65 nM, respectively). Addition of signal enhancers, such as fMWCNT, did increase the current response for Trp at the BGCE; however, a similar effect was not exhibited when fMWCNTs were

incorporated into the Trpase-modified GCEs.

Therefore, enzyme modified sensors have distinct advantages (specificity) and disadvantages (catalysis). The Trpase modifications used at the GCE surface were not suitable for the sensitive detection of Trp as localised catalysis occurred at the surface resulting in a lowered signal response. The localised catalysis resulted in the formation of an indole oxidation peak, the peak potential of which was within the Trp potential window, resulting in overlapping of the peaks and shouldering peak formation. In order to promote Trp catalysis and hinder the reverse reaction (Trp production from indole), excess substrate was required; thereby, promoting indole formation and selectivity towards Trp. Further evidence of substrate selectivity for Trp by Trpase was presented upon analysis of the peak potential shifts as a shift towards a more positive potential indicated binding of Trp to Trpase. A higher degree of substrate specificity by Trpase towards Trp was observed as no activity was exhibited towards Mel.

As a tool for Trp detection, this method of analysis would rely on a decrease in the current response at the modified surface in order to prove the presence of Trp. This would, however, be complicated by fouling at the GCE surface resulting in inaccuracies during measurement of Trp. These inaccuracies may arise in that an observed decrease in current response may be attributed to fouling and not Trpase activity on Trp. Further complications may arise during analysis of Trp in complex matrices as co-adsorption and non-specific binding may affect signal responses.

Due to a lack of sensitivity towards Trp by means of the Trpase-modified GCEs, an alternative method for the selective and sensitive detection of Trp is required. Subsequent chapters address this in the context of GCE modification with the commercial membrane, Nafion®; electrocatalysts, such as metallophthalocyanines; and, hybrid or composite layers that include fMWCNTs.

Chapter 3

pH tuning using Nafion® for detection of tryptophan*

3.1. Introduction

In today's society, there are increasing numbers of unregulated pharmaceutical formulations, dietary supplements and food products flooding the commercial market. Each of these products has a specific application employed to effectively prevent, regulate or correct specific medical and physiological conditions. For example, there are a number of products available that treat insomnia and jet lag, such as the pharmaceutical or dietary supplement, Serene Tranquillity®. These products result from better understanding of and advances in the fundamental biochemistry of the human body. The underlying mechanisms of these fundamentals determine the composition of these products, such as the use of melatonin (Mel) to control sleep disorders (Skene, 1996) and administration of tryptophan (Trp) to control Mel biosynthesis (Fernstrom & Wurtman, 1971; Biggio, et al., 1974; Young, et al., 1989).

Due to the complexity of the human diet, more complex formulations are being produced in which more than one active ingredient may be present. This results in interference when assessing the quality of these formulations. Therefore, a quick, simple, robust, sensitive and selective method of detection for the analysis of these products is required. Electrochemistry is one such technique that fulfils these requirements.

Formulations that contain Trp target conditions that are related to deficiencies in Trp and its metabolites, serotonin and Mel. Therefore, there exists the possibility that these Trp metabolites interfere in Trp detection during the quality control process of the Trp-containing product. However, it is more likely that Mel would be the interfering analyte during electrochemical analysis of Trp due to the similarity in structure, as shown in Figure 3.1, and, possible, electrocatalytic behaviour of the two molecules. Alternatively, many formulations contain added ingredients that are

* The results presented in this chapter are currently "In Press" in *Electrochimica Acta* (Frith & Limson, 2009).

known to promote health and well-being, such as ascorbic acid (AA), which is a common electrochemical interferent found in dietary supplements and blood serum.

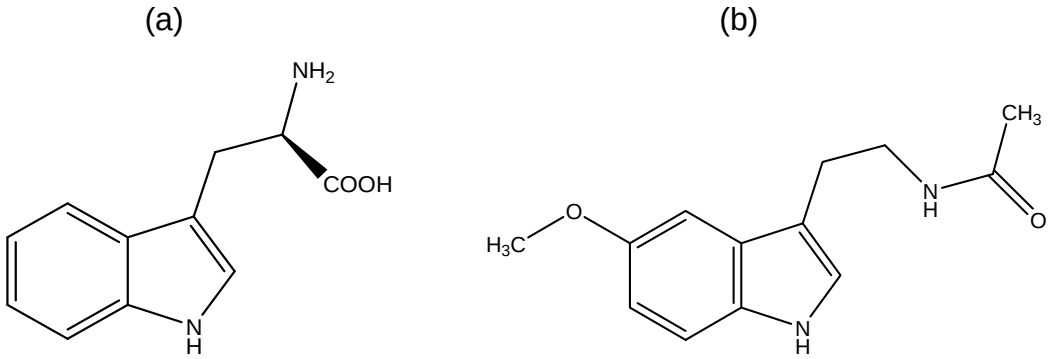

Figure 3.1: The chemical structures of (a) Trp and (b) Mel

Different electrochemical techniques and electrode modifications are required for the sensitive and selective analysis of the target analyte, Trp, in these products. Nafion® provides one such method of electrode modification that may allow for the selective detection of a particular analyte. As discussed in Chapter 1.3.2. and 1.4.3., the cation exchanging, perfluorinated polymer, Nafion® (Figure 1.5), provides for a selectively permeable polymer resin which allows for the selective detection and analysis of positively charged ions (Nagy *et al*., 1985; Kreuer *et al*., 2000). Electrochemical detection of the positively charged analytes is achieved by the accumulation of these analytes at the surface of the Nafion® film due to charge interactions between the cationic, or positively charged, analyte and the negatively charged sulphonate groups on the polymer (Nagy *et al*., 1985). The negatively charged, or anionic, analytes are repelled by their like charges on the sulphonate groups of the polymer (Heitner-Wirguin, 1996). An excellent example of application of Nafion®, in detection of positively charge analytes, is that of dopamine (DA). DA is a cation at physiological pH and will, therefore, permeate through the Nafion® film, resulting in an enhanced signal (Nagy *et al*., 1985). The troublesome interferent during DA detection is AA, which is negatively charged at physiological pH. AA will, therefore, be excluded during the simultaneous detection of DA and AA, resulting in the selective detection of DA. However, analyses of some analytes at a Nafion®-modified GCE have exhibited losses in sensitivity owing to diffusional constraints (Gogol *et al.*, 2000).

At physiological pH, Trp (pKa_1 = 2.45 & pKa_2 = 9.39) and Mel (pKa = ~1.2) have a net neutral charge. As the pH of the solution in which the analyte is analysed approaches and is dropped below the pKa of the analyte, the molecule becomes protonated (positively charged) and the number of protonated species in the solution increases. Alternatively, as the pH of the working solution approaches and is raised above the pKa of the functional groups of the analyte, the molecule becomes deprotonated (negatively charged) and the number of deprotonated species in the solution increases.

3.2. Aim

The aim of this study was to examine the effect of the pH of the electrolyte solution and manipulation of the resulting charge on the detection of Trp, Mel and DA with a Nafion®-coated GCE, and apply the findings to the detection of Trp in a real sample, such as the dietary supplement or pharmaceutical formulation, Serene Tranquility® Night with Trp (Tryptopure™).

3.3. Experimental Procedure

3.3.1. Chemicals, reagents and apparatus

Trp, Mel and DA were purchased from Sigma Aldrich (Johannesburg, South Africa), and 1.0 mM stock solutions of each were prepared using Milli-Q water (Millipore, UK), with the exception that Mel was first dissolved in 200.0 µl of absolute (99.6 %) ethanol and subsequently made up to 10.0 ml using Milli-Q water. The Britton-Robinson (BR) buffer (Britton, 1955) stock was prepared from 0.04 M solutions of phosphoric acid, acetic acid and boric acid. The pH of the stock solution was adjusted to the initial pH of 1.5 using mutual combinations of acetic, boric and phosphoric acid. A volume of 200.0 ml was removed from the stock solution and stored at 4.0 ^{o}C. BR buffer solutions were prepared similarly for the pH values of 2.0, 2.5, 3.0, 4.0, 5.0, 6.0, 7.0, 7.4, 8.0, 9.0, 9.5, 10.0 and 11.0 from the stock solution (pH 1.5) and adjusted to the chronological pH value using a 0.2 M solution of NaOH (Sigma Aldrich, South Africa). All pH measurements were carried out using the WTW pH 330i pH meter coupled to a Sentix 41 pH electrode. Nafion® was obtained, in the

form of 5.0 % solution (w/v) in a low-molecular weight alcohol, from Sigma Aldrich (South Africa).

3.3.2. Electrochemical apparatus

Set up and cleaning of the electrochemical cell and GCE pretreatment were carried out as described in Chapter 2.3. A 5.0 ml working electrolyte solution of 0.04 M BR buffer was used. The cyclic voltammetry (CV) scans were conducted from a start potential (V) ranging from -0.1 V to an end potential of 1.1 V, with a step potential of 1.8 mV, a scan rate of 50 mV/s and a 10 s pretreatment step, unless otherwise stipulated. The squarewave voltammetry (SWV) scans were conducted in the same potential range as for CV; however, the step potential was 4.0 mV, amplitude was 25.0 mV and frequency was 15.0 Hz.

3.3.3. Preparation of electrodes

A 5.0 % (w/v) Nafion® solution was diluted with methanol, where necessary, to obtain 0.5, 1.0, 2.0, 3.0, 4.0 & 5.0 % (w/v) solutions. Subsequent to GCE polishing, a volume of 1.5 µl of the desired concentration of Nafion® was carefully placed on the surface of the electrode and allowed to dry at ambient or room temperature under laminar airflow.

3.3.4. Analyte characterisation

3.3.4.1. Linearity

Standard curves of concentration versus current were produced by linearly and uniformly increasing the concentration of the analyte. This was done in a step-wise fashion using 10.0 µl aliquots of the analyte of interest with stirring in between each SWV scan. The analysed concentrations ranged from 1.96 to 19.6 µM as the final concentration.

3.3.4.2. Passivation

Fouling, or passivation, analyses were carried out by running consecutive CV scans (outlined in Chapter 3.3.2.) without stirring, cleaning of the electrochemical apparatus and polishing of the GCE between scans. The passivation is calculated as a percentage of the current response of the initial scan, described as:

Current Response Passivation (%) = (I_{pa}^{final} / $I_{pa}^{initial}$) X 100 ..... Equation (3.1)

Where I_{pa} is the current response of the anodic peak. Therefore, the initial scan is assigned a value of 100.0 %. These studies were conducted at both a modified and unmodified GCE.

3.3.4.3. Mode of transport

The mass transport of an analyte was determined by analysing the effect of scan rate. This was determined by running CV scans of the analyte of interest with scan rates of 50, 100, 200, 300, 400 and 500 mV/s; and, plotting the current response versus the square root of the scan rate.

3.3.4.4. LOD and LOQ

The LOD and LOQ were calculated as described in Chapter 2.3.2.5.

3.3.4.5. Variability and reproducibility

The variability and reproducibility were calculated as described in Chapter 2.3.2.6.

3.3.5. Electron flow characterisation for the Nafion®-GCE

Impedance spectroscopy measures the resistance in the flow of electrons given by the modifying layer at the electrode surface. The three electrode system was used for all impedance spectroscopy analyses and conducted on the Potentiostat/ Galvanostat (PGSTAT) from Autolab using Frequency Response Analysis (FRA) software Version 4.9 (Eco Chemie, Netherlands). A working electrolyte solution of 5.0 mM potassium hexacyanoferrate was prepared in 0.2 M potassium phosphate buffer, pH 7.4. The preliminary CV scan had a start potential of -0.2 V and an end potential of 0.8 V. The formal potential was determined by halving the sum of the anodic and cathodic potential values and is given by the equation (Heineman & Kissinger, 1996):

$$E^{o'} = (E_{p(a)} + E_{p(c)}) / 2 \quad \text{.....Equation (3.2)}$$

The formal potential used for all impedance analyses was approximately 0.24 V.

3.3.6. *pH studies*

SWV scans of Trp, Mel and DA were conducted from pH 1.5 to 11.0 in the presence and absence of Nafion®. The pKa values and chemical structures for both Trp and Mel were calculated and generated using the SPARC online calculator (see http://ibmlc2.chem.uga.edu/sparc/ for details).

3.3.7. Detection of tryptophan in the presence of melatonin and dopamine

SWVs of a solution containing 19.6 µM of Trp, Mel and DA were conducted at pH 3.0. SWVs were conducted using a 2.0 mg/ml solution of a dietary supplement containing Trp. The dietary supplement used was in the form of the formulation Serene Tranquility® Night with Trp (Tryptopure™) supplied by Life Enhancement (USA). The oxidation peak for Trp was identified in the formulation by means of standard additions of a Trp stock solution.

3.3.8. Statistics

All studies were conducted in triplicate. Results are presented as mean ±standard deviation.

3.4. Results and Discussion

3.4.1. Optimisation of pH and electrochemical technique

The buffering solution with a pH of 3.0 was chosen for the optimization analyses due to an optimum Trp current response and enhanced peak resolution exhibited at this pH, as described in further sections.

SWV yielded a sharp, well-defined peak (Figure 3.2) demonstrating good sensitivity. SWV was the technique of choice as it was both rapid and sensitive (Kounaves, 1997).

3.4.2. Effect of Nafion® concentration at GCE surface

Figure 3.2 illustrates the SWVs obtained during Trp detection with 0.5 % (w/v) Nafion® at the GCE surface at pH 3.0.

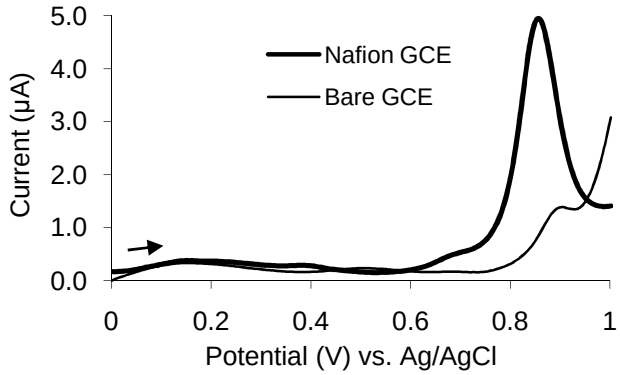

Figure 3.2: SW voltammograms of Trp with Nafion®-modified GCE and BGCE in BR buffer, pH 3.0 (with baseline correction). [Trp] = 19.6 µM; [Nafion®] = 0.5 %

The optimal Nafion® concentration for Trp detection at the GCE surface in a solution of pH 3.0 was 0.5 % (Figure 3.3). The Trp current response exhibited an increase of 4.12 ±0.128 µA when 0.5 % Nafion® was added to the bare GCE surface (Figure 3.2). This increase is attributed to the accumulating effects exhibited by the Nafion® layer (Nagy *et al*., 1985) as the Trp molecules accumulate in the water pockets that are positioned alongside the hydrophilic side-chains of the Nafion® (Heitner-Wirguin, 1996).

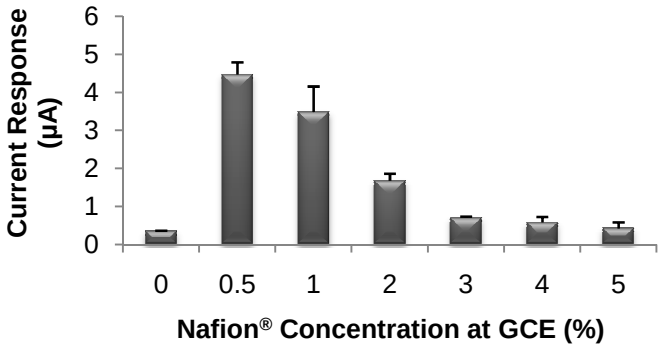

Figure 3.3: The optimisation of the Nafion® concentration (%) at the surface of the GCE when detecting Trp in BR buffer, pH 3.0, using SWV. [Trp] = 19.6 µM; *n* = 3.

A decrease in the current response was observed as the concentration of Nafion® increased beyond 0.5 % to 5.0 %, as demonstrated in Figure 3.3 and previously reported by Rocha and Carapuça (2006). This decrease can be attributed to the reduction in the number of pores in the Nafion® and a reduction in the pore sizes as more polymeric Nafion® molecules are over-layed. This would, thus, limit the effective transport of Trp through the Nafion® film.

3.4.3. Tryptophan characterisation

3.4.3.1. Linearity

Linear standard curves for the BGCE and Nafion®-GCE at pH 3.0 exhibited 98.9 and 94.9 % reproducibility, respectively. The LOD and LOQ for SWV analysis of Trp at the BGCE and Nafion®-GCE are outlined in Table 3.1.

Table 3.1: The LOD and LOQ for Trp at the BGCE and Nafion®-GCE during SWV analysis

Modification	LOD (nM)	LOQ (nM)
BGCE	14.91	45.19
Nafion®-GCE	1.62	5.40

The calculated LOD at the Nafion®-GCE was 9.2 times lower than the LOD calculated at the BGCE at pH 3.0. This demonstrates that sensitivity for Trp detection at pH 3.0 at the Nafion®-GCE was 9.2 times more sensitive than at the BGCE. This data coincides with the fact that the Trp current response at the Nafion®-GCE was substantially greater (12.7 times) than that observed at the BGCE (Figure 3.2), demonstrating that the improved sensitivity during electrochemical detection was accurate. Therefore, a lower concentration of Trp can be detected at the Nafion®-GCE at pH 3.0.

3.4.3.2. Passivation

Figure 3.4 (a) and (b) demonstrates the effects of fouling with no stirring at pH 3.0 with the BGCE and Nafion®-GCE, respectively. Figure 3.4 (c) summarises the observed passivation of Trp at the BGCE and Nafion®-GCE and represented as plots of current response passivation versus the number of scans.

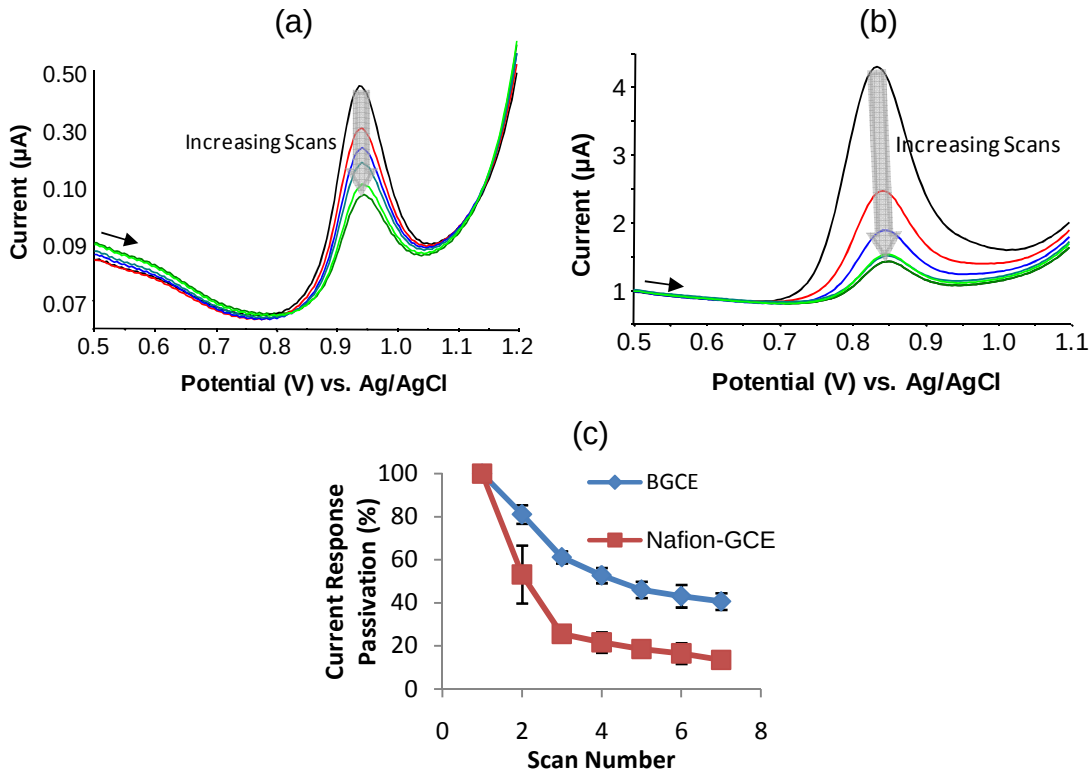

Figure 3.4: SWVs of consecutive scans of Trp oxidation at the (a) BGCE and (b) Nafion®-GCE surface (pH 3.0). (c) Trp fouling at the BGCE and Nafion®-GCE (pH 3.0) represented as current response passivation (%). [Trp] = 19.6 µM; Scan rate = 50 mV/s

From Figure 3.4 (a) and (b) it is evident that consecutive scans of Trp resulted in a decrease in the current response of the oxidation peak at both the BGCE and Nafion®-GCE, respectively, demonstrating passivation of the electrode. Passivation of the electrode is as a result of the accumulation of oxidized compounds at the GCE surface causing interference of the signal response, resulting in the observed reduction in signal. A total passivation of 86.5 ±2.5 % was observed at the Nafion®-GCE after 7 scans as opposed to 59.3 ±1.3 % for the BGCE.

Figure 3.5(a) demonstrates the effect that stirring has on consecutive SWV scans of Trp at the Nafion®-GCE under acidic conditions (pH 3.0). Figure 3.5(b) represents Trp passivation, expressed as a percentage, at the Nafion®-GCE after seven consecutive scans.

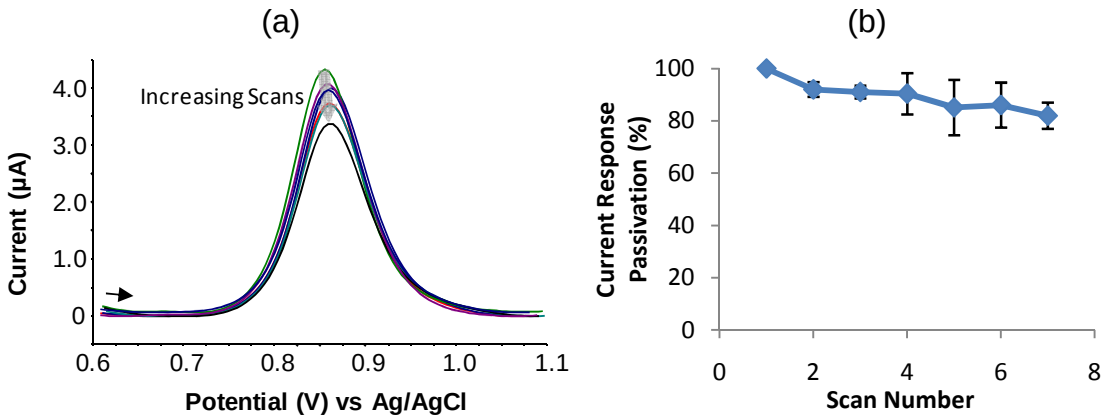

Figure 3.5: SWVs of consecutive scans of Trp oxidation with stirring between scans at the Nafion®-GCE surface (pH 3.0) (with baseline correction). (c) Trp fouling with stirring at the Nafion®-GCE (pH 3.0) represented as current response passivation (%). [Trp] = 19.6 µM;

A total passivation of 18.1 ±3.6 % was observed at the Nafion®-GCE after seven scans with stirring between each scan. The employment of stirring between scans resulted in an average of 68.4 % less passivation of the Nafion®-GCE compared to the when stirring was not employed between scans. Therefore, stirring reduced the effects of fouling at the Nafion®-GCE due to dislodging of adsorbed oxidation products. The effect of this adsorption behaviour is illustrated by the impedance plots (Figure 3.9 and 3.10) for Nafion® where increased resistance to electron flow is observed compared to the BGCE (please refer to Chapter 3.4.5.).

3.4.3.3. Mode of transport

Figure 3.6 (a) and (b) illustrates the CV analysis of Trp oxidation at the BGCE and the Nafion®-GCE, respectively, using the studied scan rates (50, 100, 200, 300, 400 and 500 mV/s). Figure 3.6 (c) represents the linearity that was obtained upon plotting the current response and the square root of the scan rate.

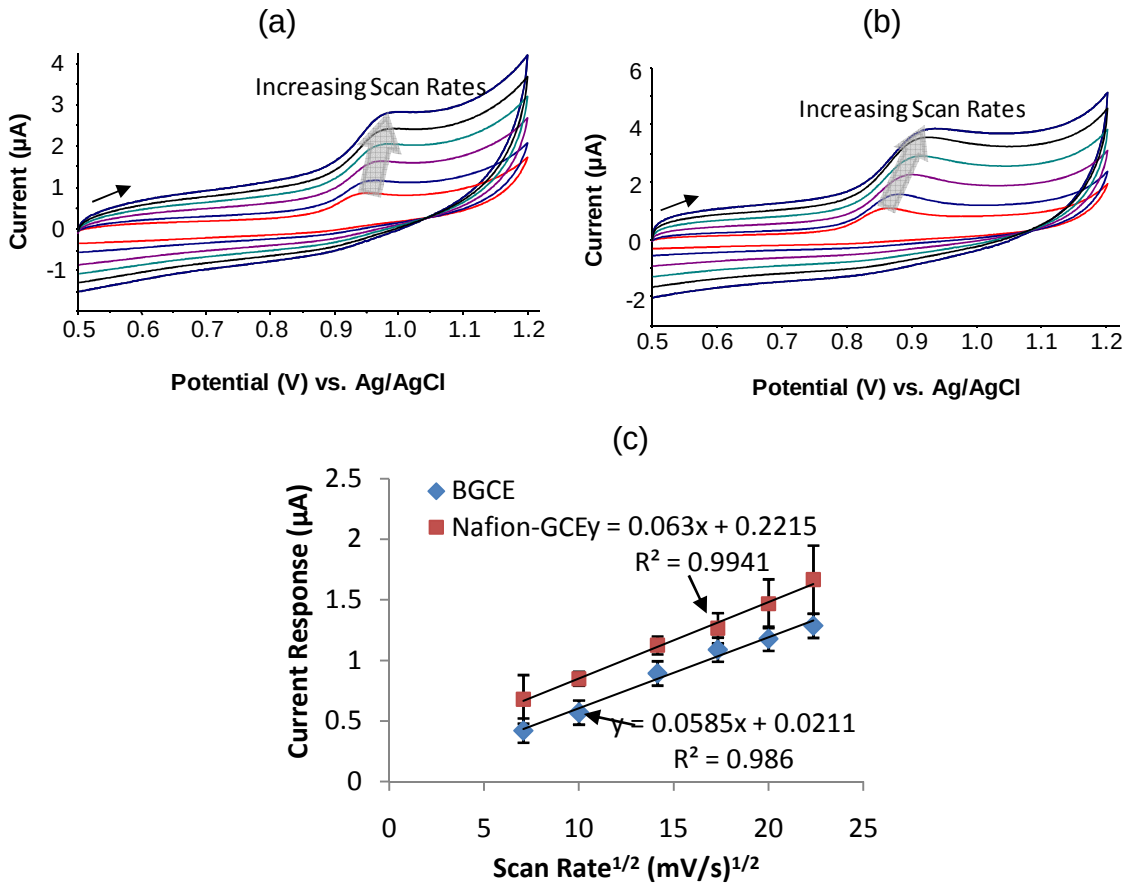

Figure 3.6: CVs of Trp at the (a) BGCE and (b) Nafion®-GCE with various increasing scan rates (pH 3.0). Effect of the square root of the scan rate on the current response of Trp at the BGCE and Nafion®-GCE (pH 3.0). [Trp] = 19.6 µM; Scan rates = 50, 100, 200, 300, 400 & 500 mV/s.

As demonstrated in the plot of current response versus the square root of the scan rate (Figure 3.6c), Trp exhibited a linear response at pH 3.0 when analysed with the BGCE and Nafion®-GCE. The linearity exhibited for the BGCE and Nafion®-GCE had an R^2 value of 0.986 and 0.994 with an average percentage of reproducibility of 90.1 and 85.0 %, respectively. The linear relationship of current response versus the square root of the scan rate indicates that Trp oxidation is diffusion controlled at both the BGCE and Nafion®-modified GCE (Nicholson & Shain, 1965).

3.4.4. Melatonin characterisation

3.4.4.1. Linearity

Mel exhibited an irreversible anodic oxidation peak at 0.82 ± 0.003 V as observed in CV analysis at the BGCE. Upon addition of Nafion® to the GCE surface, increases in current response for Mel were observed. Linear standard curves of current response versus Mel concentration at the BGCE and Nafion®-GCE exhibited 94.6 and 98.2 %

reproducibility, respectively. The LOD and LOQ for SWV analysis of Mel at the BGCE and Nafion®-GCE are outlined in Table 3.2.

Table 3.2: The LOD and LOQ for Mel at the BGCE and Nafion®-GCE during SWV analysis

Modification	LOD (nM)	LOQ (nM)
BGCE	13.35	40.44
Nafion®-GCE	1.60	5.33

A greater sensitivity for Mel detection was observed at the Nafion®-GCE over the BGCE at pH 3.0 due to the lower LOD and LOQ values at the Nafion®-GCE. The calculated LOD and LOQ observed at the BGCE and Nafion®-GCE were similar to that of Trp (Table 3.1); however, the current responses observed for Mel differ to those of Trp due to differing mechanisms of detection at the Nafion® layer and interaction between Mel and the Nafion® polymer. Therefore, a lower concentration of Mel can be detected at the Nafion®-GCE at pH 3.0.

3.4.4.2. Passivation

Figure 3.7 (a) and (b) demonstrates the effects of fouling at pH 3.0 without cleaning the BGCE and Nafion®-GCE, respectively. Figure 3.7 (c) summarises the observed passivation of Mel at the BGCE and Nafion®-GCE and are represented as plots of current response passivation, as a percentage of the initial scan, versus the number of scans.

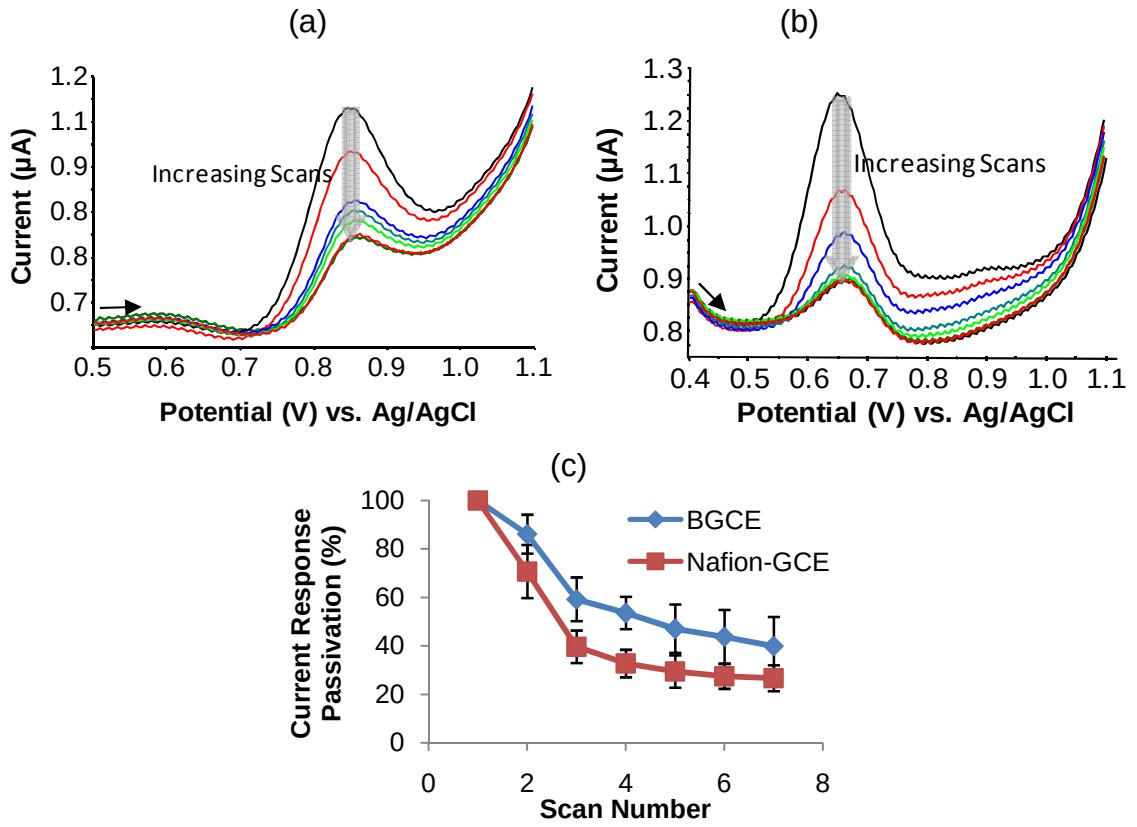

Figure 3.7: SWVs of consecutive scans of Mel oxidation at the (a) BGCE and (b) Nafion®-GCE surface (pH 3.0). (c) Mel fouling at the BGCE and Nafion®-GCE (pH 3.0) represented as current response passivation (%). [Mel] = 19.6 µM

From Figure 3.7 (a) and (b), it is evident that consecutive scans of Mel exhibited trends in current response at the BGCE and Nafion®-GCE that were similar to those found for Trp. During the fouling studies for Mel, the BGCE experienced a total passivation of 61.1 ±5.3 % after seven scans whereas the Nafion®-GCE exhibited a 73.4 ±2.4% decrease in current response. The increased passivation of Mel at the Nafion®-GCE can be attributed to the accumulation of the oxidised products at the GCE surface-Nafion® layer interface. Thus, the Nafion® layer trapped the oxidised Mel products at the GCE surface, limiting diffusion of products away from the Nafion®-GCE. However, this exhibited effect could be limited with stirring.

3.4.4.3. Mode of Transport

Figure 3.8 (a) and (b) illustrates the CV analysis of Mel oxidation at the BGCE and the Nafion®-GCE, respectively, using the studied scan rates (50, 100, 200, 300, 400 and 500 mV/s). Figure 3.8 (c) represents the linearity that was obtained upon plotting the current response and the square root of the scan rate for both the BGCE and Nafion®-GCE.

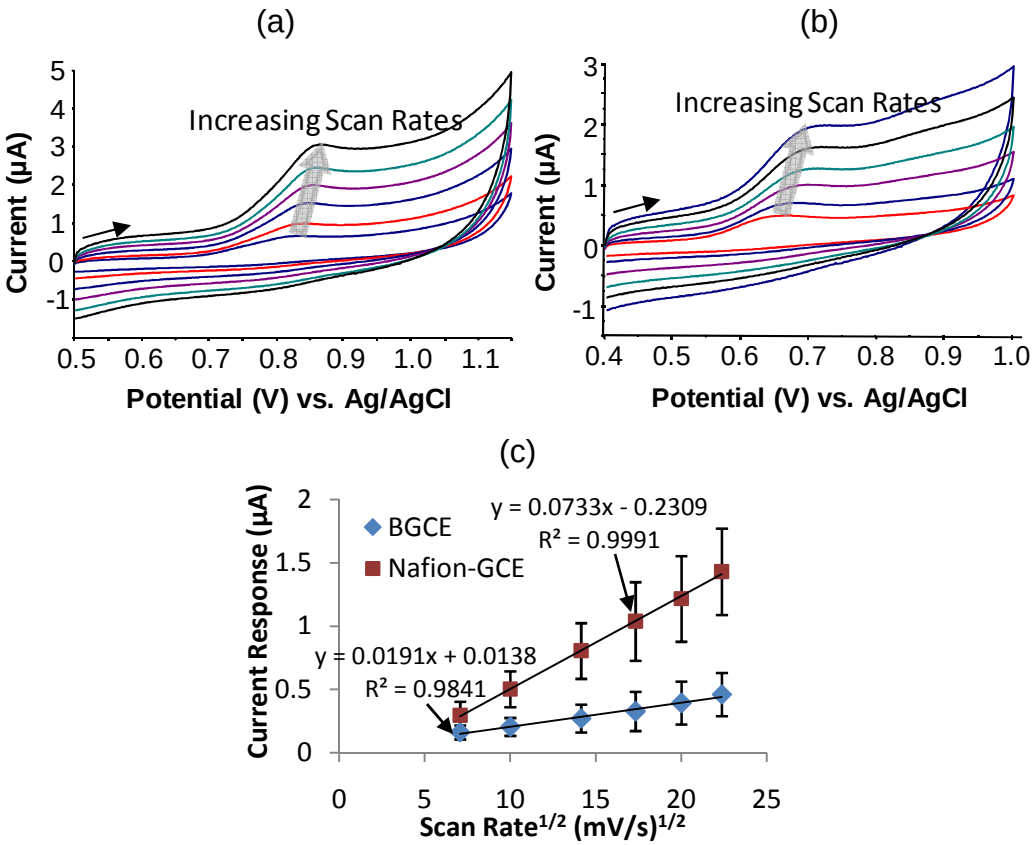

Figure 3.8: CVs of Mel at the (a) BGCE and (b) Nafion®-GCE with various increasing scan rates (pH 3.0). Effect of the square root of the scan rate on the current response of Mel at the BGCE and Nafion®-GCE (pH 3.0). [Mel] = 19.6 µM; Scan rates = 50, 100, 200, 300, 400 & 500 mV/s.

As demonstrated in the plot of current response versus the square root of the scan rate (Figure 3.8c), Mel exhibited a linear response at pH 3.0 when analysed with the BGCE and Nafion®-GCE. The linearity exhibited for the BGCE and Nafion®-GCE had an R^2 value of 0.999 and 0.984 with an average percentage of reproducibility of 75.7 and 88.1 %, respectively. The linear relationship of current response versus the square root of the scan rate indicates that Mel oxidation was a diffusion-controlled process at both the BGCE and Nafion®-modified GCE (Nicholson & Shain, 1965).

3.4.5. Electron flow characteristics at the Nafion®-GCE

The Nyquist plot (Figure 3.9) illustrates that the BGCE exhibited a linear response demonstrating that there was little to no hindrance, or resistance, in electron flow from solution to the GCE surface. The Nafion®-GCE exhibited resistance in electron flow as a variation in linearity, seen by the large semi-circle, was observed. The size of this semi-circle is indicative of the degree of electron flow resistance in solution (Hu *et al*., 2006).

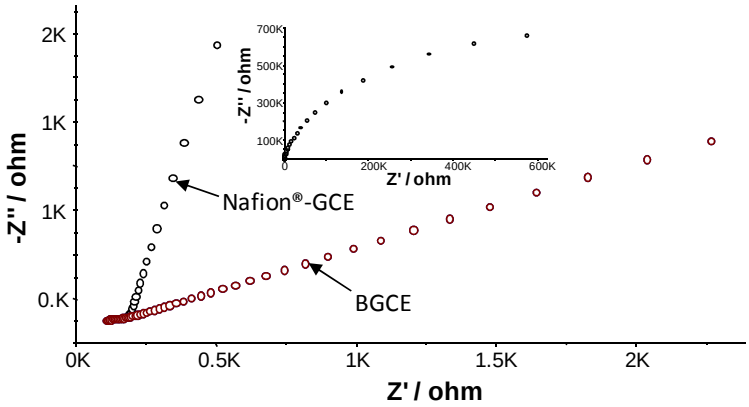

Figure 3.9: Nyquist plots, focusing on the lower ohmic values, of the BGCE (red) and Nafion®-GCE (black) using 5 mM potassium hexacyanoferrate in 0.2 M potassium phosphate buffer, pH 7.4. Insert: The semi-circle exhibited in the complete Nyquist plot for the Nafion®-GCE.

The insulatory effects given by the layer on the GCE surface are indicated in the Bode plot (Figure 3.10). The Bode plot for the BGCE and Nafion®-GCE in 5 mM potassium hexacyanoferrate is given in Figure 3.10.

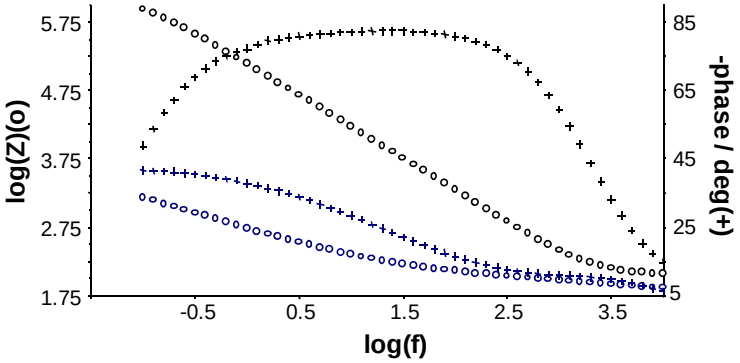

Figure 3.10: Bode plots of the BGCE (blue) and Nafion®-GCE (black) using 5 mM potassium hexacyanoferrate in 0.2 M potassium phosphate buffer, pH 7.4.

A large variation in the phase degree is indicative of a layer more likely to act as a capacitor, as observed for the Nafion®-GCE. The BGCE demonstrated a linear phase response indicating that there is no capacitance. Therefore, the Nafion® forms an insulating layer on the GCE surface thereby allowing the GCE to act as a capacitor. Furthermore, any observed effects on analyte detection at the Nafion®-GCE are as a result of the exerted effects of the Nafion® layer and are not due to imperfections in the layer.

3.4.6. pH tuning for enhanced tryptophan detection

Figure 3.11 illustrates the different Trp species that predominate when analysed in the working solutions with varying pH values.

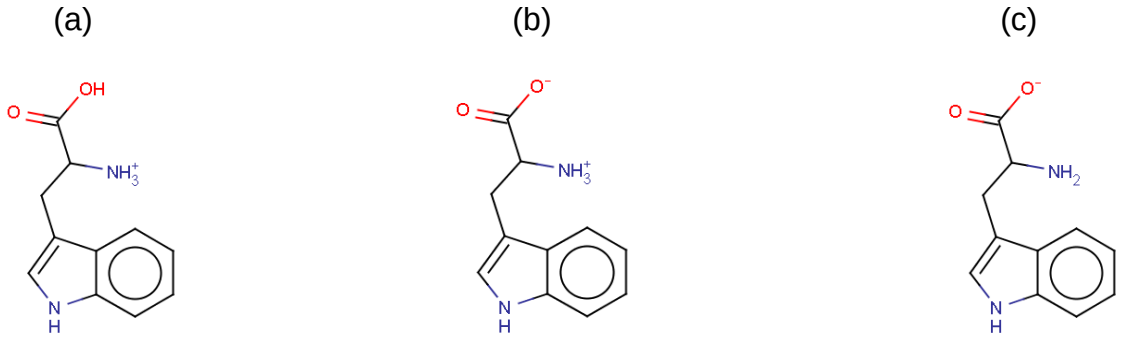

Figure 3.11: The chemical structures of the predominant species of Trp at (a) pH 2.5, (b) pH 7.4 and (c) pH 9.5.

The pH profile of current response versus pH for Trp at the BGCE and Nafion®-GCE is illustrated in Figure 3.12.

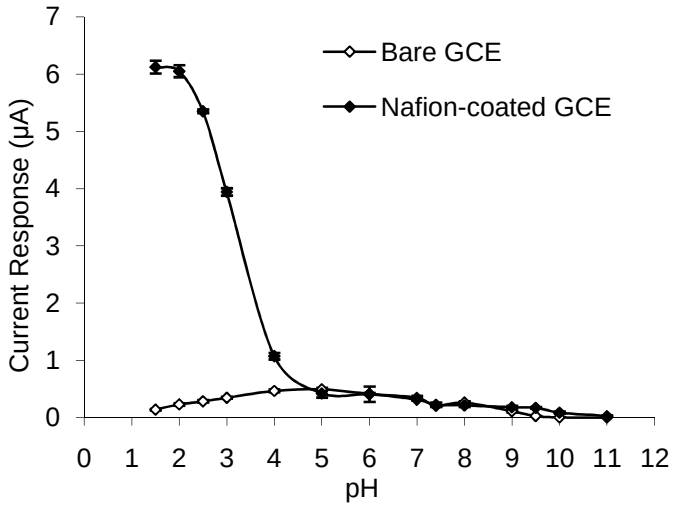

Figure 3.12: pH profile with respect to current response for Trp, in BR buffer using SWV, when analysed with the BGCE and Nafion®-GCE. [Trp] = 19.6 µM; *n* = 3.

When Trp was analysed using the Nafion®-GCE, a progressive increase in current response for Trp was observed as the pH of the solution approaches the pKa_1 value (2.38) for Trp and increases further with acidity, as illustrated in Figure 3.12. This increase in current response for Trp can be attributed to an increase in the protonation of the Trp molecule, as seen in Figure 3.11(a). The protonation would, therefore, result in the Trp molecule having a net positive charge, thus becoming a

cation. Due to the fact that Nafion® is a cation exchanger, more cationic species diffuse through the Nafion® film allowing for the accumulation of these cationic species at the GCE surface. Although not clearly seen in Figure 3.12, a decrease in the current response would be expected at and above the pKa_2 value (9.39) of Trp. This would be due to the deprotonation of the Trp molecule, resulting in a negatively charged or anionic species, as illustrated in Figure 3.11(c). The anionic species would be repelled from or inhibited by the Nafion® film. However, the somewhat extreme pH values of 10.0 and 11.0 caused much of the Trp to be degraded, resulting in limited detection and, hence, interpretation.

3.4.7. pH tuning for melatonin detection

In order to determine an optimal pH with which to achieve a suitable decrease in the Mel current response for selective detection of Trp, a pH profile for Mel was conducted. Figure 3.13 illustrates the pH profile of current response versus pH for Mel at the BGCE and Nafion®-GCE.

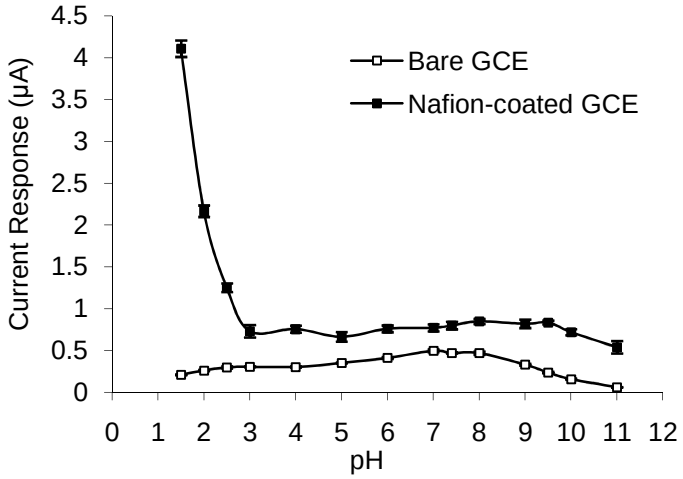

Figure 3.13: pH profile with respect to current response for Mel, in BR buffer using SWV, when analysed with the BGCE and Nafion®-GCE. [Mel] = 19.6 µM; *n* = 3.

When analysing Mel using the Nafion®-GCE, there was an increase in the current response for Mel when the pH of the electrolyte solution approached the pKa of Mel (~1.2), as illustrated in Figure 3.13. This was as a result of protonation of Mel at the amine group of the side chain at the C3 atom (refer to Figure 3.14). This, in turn, results in the accumulation of Mel species with a net positive charge. The positively charged species will then move through the Nafion® film unhindered causing the

observed increase in the Mel current response. The remaining neutral species present between pH 1.5 and 2.5 will diffuse through the Nafion® film at a rate similar to that for the rest of the pH profile.

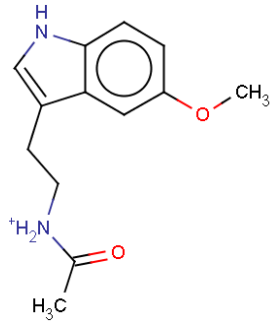

Figure 3.14: The positively charged species for Mel (pKa = ~1.2)

Nafion® has a hydrophobic backbone with hydrophilic side chains (Figure 1.5) giving it the ability to accumulate water (Heitner-Wirguin, 1996). The sulphonate groups of the sidechains face the aqueous environment (Brookman *et al.*, 1986). As a consequence of this, a general increase in the current response for Mel was observed across the pH profile as represented in Figure 3.13. This was due to the amphiphilic character of Mel, the structure of which is shown in Figure 3.14, as it is less hydrophilic in nature than Trp. Due to this amphiphilic character, Mel will reach the surface of the modified GCE owing to its ability to interact with both the hydrophilic sidechains and the hydrophobic backbone. Once at the GCE surface, it is expected that Mel will undergo electrostatic interactions with the suphonate groups of the Nafion® at the GCE surface.

3.4.8. Oxidation peak potentials at the BGCE

Figure 3.15 demonstrates the effect that pH has on the anodic oxidation peak potentials for Trp, Mel and DA at the BGCE.

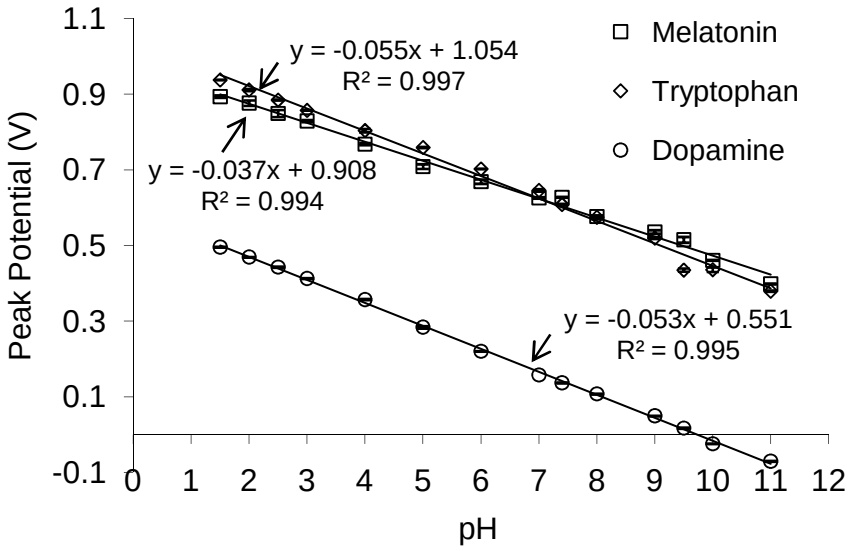

Figure 3.15: The shift in peak potential (V) with pH for Trp, Mel and DA in BR buffer at the BGCE when analysed using SWV. [Trp] = [Mel] = [DA] = 19.6 µM; Scan rate = 50 mV/s; *n* = 3

The anodic potentials of Mel and Trp are in close proximity of each other (in contrast to DA) at all pH values which could lead to masking or overlapping peaks (Figure 3.15). The peak potentials of all analytes exhibited a linear shift towards more negative potentials with increasing alkalinity, as illustrated in Figure 3.15, demonstrating the involvement of protons which can be expressed as:

Ep (Trp) = -0.055pH + 1.054	(R^2 = 0.997)	Equation (3.3)
Ep (Mel) = -0.037pH + 0.908	(R^2 = 0.994)	Equation (3.4)
Ep (DA) = -0.053pH + 0.551	(R^2 = 0.995)	Equation (3.5)

The number of protons and/or electrons involved in the process can then be determined using Equation (3.6) (Biniak *et al.*, 2000):

$$E = E^{\theta} - 0.059\ (m/n)\ \text{pH} \quad \text{.....} \quad \text{Equation (3.6)}$$

Where E is electrode potential for the studied process, E^{θ} is the formal electrode potential, m is the number of protons and n is the number of electrons in the reaction. The theoretical value for the pH/peak potential relationship for the transfer of an equal number of protons to electrons is -59 $mV.pH^{-1}$ (Biniak *et al*., 2000). In order for the theoretical value, -59 $mV.pH^{-1}$, to hold true, m must equal n. The pH/peak potential relationship for Trp and DA, seen as the slope in Equations (3.3)

and (3.5), is similar to that of the theoretical value. This reveals that the number of electrons transferred equals the number of protons involved in the process. The results concur with Babaei and coworkers (2008) in which Trp is oxidised by a two electron/two proton process at the amine group in the indole ring and methyl group in the side chain. DA is oxidised via a two electron/two proton process (Young & Babbitt, 1983).

When the pH/peak potential relationship, or slope, has a value that is less or greater than that of the theoretical value, an imbalance occurs in the number of electrons and protons involved in the redox process. This was demonstrated for Mel in Equation (3.4) in which a slope of -0.037 $mV.pH^{-1}$ was observed. Radi and Bekhiet (1998) describe Mel oxidation as having a two electron/one proton oxidation in which the initial oxidative step results in the formation of the cation radical and the second oxidative step involves electron abstraction and simultaneous proton loss.

3.4.9. Effect of Nafion® on oxidation peak potentials

Figure 3.16 demonstrates the effect that pH has on the anodic oxidation peak potentials for Trp, Mel and DA at the Nafion®-GCE.

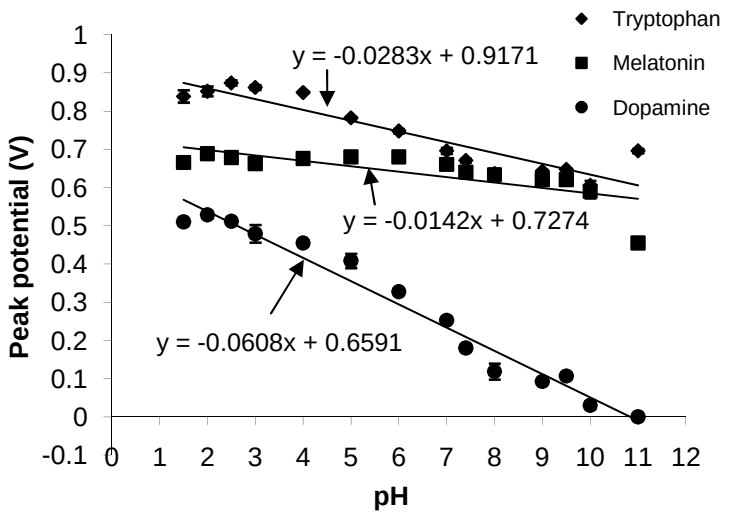

Figure 3.16: The shift in peak potential with pH when analysing solutions of Trp, Mel and DA with the Nafion®-GCE in BR buffer with SWV analysis. [Trp] = [Mel] = [DA] = 19.6 μM; *n* = 3.

Anodic potentials for all three analytes decreased with increasing alkalinity at a Nafion®-GCE. However, these did not shift with pH as uniformly as the studies at the BGCE (Figure 3.15). The slope of the linear trend observed for the shift in peak

potential with pH for DA at the Nafion®-GCE remained similar to that obtained for the BGCE (-60 mV/pH). This demonstrates that the Nafion® layer did not interfere with the DA oxidation process. For Trp and Mel oxidation at the Nafion®-GCE, a decrease in the slope of the linear trend of peak potential versus pH was observed (Figure 3.16). Therefore, Nafion® may have the ability to stabilise the effect that the changing ion and proton concentration has on the peak potential. This may be attributed to the existence of an acidic microenvironment between the GCE surface and Nafion® layer as a result of the trapping of hydrogen ions within the Nafion® layer and/or at the Nafion® film/GCE surface interface.

The observed shift in the slope of the peak potential versus pH of the electrolyte solution effectively facilitates the separation of the anodic peak potentials for Trp and Mel allowing improved selectivity. A marked peak separation was observed in working solutions with acidic pH values (pH 1.5 to pH 4.0) for Mel and Trp. The highest resolution was observed at pH 2.5 with peak potentials for Trp, Mel and DA being 0.86 V, 0.68 V and 0.52 V, respectively. Theoretically, the peak resolution allows for the simultaneous detection of Mel and Trp. A working solution of pH 3.0 yields a current response for Trp (3.94 µA) that is 3.21 µA greater than that of Mel (0.73 µA), thus facilitating further selectivity by utilising the current response.

3.4.10. Tryptophan detection in mixed solutions

Simultaneous detection of Trp, Mel and DA at a Nafion®-GCE in a mixed solution at pH 2.5 and 3.0 resulted in three well defined peaks as shown in Figure 3.17. Figure 3.17(a) shows the effect of Nafion® on current response and peak potential when compared to studies at the BGCE at pH 3.0. Poor resolution of Trp and Mel at the BGCE is clearly observed (dotted line). Figure 3.17(b) demonstrates the effect that simultaneous detection of the analytes at the Nafion®-GCE had on current response and peak potential versus SWVs of the individual analytes at pH 2.5.

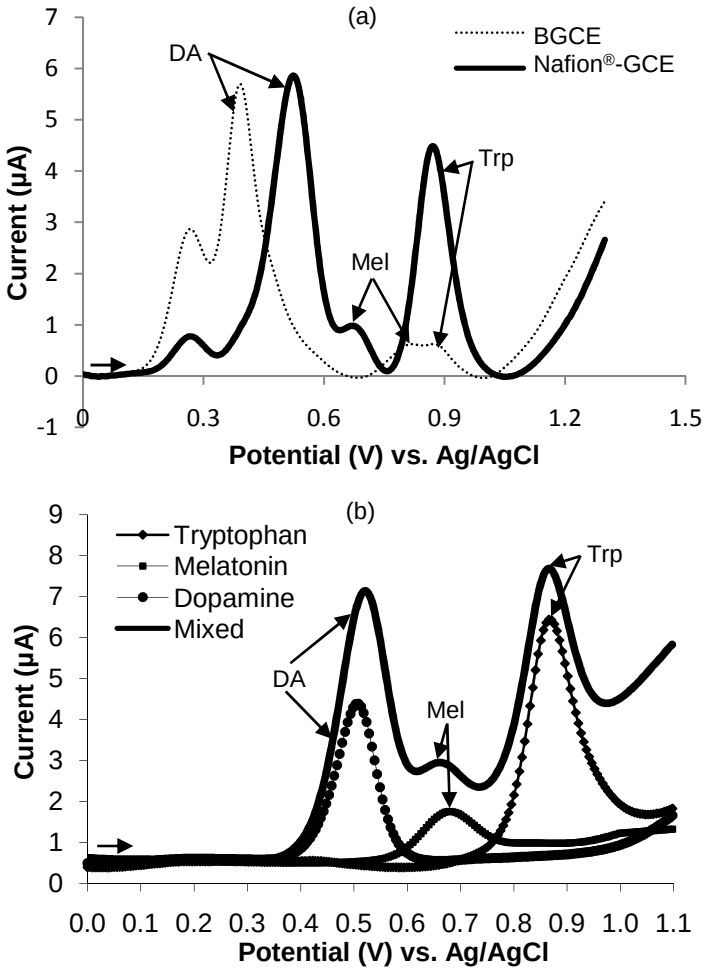

Figure 3.17: (a) SWVs of the simultaneous detection of Trp, Mel and DA at the Nafion®-GCE versus the BGCE (pH 3.0) (with baseline correction). (b) SWVs of the simultaneous detection of Trp, Mel and DA versus individual analysis at the Nafion®-GCE (pH 2.5). [Trp] = [Mel] = [DA] = 19.6 µM

Potential shifts observed for DA and Mel, and decreases in current strength compared to studies in single analyte solutions can be attributed to co-adsorption effects. Potential shifts and changes in current response for all analytes in a mixed solution were observed at the Nafion®-GCE when compared to the BGCE. Suitable separation was, therefore, achieved at pH 3.0 at the Nafion®-GCE as the current response for Mel was greatly reduced and is, thus, less of an interferent for Trp analysis.

3.4.11. Tryptophan detection in complex matrices

An example of a complex matrix is the pharmaceutical formulation Serene Tranquility™ Night with Trp. This formulation contains Trp as well as various interferents, namely Mel, which is required for the effective use of this formulation as

an evening dietary supplement. Figure 3.18 demonstrates the effects that the Nafion®-GCE has on Trp detection at (a) acidic and (b) physiological pH when in a dietary supplement or formulation.

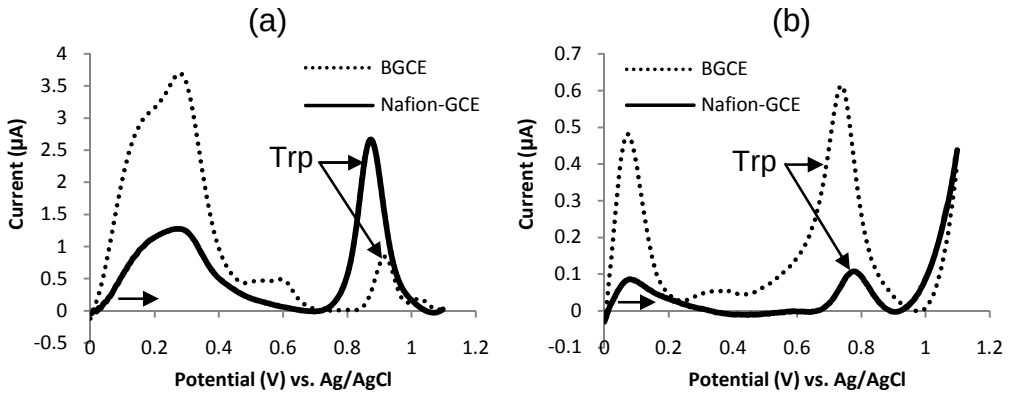

Figure 3.18: SWVs of a 2.0 mg/ml Trp-containing formulation at (a) pH 3.0 and (b) pH 7.4 using a BGCE and Nafion®-GCE (baseline correction used for better comparison of peak responses). [$Trp_{form.}$] = 3.84 µM

From Figure 3.18, it is evident that Trp was successfully detected in the pharmaceutical formulation that contains both Mel and Trp in the presence of other interferents which includes ascorbic acid, malic acid, glycine, glucose, citric acid and arginine. The effect of improved current response and enhanced peak resolution for Trp detection under acidic conditions (pH 3.0) at the Nafion®-GCE versus the BGCE is shown in Figure 3.18(a). A shift in the Trp peak potential towards a less positive potential was exhibited for the Nafion®-GCE under acidic conditions compared to the BGCE, as illustrated in Figure 3.18(a). The effect of pH on Trp detection is shown through comparison with studies at pH 7.4 (Figure 3.18b), in which a decrease in current response for Trp at the Nafion®-GCE was observed. Interference caused by the oxidisable components in the formulation, under acidic and physiological conditions, was limited due to the charge selective properties exhibited by the Nafion® layer. Therefore, the effects exhibited by Nafion® under acidic conditions demonstrated improved Trp selectivity due to lowered anodic interference and positive charge of Trp at this pH, as described previously.

Due to the analyses at pH 3.0 having the most pronounced effects on current response, pH 3.0 was used for the standard additions in the formulation. The concentration of Trp in a measured volume of the dietary supplement at pH 3.0 was

determined by standard addition to within 10.07 ±0.19 % and 1.01 ±0.13 % of the stated Trp concentration at the BGCE and Nafion®-GCE, respectively. The higher degree of accuracy in the determination of Trp at pH 3.0 at the Nafion®-GCE, compared to the BGCE, is due to the minimisation of interference from other analytes. Therefore, the concentration of Trp in the pharmaceutical formulation, which includes Mel, can be suitably determined using the Nafion®-GCE.

3.5. Conclusions

When analysed at a BGCE at pH 3.0, Trp was the dominating analyte when analysed in the presence of the interferents, Mel and DA. At a Nafion®-modified electrode at a pH of 3.0 and below, an increase in the current response for Trp was observed with favourable peak separation of the Trp and Mel oxidation peaks occurring at this pH. Therefore, Trp can be sensitively and selectively detected, in the presence of Mel, by simultaneously using a Nafion® layer on the electrode surface and manipulating the pH of the working solution to optimize detection of the Trp. This is due to protonation of the Trp molecules, and resultant positively charged species, which leads to the enhanced movement of the positive Trp species through the Nafion® layer to the GCE surface and the ensuing improved current response. Furthermore, Trp can be selectively detected in a complex matrix such as the pharmaceutical formulation used with little interference from the matrix components at pH 3.0. Moreover, the concentration of Trp in the formulation can be detected to with 9.06 % greater accuracy at the Nafion®-GCE than at the BGCE.

Chapter 4

Detection using a Nafion® and fMWCNT layer

4.1. Introduction

The selective detection of tryptophan (Trp) over melatonin (Mel) can be achieved through peak elimination, based on pH and charge, and peak potential separation, which is based on electrocatalytic effects brought on by the modified layer, namely Nafion®, as demonstrated in Chapter 3. However, scope remains for an improvement in current response for these analytes.

The interference of ascorbic acid (AA) is a common problem during the detection of dopamine (DA) and, therefore, when testing the efficacy of a GCE modification in the charge-based elimination of an interfering analyte, the detection of DA over AA provides for an excellent standard during testing of a proof of concept. Methods used to selectively detect DA over AA include modification of an electrode with Nafion®, as previously discussed in Chapter 1.3.3. and Chapter 3.1. The benefits of MWCNTs in improving detection of DA current response, as well as resolution of peak potentials, has been demonstrated (Valentini *et al.*, 2003). Analysis of Trp with MWCNTs has previously been carried out at a MWCNT paste electrode in presence and absence of cobalt salophen (Shahrokhian & Fotouhi, 2007). However, analysis of Trp at an electrode modified with carbon nanotubes and Nafion® has not been examined in literature to date. Moreover, analysis of Mel with MWCNTs, or Nafion® with MWCNTs, has not yet been examined in the literature to date.

4.2. Aim/s

The aim of this study was to:

1) Test the efficacy of fMWCNTs in enhancing analyte response at the GCE surface in the presence of a dispersing agent/polymer (Nafion®) using DA as a standard analyte; and,
2) Selectively detect Trp over Mel and DA over AA using a GCE modified with a mixture of Nafion® and fMWCNTs.

4.3. Experimental Procedure

4.3.1. Chemicals and reagents

Trp, Mel and MWCNTs were purchased and prepared as previously described in Chapter 3.3.1. and Chapter 2.3.3.1. DA and AA were purchased from Sigma Aldrich, South Africa, and prepared in Milli-Q water to a concentration of 1.0 mM and 10.0 mM, respectively. A 0.5 % (w/v) solution of Nafion® (Sigma) was prepared as previously described (Chapter 3.2.2.). A Nafion®/fMWCNT solution was prepared by adding 1.3 mg fMWCNTs to 1.0 ml of a 0.5 % (w/v) solution of Nafion®. The electrolyte solutions used were 0.04 M Britton-Robinson buffer, pH 3 (Britton, 1955), and 0.2 M potassium phosphate buffer, pH 7.4. The pH measurements were conducted on a WTW pH 330i pH meter, coupled to a Sentix 41 pH electrode.

4.3.2. Functionalisation of MWCNTs

The MWCNTs were functionalised as described in Chapter 2.3.3.1.

4.3.3. Preparation of electrodes

The GCE was modified by carefully applying 10µl of the Nafion®/fMWCNT mixture to the GCE surface and allowing the applied mixture to dry under ambient temperatures with laminar air flow for approximately 5 mins.

4.3.4. Electrochemical apparatus and electrode pretreatment

Set up and cleaning of the electrochemical cell and electrode pretreatment was carried out as described in Chapter 2.3. A 5 ml working electrolyte solution of 0.2 M potassium phosphate buffer (Merck), pH 7.4, was used. The cyclic voltammetry (CV) scans were conducted from a start potential (V) ranging from -0.1 V to an end potential of 1.1 V, with a step potential of 1.8 mV and a scan rate of 50 mV/s, unless otherwise stipulated.

4.3.5. Analyte characterisation and electrode kinetics

4.3.5.1. Passivation

Fouling, or passivation, analyses were conducted as outlined in Chapter 3.3.4.2.

4.3.5.2. Mode of transport

Diffusion characteristics were assessed as previously described (Chapter 3.3.4.3.).

4.3.5.3. LOD and LOQ

The LOD and LOQ were calculated as described in Chapter 2.3.2.5.

4.3.6. Statistics

All studies were conducted in triplicate. Results are presented as the mean ±standard deviation.

4.4. Results and Discussion

4.4.1. Dopamine analysis at the Nafion®/fMWCNT-GCE

Figure 4.1 demonstrates the effects that various GCE surface modifications have on DA detection at physiological pH.

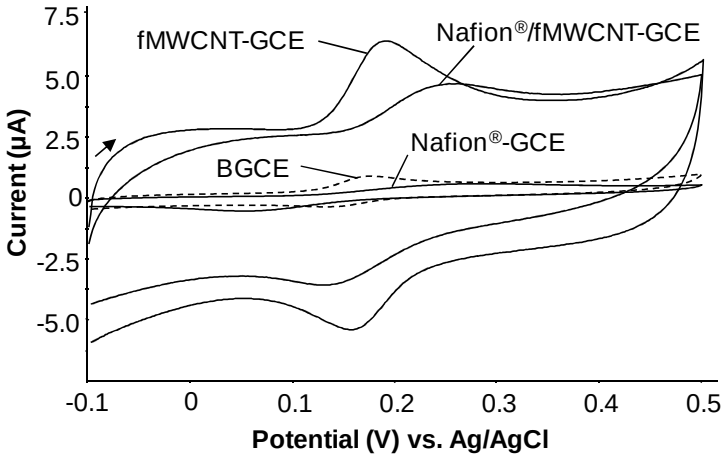

Figure 4.1: CVs of DA at the BGCE, Nafion®-GCE, fMWCNT-GCE and Nafion®/fMWCNT-GCE at pH 7.4. [DA] = 19.6 µM; Scan rate = 50 mV/s.

Table 4.1 shows the peak potentials and current responses for DA at the BGCE, Nafion®-GCE, fMWCNT-GCE and Nafion®/fMWCNT-GCE.

Table 4.1: Anodic current responses and peak potentials (vs. Ag/AgCl) for DA at the BGCE, Nafion®-GCE, fMWCNT-GCE and Nafion®/fMWCNT-GCE using CV analysis with the respective shifts in current and potential versus the BGCE

Modification	Current (µA)	Current shift (vs. BGCE)	Potential (V)	Potential shift (vs. BGCE)
BGCE	0.49 (±0.073)	-	0.17 (±0.001)	-
Nafion®-GCE	0.29 (±0.022)	-0.20	0.26 (±0.003)	+0.09
fMWCNT-GCE	2.80 (±0.101)	+2.31	0.19 (±0.005)	+0.02
Nafion®/fMWCNT-GCE	1.29 (±0.066)	+0.80	0.24 (±0.001)	+0.07

The Nafion®-modified GCE exhibited a current response that was lower than that of the BGCE. This reduction in the current response may be attributed to the slow diffusion of DA towards the GCE surface and the insulating effects on the GCE exhibited by the Nafion® polymer, as observed in impedance spectroscopy analysis of this layer (Chapter 3.4.6. and Hu *et al*., 2006). An increase in current response for DA was observed at the fMWCNT-GCE over that of the BGCE. This may be attributed to the electron transport enhancing effects exhibited by the fMWCNTs (Britto *et al*., 1996; Luo *et al.*, 2001; Zhang *et al*., 2005). Furthermore, this increase may be attributed to electrostatic attractive forces between the charged carboxyl groups on the CNTs and cationic DA.

A decrease in current response was observed for DA at the Nafion®/fMWCNT-GCE compared to the response at the fMWCNT-GCE (Figure 4.1) due to the previously mentioned effects exhibited by the Nafion® layer on DA detection. A potential shift towards a more positive potential was observed in the presence of Nafion® and fMWCNTs demonstrating increased difficulty of DA oxidation. However, the increase in DA current response and shift towards a more positive potential occurring at the Nafion®/fMWCNT-GCE over the BGCE and Nafion®-GCE were similar to the findings of Wang and co-workers (2006).

The large difference in the baselines for the forward and reverse scans (capacitance) for the fMWCNT-modified GCEs in Figure 4.1 is attributed to the catalytically active surface or number of functional carboxyl groups on the surface of the MWCNTs and, thus, how well the fMWCNTs are functionalised (Britto *et al*., 1996).

4.4.1.1. Dopamine passivation

Figure 4.2 demonstrates the effects of passivation seen as electrode fouling, as outlined in Chapter 3.4.3.2., for DA at the Nafion®/fMWCNT-GCE, compared to fouling studies at the BGCE and fMWCNT-GCE.

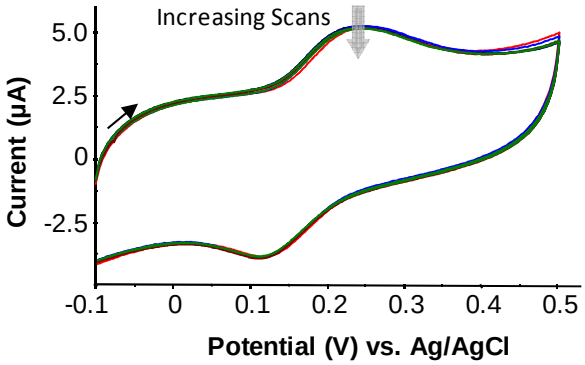

Figure 4.2: CVs of DA fouling at the Nafion®/fMWCNT-GCE surface (pH 7.4). [DA] = 19.6 µM; Scan rate = 50 mV/s

The Nafion®/fMWCNT-GCE exhibited an electrode passivation, or change in current response, of less than 15.0 ±1.8 % as observed in the plot of current response passivation (calculated as a percentage of the initial response) versus the number of scans (Figure 4.3). A similar response was observed at the fMWCNT-GCE after six consecutive scans.

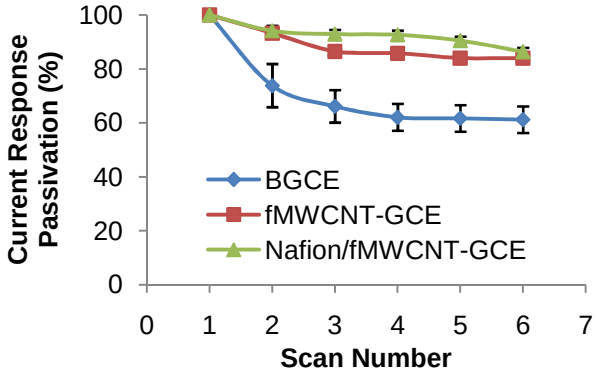

Figure 4.3: DA fouling at the BGCE, fMWCNT-GCE and Nafion®/fMWCNT-GCE (pH 7.4). [DA] = 19.6 µM

The Nafion®/fMWCNT-GCE exhibited a lower degree of fouling for DA than that observed at the BGCE (48.9 ±4.8 %) when contrasted to the fouling of 73.5 ±3.2 % observed at a Nafion®-GCE for Trp (Chapter 3.4.3.2.). This demonstrates that upon the addition of fMWCNT to the GCE surface, an increase in stability is observed and

passivation, experienced with the Nafion® layer, is greatly diminished. This is due to the ability of the fMWCNTs to resist passivation (Merkoçi *et al.*, 2005; Valentini *et al.*, 2005) and can be attributed to the physical/chemical properties exhibited by the fMWCNTs in the Nafion®/fMWCNT-GCE (Wang *et al.*, 2003). The fMWCNTs would, theoretically, form a mechanical barrier that would allow the transfer of electrons without the direct interaction between the GCE surface and analyte, thus preventing fouling of the electrode by DA.

4.4.1.2. Mode of transport for dopamine

Diffusion characteristics of DA were studied at the Nafion®/fMWCNT-GCE and an increase in the current response was observed upon an increase in the scan rate of the CV analyses (Figure 4.4 and Figure 4.5).

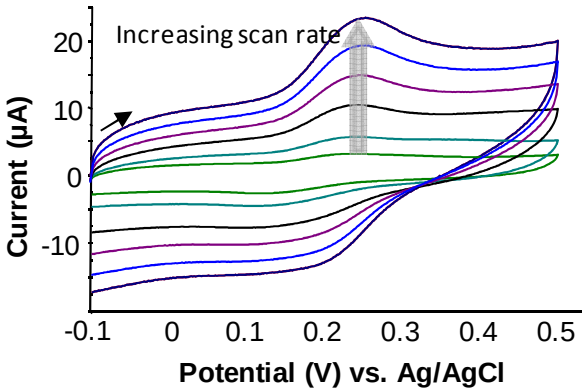

Figure 4.4: CVs of DA at the Nafion®/fMWCNT-GCE with various scan rates (pH 7.4). [DA] = 19.6 µM; Scan rates = 50, 100, 200, 300, 400 & 500 mV/s.

Figure 4.5 demonstrates the two linear trends observed for the increase in the square root of the scan rate versus the DA current response.

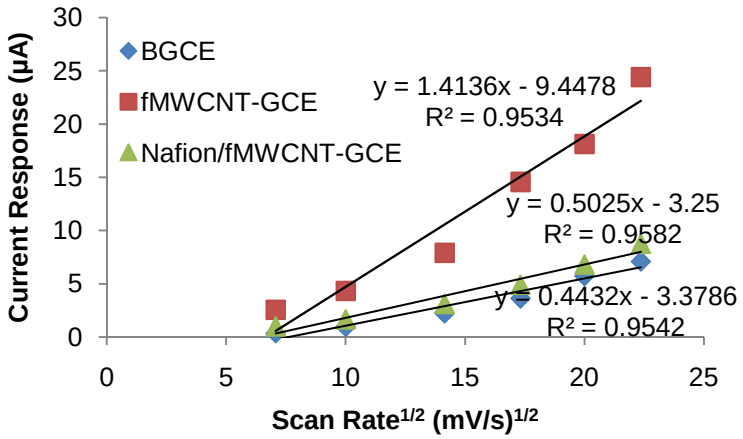

Figure 4.5: Effect of the square root of the scan rate on the current response of DA at the Nafion®/fMWCNT-GCE (pH 7.4). [DA] = 19.6 µM

The linear trend reveals that DA oxidation at the Nafion®/fMWCNT-GCE (R^2 = 0.954) occurs through a diffusion controlled process (Nicholson & Shain, 1965). The positive slope is indicative of an increase in the concentration of oxidised DA at the GCE surface with an increase in scan rate (Wopschall & Shain, 1967). At higher scan rates, minimal depletion of the adjacent solution at the GCE surface occurs due to the influence of the concentration of oxidised DA (Heineman & Kissinger, 1994). Higher current responses are also observed at the higher scan rates as the anodic peak response is dependent on the succeeding chemical reaction given by the cathodic peak (Wopschall & Shain, 1967). This is confirmed in Figure 4.4 as at higher scan rates the response for the anodic peak does not equal that of the cathodic peak. Therefore, kinetic limitations may occur at higher scan rates during DA analysis at the Nafion®/fMWCNT-GCE.

4.4.2. Electrocatalytic oxidation of ascorbic acid

A CV illustrating the electrochemical analysis of AA at the BGCE is shown in Figure 4.6.

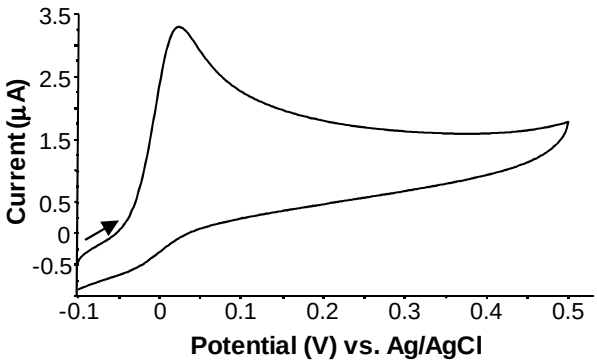

Figure 4.6: CV showing the irreversible oxidation of AA at a BGCE (pH 7.4). [AA] = 150 µM; Scan rate = 50 mV/s

Electroanalysis of AA oxidation at the BGCE, illustrated in Figure 4.6, exhibited an irreversible anodic peak at 0.015 ±0.02 V. AA oxidation involves a two-electron, one proton process that forms dehydroascorbic acid (Deakin *et al*., 1986; Hu & Kuwana, 1986). The irreversible oxidation of AA arises from the second oxidation step which involves one electron (1 e^-), as described by Hu and Kuwana (1986). The non-uniform peak shape for the AA anodic peak indicates that there is a slower diffusion of oxidised products away from the GCE surface compared to DA (Chapter 5.2.1). The LOD and LOQ for AA at the BGCE were 0.220 and 0.667 µM, respectively.

4.4.3. Ascorbic acid analysis at the Nafion®/fMWCNT-GCE

A comparison of AA analysis with the various GCE surface modifications can be seen in Figure 4.7.

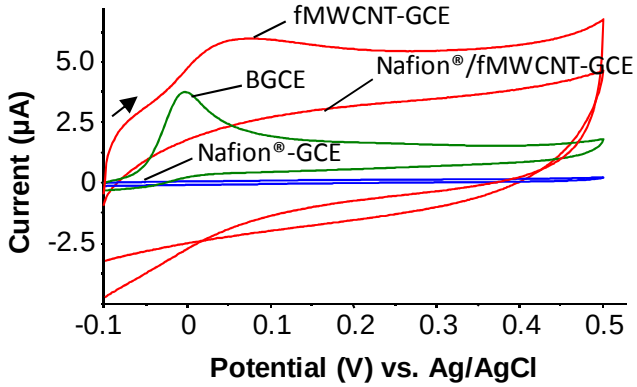

Figure 4.7: CVs of AA at the BGCE, Nafion®-GCE, fMWCNT-GCE and Nafion®/fMWCNT-GCE at pH 7.4. [AA] = 150 µM; Scan rate = 50 mV/s.

Table 4.2 shows the peak potentials and current responses for AA (150 µM) at the BGCE, Nafion®-GCE, fMWCNT-GCE and Nafion®/fMWCNT-GCE.

Table 4.2 Anodic current responses and peak potentials (vs. Ag/AgCl) for AA at the BGCE, Nafion®-GCE, fMWCNT-GCE and Nafion®/fMWCNT-GCE using CV analysis with the percent AA exclusion and shifts in potential

Modification	Current (µA)	AA Exclusion vs. BGCE (%)	Potential (V)	Potential shift (vs. BGCE)
BGCE	3.34 (±0.033)	0	0.00 (±0.013)	-
Nafion®-GCE	0.01 (±0.033)	99.70	0.17 (±0.020)	+ 0.17
fMWCNT-GCE	1.92 (±0.142)	42.52	0.04 (±0.010)	+ 0.04
Nafion®/fMWCNT-GCE	-	100.00	-	N/A

The Nafion®-GCE, fMWCNT-GCE and Nafion®-fMWCNT-GCE resulted in a decrease in the current response for AA when compared to the anodic current response observed at the BGCE. A shift towards a more positive potential and broadening of the AA oxidation peaks occurred at the modified layers when compared to the peak obtained at the BGCE. This can be attributed to a decrease in the ease of oxidation and slower electron transfer kinetics experienced with the modified layers compared to the BGCE as the negatively charged layers would hinder the movement of anionic AA at the GCE surface. Therefore, an increase in the concentration of negatively charged groups at the GCE surface should theoretically result in complete hindrance of analyte movement towards the GCE surface, as shown at the Nafion®-fMWCNT-GCE (Figure 4.7).The results obtained for AA at the Nafion®/fMWCNT-modified GCE compare favourably with those obtained by Wang and co-workers (2003) and Rivas and co-workers (2007) at the same electrode at which 100.0 % exclusion of AA was reported.

Figure 4.8 further illustrates the differences in the CV current response in the presence and absence of AA at (a) Nafion®/fMWCNT-GCE and (b) Nafion®-GCE.

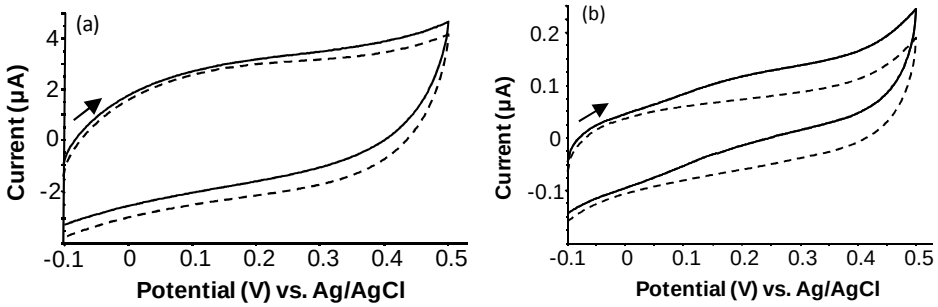

Figure 4.8: CVs of AA (solid) versus the buffer (dashed) at (a) Nafion®/fMWCNT-GCE and (b) Nafion®-GCE (pH 7.4). [AA] = 150.0 µM; Scan rate = 50 mV/s.

As observed in Figure 4.8(a), AA (150.0 µM) was excluded at the Nafion®/fMWCNT-GCE at pH 7.4 with only a minor shift in the CV baseline being observed upon the inclusion of AA. The AA response was also greatly reduced when analysed with the Nafion®-GCE (Figure 4.8b); however, a more visible baseline shift (+0.17 ±0.020 V versus BGCE) was observed compared to studies at the Nafion®/fMWCNT-GCE.

4.4.3.1. Influence of scan rate on ascorbic acid detection

In order to determine the effects of scan rate on AA detection, AA was analysed using increasing scan rates at the Nafion®/fMWCNT-GCE (Figure 4.9).

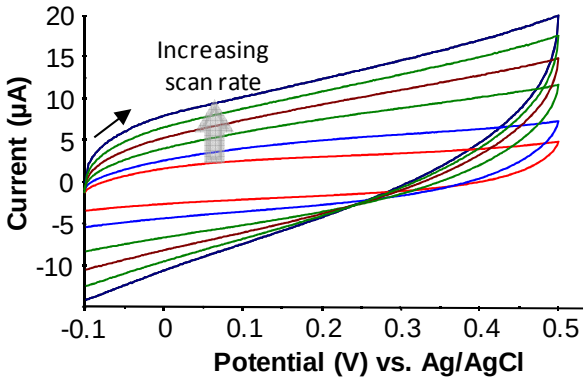

Figure 4.9: CVs of AA at the Nafion®/fMWCNT-GCE with various scan rates (pH 7.4). [AA] = 150 µM; Scan rates = 50, 100, 200, 300, 400 & 500 mV/s.

However, the AA oxidation peak remained absent when analysed up to a scan rate of 500 mV/s. This demonstrates that increased scan rates had no effect on AA detection.

4.4.4. Detection of tryptophan at a Nafion®/fMWCNT-GCE

Upon analysis of tryptophan (Trp) with the Nafion®/fMWCNT-GCE, an increase in the current response was observed above that observed at the Nafion®-GCE and BGCE (Figure 4.10). The Trp current response at the fMWCNT-GCE (3.24 µA) was excluded as the peak current responses observed at the Nafion®-modified and bare GCEs would be misrepresented.

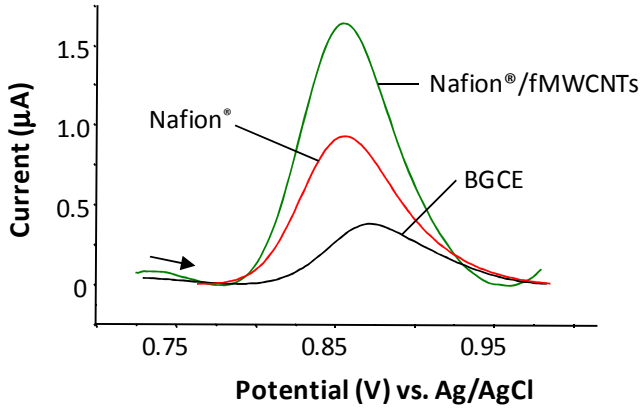

Figure 4.10: Anodic oxidation peaks obtained for Trp during CV analysis at the BGCE, Nafion®-GCE and Nafion®/fMWCNT-GCE in BR buffer, pH 3.0. Only the baseline-corrected forward scans are shown. The arrow indicates the direction of the CV scan. [Trp] = 19.6 µM; Scan rate = 50 mV/s.

The observed increase in the Trp current response at the Nafion®/fMWCNT-GCE can be attributed to properties exhibited by the fMWCNTs on Trp at pH 3.0 (Figure 4.10), as observed for studies with DA. The Nafion®/fMWCNT-GCE exhibited no change in potential compared to the Nafion®-GCE demonstrating that addition of fMWCNTs did not affect electrode kinetics. However, when compared to the BGCE, the shift of -0.02 V (vs. Ag/AgCl) for the Trp anodic peak potential at the Nafion®/fMWCNT-GCE and Nafion®-GCE demonstrated minimal increases in the ease of oxidation. The shift observed for Nafion®/fMWCNT-GCE is due to an increase in the ease of electron flow through the polymer and, in particular, along the CNTs. The ease of electron flow may be attributed to the dispersion of the fMWCNTs in the polymer layer (Su *et al*., 2006) as there would be little to no impairment in the mechanical and electrocatalytic properties of the CNTs in the Nafion®/fMWCNT suspension (Wang *et al.*, 2003). This effectively demonstrates the enhancing effects that an increased surface area, offered by the fMWCNTs, would have towards the current response of an analyte.

It must be noted that the observed current responses for the BGCE and Nafion®-GCE are lower than those previously reported in Chapter 3 due to the use of a different electrochemical waveform: cyclic voltammetry. CV yields lower current responses compared to SWV (Kounaves, 1997).

Upon Trp analysis at pH 7.4 with the Nafion®/fMWCNT-GCE, an increase in the current response was also observed above that of the Nafion®-GCE and BGCE, with a significant lowering of the potential to 0.68 ±0.003 V (vs. Ag/AgCl) indicating an increase in the ease of oxidation of Trp at this layer (Figure 4.11).

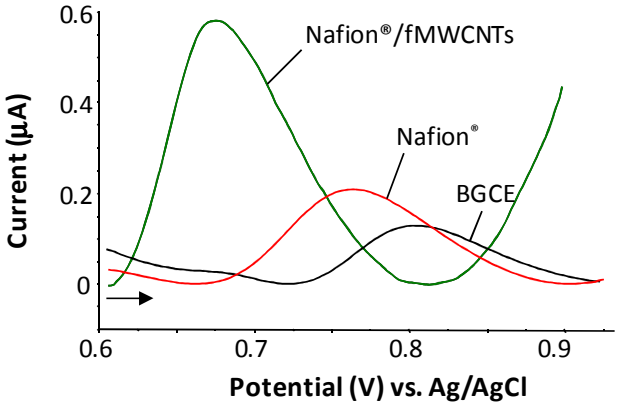

Figure 4.11: Anodic oxidation peaks obtained for Trp during CV analysis at the BGCE, Nafion®-GCE and Nafion®/fMWCNT-GCE in phosphate buffer, pH 7.4. Only the baseline-corrected forward scans are shown. [Trp] = 19.6 µM; Scan rate = 50 mV/s.

Table 4.3 summarises the current response values and peak potentials that were obtained for Trp at the BGCE, Nafion®-GCE, fMWCNT-GCE and Nafion®/fMWCNT-GCE at pH 3.0 and 7.4. At all surfaces, the highest current response was observed at pH 3.0.

Table 4.3: Anodic current responses and peak potentials (vs. Ag/AgCl) for CV analyses of Trp at the BGCE, Nafion®-GCE, fMWCNT-GCE and Nafion®/fMWCNT-GCE at pH 3.0 and 7.4

Modification	pH 3.0		pH 7.4	
	Current (µA)	Potential (V)	Current (µA)	Potential (V)
BGCE	0.40 (±0.131)	0.88 (±0.001)	0.17 (±0.060)	0.80 (±0.002)
Nafion®-GCE	0.94 (±0.104)	0.86 (±0.006)	0.21 (±0.052)	0.76 (±0.005)
fMWCNT-GCE	2.65 (±0.164)	0.86 (±0.010)	1.46 (±0.108)	0.68 (±0.009)
Nafion®/fMWCNT-GCE	1.84 (±0.197)	0.86 (±0.002)	0.60 (±0.081)	0.67 (±0.003)

The Trp current response at the Nafion®/fMWCNT-GCE was greater than that at the BGCE and Nafion®-GCE at pH 3.0 (Figure 4.10) and pH 7.4 (Figure 4.11) due to the conducting properties of the fMWCNTs. The Trp current response at the Nafion®/fMWCNT-GCE at pH 3.0 was 1.24 µA greater than that observed at pH 7.4. Briefly, this is due to the charge interactions between the Nafion® polymer and the positively charged Trp species that dominate in the solutions at a more acidic pH (3.0). Furthermore, at pH 3.0 the predominating negatively charged fMWCNTs have a tendency to attract the positive charges present at the protonated amine group on the Trp molecule; thereby, enhancing the current. Therefore, the functional effectiveness of the fMWCNTs is affected by the pH and resultant charge on the nanotube and analyte. Furthermore, the current response observed for Trp at pH 3.0 at the fMWCNT-modified GCEs can be further attributed to an increased surface area at the GCE surface due to the presence of fMWCNTs (Peigney *et al.*, 2001).

4.4.5. Detection of melatonin at a Nafion®/fMWCNT-GCE

The anodic oxidation peaks for Mel at the BGCE, Nafion®-GCE and Nafion®/fMWCNT-GCE at pH 3.0 (Figure 4.12) and 7.4 (Figure 4.13) are illustrated.

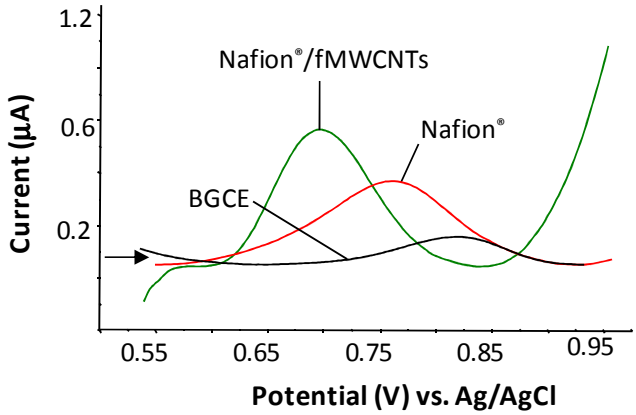

Figure 4.12: Anodic oxidation peaks for Mel during CV analysis at the BGCE, Nafion®-GCE and Nafion®/fMWCNT-GCE in BR buffer, pH 3.0. Only the baseline-corrected forward scans are shown. [Mel] = 19.6 µM; Scan rate = 50 mV/s.

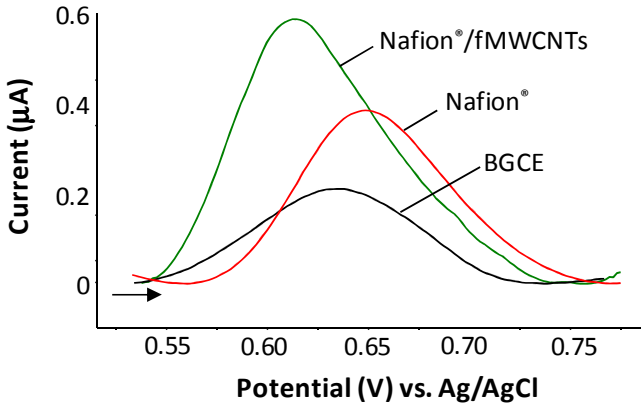

Figure 4.13: Anodic oxidation peaks for Mel during CV analysis at the BGCE, Nafion®-GCE and Nafion®/fMWCNT-GCE in phosphate buffer, pH 7.4. Only the baseline-corrected forward scans are shown. [Mel] = 19.6 µM; Scan rate = 50 mV/s.

Table 4.4 summarises the current response values and peak potentials that were obtained for Mel at the BGCE, Nafion®-GCE and Nafion®/fMWCNT-GCE at pH 3.0 and 7.4.

Table 4.4: Anodic current responses and peak potentials (vs. Ag/AgCl) from CV analyses for Mel at pH 3.0 and 7.4

Modification	pH 3.0		pH 7.4	
	Current (µA)	Potential (V)	Current (µA)	Potential (V)
BGCE	0.18 (±0.026)	0.82 (±0.003)	0.21 (±0.020)	0.63 (±0.001)
Nafion®-GCE	0.42 (±0.072)	0.76 (±0.005)	0.38 (±0.045)	0.65 (±0.002)
Nafion®/fMWCNT-GCE	0.65 (±0.052)	0.69 (±0.002)	0.58 (±0.032)	0.62 (±0.002)

Increases in current responses were observed at the Nafion®/fMWCNT-GCE over the BGCE and Nafion®-GCE at pH 3 and pH 7.4, as observed for Trp in Chapter 4.4.4. Shifts towards less positive potentials were observed at the Nafion®/fMWCNT-GCE at pH 3.0 and 7.4 when compared to the peak potential obtained with the Nafion®-GCE (Figure 4.12; Figure 4.13 and Table 4.4). This demonstrates that an increase in the ease of oxidation occurred when fMWCNTs were incorporated into the Nafion® layer. fMWCNTs allow for easier analyte oxidation due to improved electron transport along the numerous CNT walls present in the MWCNT structure. Interestingly, a shift of +0.02 V (vs. Ag/AgCl) was observed at the Nafion®-GCE compared to the BGCE demonstrating that at the Nafion®-modified GCE at pH 7.4,

Mel oxidation increases in difficulty due to effects exerted by the Nafion® polymer on Mel.

4.4.6. Tryptophan and melatonin peak potential comparisons

Separation of the Trp and Mel peaks was obtained when analysed at pH 3.0 at the Nafion®/fMWCNT-GCE, as illustrated in Figure 4.14. This separation is achieved through an increased difference between the peak potentials for Trp and Mel, similarly to that achieved with the Nafion®-GCE (Chapter 3).

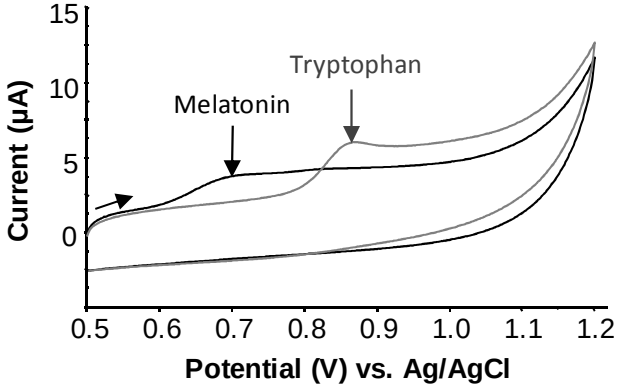

Figure 4.14: CVs of Trp (grey) and Mel (black) at the Nafion®/fMWCNT-GCE at pH 3.0. [Trp] = 19.6 µM; [Mel] = 19.6 µM; Scan rate = 50 mV/s.

Alternatively, at pH 7.4, no clear separation was achieved between the Trp and Mel anodic peak potentials with the Nafion®/fMWCNT-GCE, as illustrated in Figure 4.15. Subsequent to the isolation and correction of the baseline (Figure 4.15 Insert), no clear separation of the peaks was observed as the peak potentials exhibited a difference of 0.06 V.

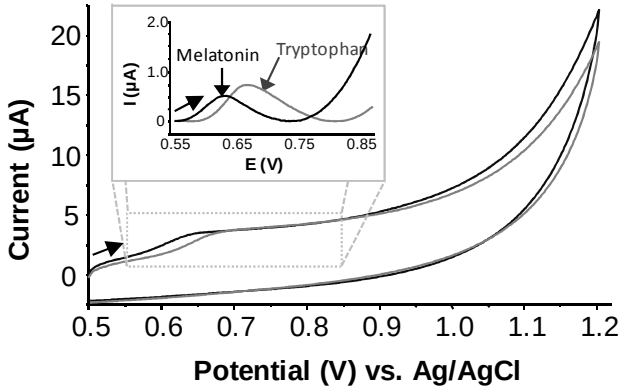

Figure 4.15: CVs of Trp and Mel at pH 7.4 at the Nafion®/fMWCNT-GCE. Insert: The anodic peaks for Trp and Mel (only forward scans are shown). [Trp] = 19.6 µM; [Mel] = 19.6 µM; Scan rate = 50 mV/s.

Table 4.5 shows the peak potentials that were obtained for Trp and Mel at the BGCE, Nafion®-GCE and Nafion®/fMWCNT-GCE at pH 3.0 and 7.4 during CV analyses.

Table 4.5: The anodic peak potentials (V) for Trp and Mel at pH 3.0 and pH 7.4 during CV analyses at the BGCE, Nafion®-GCE and Nafion®/fMWCNT-GCE with the values in brackets indicative of any change versus the BGCE.

	pH 3.0		pH 7.4	
Modification	Trp (V)	Mel (V)	Trp (V)	Mel (V)
BGCE	0.88	0.82	0.80	0.63
Nafion®-GCE	0.86 (-0.02)	0.76 (-0.06)	0.76 (-0.04)	0.65 (+0.02)
Nafion®/fMWCNT-GCE	0.86 (-0.02)	0.69 (-0.13)	0.68 (-0.12)	0.62 (-0.01)

Similarly to the findings reported in Chapter 3.4.9., further separation between the Trp and Mel oxidation peaks was observed at pH 3.0 compared to pH 7.4, as outlined in Table 4.5. Upon examination of the values for the peak potentials, a step-wise increase in the separation of the Trp and Mel oxidation peaks was achieved at pH 3.0 at the Nafion®-GCE and Nafion®/fMWCNT-GCE with the greatest separation occurring at the Nafion®/fMWCNT-GCE. It must be noted, however, that further separation in the anodic peak potentials was achieved during SWV analysis at the Nafion®-GCE; therefore, the same may apply, in theory, at the Nafion®/fMWCNT-GCE.

Therefore, analysis with the Nafion®/fMWCNT-GCE at pH 3.0 resulted in optimal separation between the Trp and Mel oxidation peaks in order for the sensitive and selective detection of Trp to occur.

4.5. Conclusions

Inclusion of fMWCNTs to the Nafion®-modified GCE resulted in improved sensitivity of the modified GCE towards DA, Trp and Mel; and, improved stability towards these analytes after a set number of consecutive scans. Increased sensitivity was achieved through utilisation of the electrical conduction properties exhibited by the CNTs at neutral pH or on molecules with a net neutral charge. Stability, assessed through GCE passivation, was enhanced due to the physico-chemical properties of fMWCNTs and their ability to resist passivation due to their semiconducting

properties (Merkoçi *et al.*, 2005). DA exhibited favourable charge interaction with the Nafion®/fMWCNT layer and was suitably detected.

AA interference during DA detection was suitably eliminated upon addition of fMWCNTs to the Nafion®-GCE at physiological pH due to unfavourable charge interactions between the anionic AA molecules, anionic sulphonate groups of Nafion® and ionised carboxyl groups of the fMWCNTs; and, a change in the electrode kinetics.

The fMWCNT properties exhibited towards Trp and Mel oxidation resulted in shifts in the peak potentials similar to those exhibited at the Nafion®-GCE (Chapter 3). The shift in potential, for Mel in particular, facilitated the separation of the Trp and Mel oxidation peaks, thus facilitating the selective detection of Trp over Mel at pH 3.0 through peak resolution.

Therefore, fMWCNTs used in conjunction with Nafion® in a Nafion®/fMWCNT composite sensor can be used to enhance detection when selectively detecting an analyte. Therefore, fMWCNTs may offer advantages in detection of an analyte, which may be applied to both sensitivity and selectivity.

Chapter 5

The voltammetric analysis and detection of dopamine, tryptophan and melatonin using a CoTSPc/fMWCNT nanocomposite layer

5.1. Introduction

The catalytic properties of metallophthalocyanines (MPcs) make them highly attractive as electrode modifiers in sensor development. Indeed, enhancements in sensitivity have been offered by MPcs for dopamine (DA; Kang *et al.*, 1997). However, minimal work has been conducted on the electrochemical detection of tryptophan (Trp) or melatonin (Mel) with electrodes modified with MPcs. Recently, hybrid sensors combining the catalytic properties of MPcs with the benefits offered by nanostructured materials, such as nanoparticles (Wang *et al.*, 2006a) and carbon nanotubes (Ozoemena *et al*., 2006), have shown promise. Limited detection of DA has previously (Oni & Nyokong, 2001) been achieved with CoPc, FePc, ZnPc and the tetrasulphonated derivatives (TSPc) of each at a carbon paste electrode. However, no such hybrid sensor has been examined in which MTSPcs are coupled to carbon nanotubes at a GCE for detection of DA, ascorbic acid (AA), Trp and Mel.

Tetrasulphonated MPcs (MTSPcs) are highly soluble in aqueous solutions (Zecevic *et al*., 1985), which makes the MTSPc-modification of carbon electrodes highly troublesome. Previous methods of MTSPc-modification of carbon electrodes include mechanical entrapment using graphite powder used in carbon paste electrodes (Oni & Nyokong, 2001); adsorption (Griveau *et al*., 2003); entrapment using lysine films at a GCE (Luz *et al*., 2006); electropolymerisation (Yilmaz *et al*., 2007); and, multi-layered covalent attachments (Li *et al*., 2003).

The use of carbon nanotubes (CNTs) in MTSPc immobilisation was previously carried out for cobalt phthalocyanine on MWCNTs on a pyrolytic graphite electrode (Siswana *et al*., 2006); and, cobalt phthalocyanine and nickel tetrasulphonated phthalocyanine on single-walled CNTs on a GCE (Francisco Silva *et al.*, 2007). Bonding of CoTSPc (Figure 5.1) to the fMWCNTs is believed to have occurred through hybridisation through π-π interactions of the phthalocyanine complex and the walls of the fMWCNTs (Schulte *et al*., 2008).

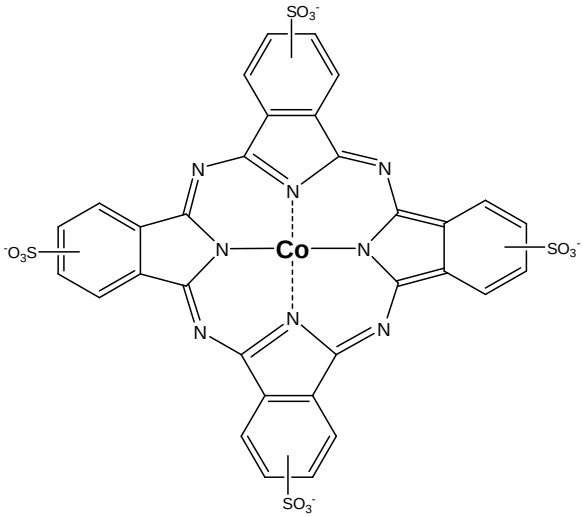

Figure 5.1: The chemical structure of CoTSPc.

Studies in Chapter 3 and 4 also show that fMWCNTs not only enhance the current response but also offer signal separation through lowering of the anodic peak potentials, as observed for fMWCNTs alone for DA, AA, Trp and Mel. These studies, thus, aim to examine a combination of cobalt TSPcs and fMWCNTs for enhanced detection of DA, AA, Trp and Mel as well as peak potential separation. This chapter first examines DA, Trp and Mel, while Chapter 6 focuses on AA exclusion.

5.2. Aim

The aim of this study was to examine the effects that a CoTSPc and fMWCNT hydrid sensor would have on DA, Trp and Mel detection. The specific aims included:

1) Identification of a co-ordinating metal and substituted MPc suitable for DA detection;
2) Determination of the effect that incorporated fMWCNTs would have on:
    i. DA detection; and,
    ii. MPc stability at the GCE surface; and,
3) Assessment of the characteristics for DA detection at the hybrid sensor, with focus on the:
    i. Establishment of linear concentration ranges;
    ii. Effects of electrode passivation;
    iii. Determination of diffusion characteristics; and,

iv. Determination of LODs and LOQs.

4) Determination of the effect that the optimised MTSPc/fMWCNT-GCE has on Trp and Mel detection at a previously determined optimal pH value (pH 3.0) and physiological pH (pH 7.4).

5.3. Experimental procedure

5.3.1. Chemicals and reagents

DA, Trp and Mel (Sigma) was prepared as previously mentioned (Chapter 3.3.1. and 4.2.1.). The metallophthalocyanines (MPcs) were supplied by Sigma Aldrich (South Africa) with CoTSPc kindly provided by Prof. T. Nyokong (Rhodes University, South Africa). The MPcs used included cobalt Pc, cobalt tetrasulphonated Pc and copper tetrasulphonated Pc, designated CoPc, CoTSPc and CuTSPc, respectively. The MPcs and MTSPcs were suspended in distilled dimethylformamide (dDMF). The electrolyte solution used was 0.2 M potassium phosphate buffer, pH 7.4. The pH measurements were conducted on a WTW pH 330i pH meter, coupled to a Sentix 41 pH electrode.

5.3.2. Functionalisation of MWCNTs

The MWCNTs were functionalised as described in Chapter 2.3.3.1.

5.3.3. Preparation of metallophthalocyanines (MPc) suspensions

The MPc suspensions were prepared similarly to that in Francisco Silva *et al.* (2007). The following were prepared or suspended in dDMF: fMWCNTs; CoTSPc; CoPc; CoTSPc + fMWCNTs; CoPc + fMWCNTs; and, CuTSPc + fMWCNTs. The final concentrations of the MPcs and fMWCNTs were 3.8 mM (±0.4 mg/ml) and 1.3 mg/ml, respectively. The fMWCNT and MPc mixtures were sonicated for 30 min in order to suspend the composites and separate any aggregated molecules. These mixtures were sonicated for 2.0 min in order to resuspend the settled fMWCNTs prior to GCE modification.

5.3.4. Preparation of electrodes

The GCE was modified by carefully applying 10.0 μl of the fMWCNT and MPc mixtures to the GCE surface and allowing the applied mixture to dry under ambient

temperatures with laminar air flow for approximately 1.5 hours.

5.3.5. Electrochemical apparatus and electrode pretreatment

The electrochemical cell and pretreatment was carried out as described in Chapter 2.3.2. A 5.0 ml working solution of 0.2 M potassium phosphate buffer (Merck), pH 7.4, was used. The cyclic voltammetry (CV) scans were conducted from a start potential (V) of -0.1 V to an end potential of 0.5 V, with a step potential of 1.8 mV and a scan rate of 50 mV/s, unless otherwise stipulated. The squarewave voltammetry (SWV) scans were conducted in the same potential range as for CV; however, the step potential was 4 mV, amplitude was 25 mV and frequency was 15.0 Hz.

5.3.6. Analyte characterisation and electrode kinetics

5.3.6.1. Linearity

Standard curves of concentration versus current were produced as previously outlined in Chapter 3.3.4.1.

5.3.6.2. Passivation

Fouling, or passivation, analysis was carried out as previously described in Chapter 3.3.4.2.

5.3.6.3. Mode of transport

Diffusion characteristics were determined as described in Chapter 3.3.4.3.

5.3.6.4. LOD and LOQ

The LOD and LOQ were calculated as described in Chapter 2.3.2.5.

5.3.7. Statistics

All studies were conducted in triplicate. Results are presented as the mean ±standard deviation.

5.4. Results and Discussion

5.4.1. Dopamine detection with MPc/fMWCNTs hybrid layers

Figure 5.2 shows representative CV illustrating increases in current response over a BGCE at surface modified with fMWCNTs (a) and composites of CoTSPc (b), CuTSPc (c) and CoPc (d) with fMWCNTs.

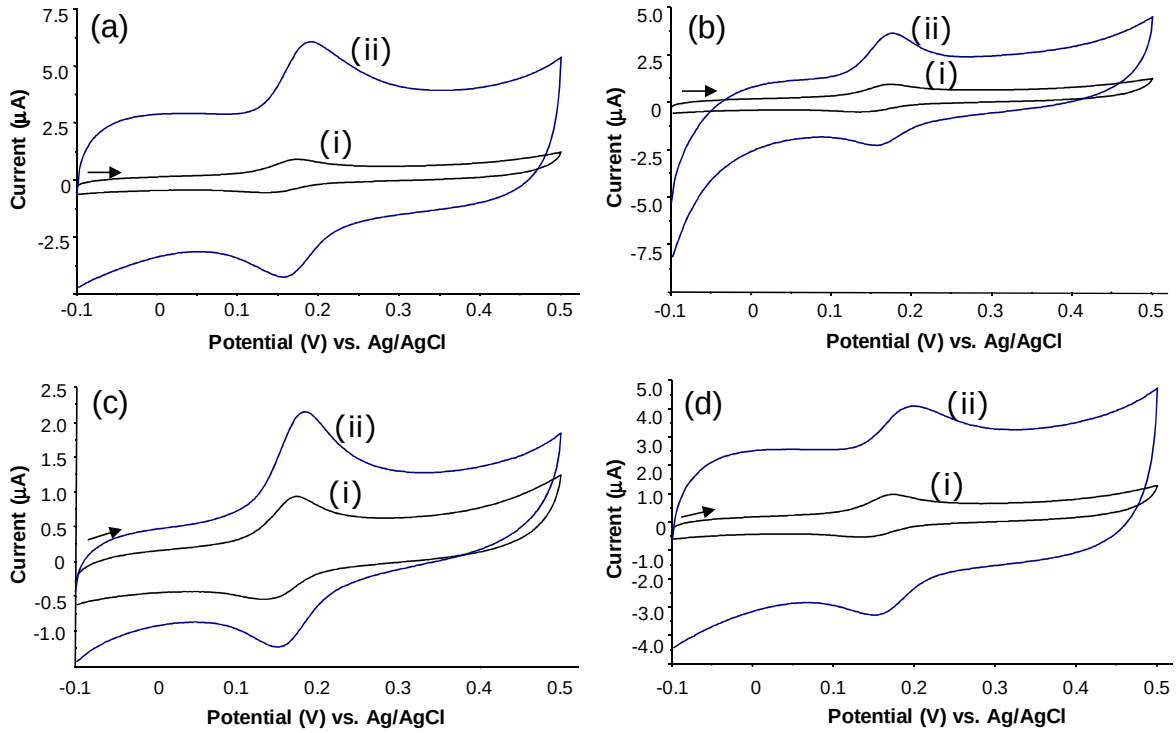

Figure 5.2: CV scans of DA at (a) fMWCNT-GCE; (b) CoTSPc/fMWCNT-GCE; (c) CuTSPc/fMWCNT-GCE; and (d) CoPc/fMWCNT-GCE. (i) Bare-GCE and (ii) modified GCE (pH 7.4). [DA] = 19.6 µM; Scan rate = 50 mV/s.

Table 5.1 summarises the mean current responses and peak potentials that were obtained for DA at the BGCE, fMWCNT-GCE, CoPc-GCE, CoTSPc-GCE, CoPc/fMWCNT-GCE, CuTSPc/fMWCNT and CoTSPc/fMWCNT-GCE.

Table 5.1: The current responses and peak potentials (vs. Ag/AgCl) of DA, with the respective shifts compared to the BGCE, which were obtained at the BGCE and the MPc, MTSPc and fMWCNT composite GCEs during CV analysis

Modification	Current (µA)	Current shift (vs. BGCE)	Potential (V)	Potential shift (vs. BGCE)
BGCE	0.49 (±0.07)	-	0.17 (±0.001)	-
fMWCNT-GCE	2.80 (±0.10)	+2.31	0.19 (±0.005)	+0.02
CoPc-GCE	0.20 (±0.03)	-0.29	0.23 (±0.018)	+0.06
CoTSPc-GCE	0.23 (±0.12)	-0.26	0.20 (±0.002)	+0.03
CoPc/fMWCNT-GCE	1.26 (±0.06)	+0.77	0.20 (±0.009)	+0.03
CuTSPc/fMWCNT-GCE	1.28 (±0.09)	+0.79	0.18 (±0.005)	+0.01
CoTSPc/fMWCNT-GCE	1.86 (±0.08)	+1.37	0.17 (±0.003)	±0.00

The expected increases in the DA current response at the modified GCEs were observed, as previously shown in Chapter 4.4.1. Decreases in current response were observed at the CoPc-GCE and CoTSPc-GCE, suggesting that the method of immobilisation of the MPcs was not optimal. This is attributed to the solubility of CoTSPc in an aqueous solution as the CoTSPc is susceptible to leaching upon immersion of the CoTSPc-GCE in the aqueous working solution, affecting catalysis of DA at the GCE surface. However, fMWCNTs in combination with CoPc, CuTSPc and CoTSPc resulted in an increase in the current response over the BGCE. This effect may, however, be solely related to the fMWCNTs. The decrease in potential (vs. Ag/AgCl) to 0.17 ±0.003 V at the CoTSPc/fMWCNT-GCE over that of the fMWCNT-GCE (0.19 ±0.001 V) and CoTSPc (0.20 ±0.002 V) suggests a synergistic effect. The shifts in potential may also represent an improvement in the stabilisation of CoTSPc immobilisation, thus preventing leaching. This particular benefit of fMWCNTs in sensor development may be extended to other analytes.

In order to assess the effect that the central metal cation has on DA detection, a comparison in the current responses for CoTSPc/fMWCNT-GCE and CuTSPc/fMWCNT-GCEs was conducted (Figure 5.2b and c, respectively). The cobalt-containing TSPc/fMWCNT-GCE exhibited a greater current response for DA (1.86 ±0.08 µA) compared to the copper-containing TSPc/fMWCNT-GCE (1.28 ±0.09

μA). Therefore, cobalt is more catalytically active as cobalt is a redox active central metal cation; whereas copper exhibits ring-based redox activity (Zagal *et al*., 1992).

In order to assess the effects that the functional groups on the outer ring of the MPc have on DA detection, a comparison between the current responses achieved from detection with sulphonated and non-sulphonated MPcs was conducted (Figure 5.2(b) and (d), respectively). The effect of the tetrasulphonated CoPc in the CoTSPc/fMWCNT-GCE resulted in an increased current response for DA (1.86 ±0.08 μA) and shift towards a more negative anodic peak potential (0.17 ±0.003 V vs. Ag/AgCl) when compared to that of the non-sulphonated CoPc (CoPc/fMWCNT-GCE) (1.26 ±0.06 μA and 0.20 ±0.009 V vs. Ag/AgCl). This demonstrates that the outer ring and any additional functional groups of the MPc are involved in the oxidation processes catalysed by the MPc. The sulphonate groups on the MPc also incorporate the factor of charge as they are negatively charged ($-SO^{2-}_4$). This, therefore, allows them to act as cation exchangers (Oni & Nyokong, 2001), much like that of the sulphonate groups on the Nafion® polymer, which attract cations resulting in enhanced cation detection.

Interestingly, the current responses for CuTSPc/fMWCNT-GCE (Figure 5.2c) and CoPc/fMWCNT-GCE (Figure 5.2d) were similar with a difference less than 20 nA. When compared against the CoTSPc/fMWCNT-GCE (1.86 ±0.08 μA), the DA responses for both the CuTSPc/fMWCNT-GCE (1.28 ±0.09 μA) and CoPc/fMWCNT-GCE (1.26 ±0.06 μA) were considerably lower. Therefore, by combining the catalytic effects of the central metal cation with that of the sulphonate functional groups, and fMWCNTs, a combined catalytic response was observed for DA at this hybrid surface (Figure 5.2b).

As demonstrated in Figure 5.2, DA exhibited a reversible oxidation for the bare and modified GCE. The difference in the peak potentials between the oxidised and reduced species decreased from 0.03 V (vs. Ag/AgCl) for the BGCE to 0.013 V (vs. Ag/AgCl) for the CoTSPc/fMWCNT-GCE demonstrating an improvement in the electrode kinetics (Heineman & Kissinger, 1996).

5.4.2. Enhancing sensitivity

In order to further enhance the sensitivity for DA at the CoTSPc/fMWCNT-GCE, a more rapid and sensitive electrochemical waveform was employed. Therefore, SWV was employed over CV as SWV fulfil these criteria. As illustrated in Figure 5.3, an increase of 28.7 ±2.05 µA was obtained for DA at the CoTSPC/fMWCNT-GCE over the BGCE, demonstrating a substantial increase in current response over CV.

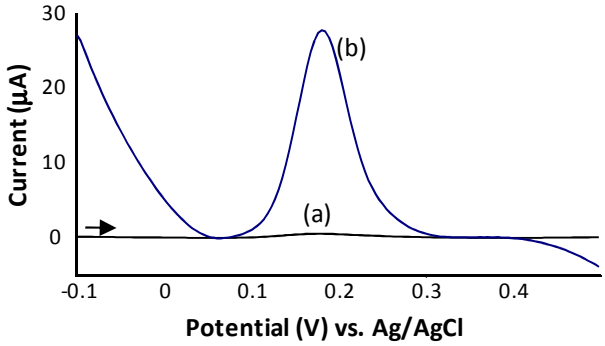

Figure 5.3: SWV of DA at (a) bare-GCE and (b) CoTSPc/fMWCNT-GCE (pH 7.4) (with baseline correction). [DA] = 19.6 µM

Table 5.2 shows the LODs and LOQs achieved for DA at the BGCE and CoTSPc/fMWCNT-GCE using SWV.

Table 5.2: The LOD and LOQ for SWV analysis of DA at the BGCE and CoTSPc/fMWCNT-GCE

Modifications	LOD (µM)	LOQ (µM)
Bare	0.613	1.857
CoTSPC/fMWCNT	0.0143	0.0433

SWV was employed for preparation of the DA and AA standard curves, as SWV is more suitable for quantitative analyses than CV; however, CV was performed for the qualitative analyses, such as the fouling/passivation and diffusion studies (Heineman & Kissinger, 1996).

5.4.3. Electrode kinetics for dopamine at the BGCE and modified-GCEs

5.4.3.1. Linearity

Standard curves for DA at the BGCE and CoTSPc/fMWCNT-GCE (Figure 5.4 (a) and Figure 5.4 (b), respectively) during SWV analysis (Figure 5.4i) were produced by plotting the increase in current response of the oxidation, or anodic, peak versus the linear increase in the concentration of DA (Figure 5.4ii).

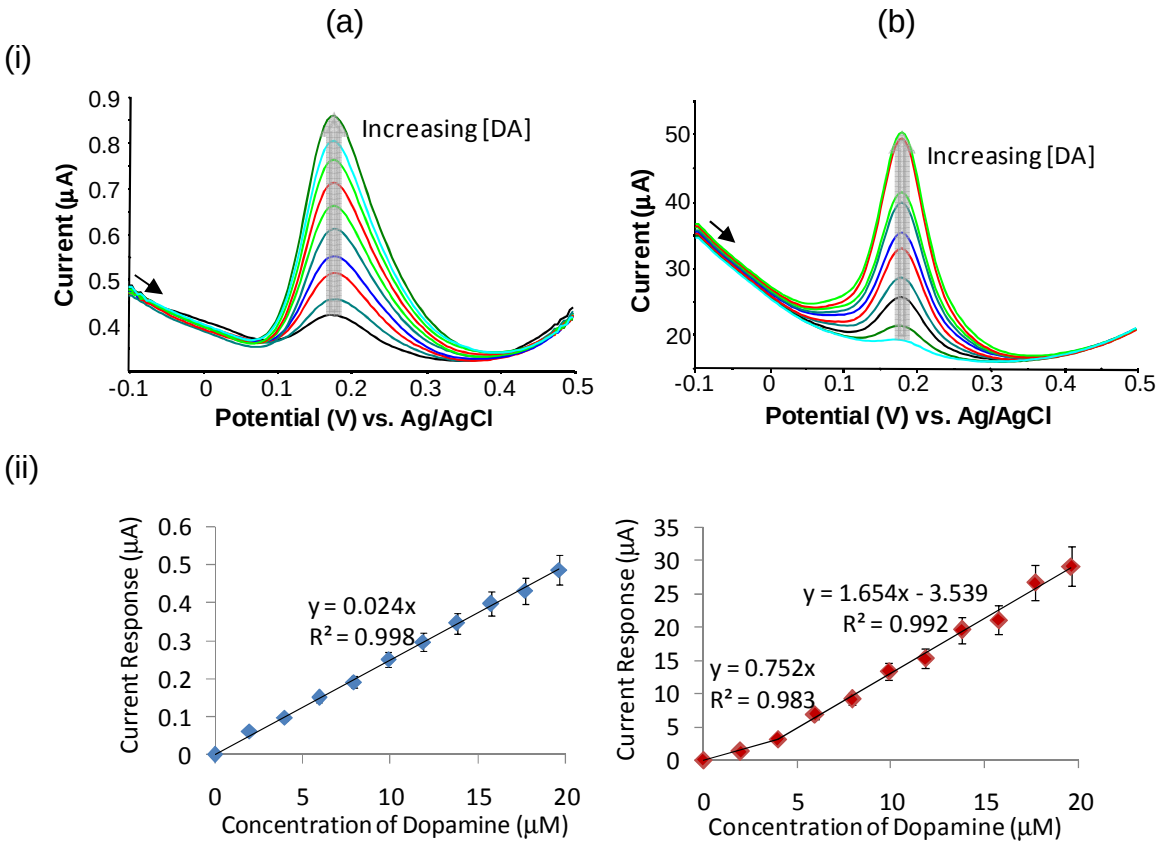

Figure 5.4: (i) SWV scans of uniform increases in the concentration of DA from 0 to 19.6 µM at (a) BGCE and (b) CoTSPc/fMWCNT-GCE (pH 7.4). (ii) Standard curves of DA concentration versus the current response for (a) and (b). (*n* = 3)

Figure 5.4(ii)a demonstrates that a linear response was achieved for DA at the BGCE for the concentration range studied (0 to 19.6 µA) with excellent reproducibility (92 %) and an R^2 value of 0.988. A reproducible linear response (R^2 = 0.992) with 10.2 % variability in response was observed for DA at the CoTSPc/ fMWCNT-GCE (Figure 5.4b) from 3.98 µM to the highest concentration studied (19.6 µM). Due to the slope at the CoTSPc/fMWCNT-GCE being 68.7 times greater than that at the BGCE, easier, more sensitive analyses can be achieved when detecting DA at the CoTSPc/fMWCNT-GCE.

A standard curve for the CoTSPc-GCE could not be generated for comparative purposes as leaching of the CoTSPc occurs upon immersion of the modified GCE into the aqueous working solution.

5.4.3.2. Passivation

Fouling of the electrode during consecutive scans of DA occurred at the BGCE (a) and, to a lesser degree, at the CoTSPc/fMWCNT-GCE (b), as illustrated in Figure 5.5.

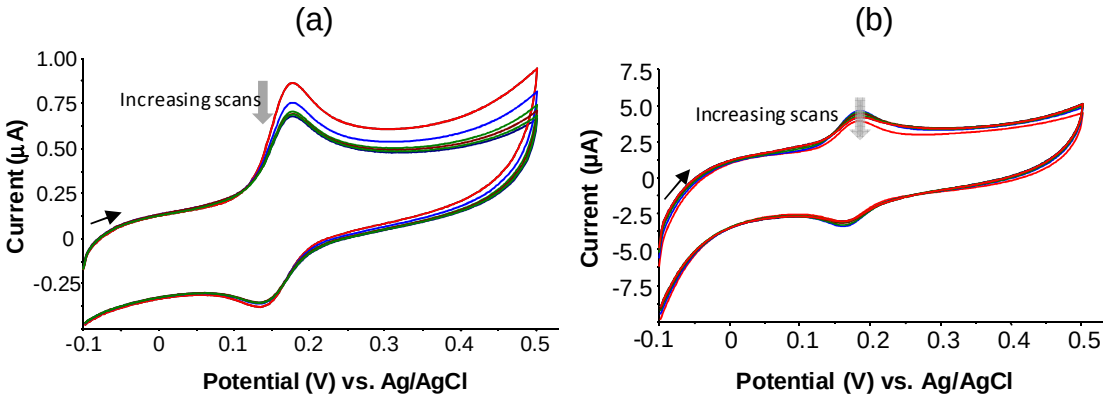

Figure 5.5: CVs of DA fouling at the (a) BGCE and (b) CoTSPc/fMWCNT-GCE (pH 7.4). [DA] = 19.6 µM; Scan rate = 50 mV/s.

For comparative purposes, Figure 5.6 compares passivation at the BGCE, fMWCNT-GCE, CoTSPc-GCE and CoTSPc/fMWCNT-GCE. A total percentage current response decrease of 15.0 ±1.1 % was observed at the fMWCNT-GCE after six consecutive scans. The BGCE, CoTSPc-GCE and CoTSPc/fMWCNT-GCE exhibited a total percentage decrease of up to 40.0 % after six consecutive scans, as demonstrated in Figure 5.6.

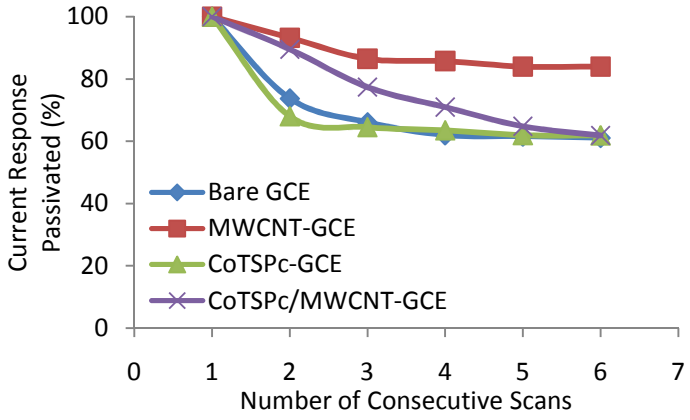

Figure 5.6: DA fouling at the BGCE and modified GCEs (pH 7.4). [DA] = 19.6 µM, Scan rate = 50 mV/s.

The total percentage current response loss for the CoTSPc-GCE and CoTSPc/fMWCNT-GCE was approximately the same as that of the BGCE after six

scans (40 ±2.0 %), as demonstrated in Figure 5.6. This indicates that after approximately six scans, the CoTSPc and CoTSPc/fMWCNT layers offer no immediate benefit in terms of the decrease in current response compared to the clear benefits afforded by the fMWCNTs. Upon inspection of the gradients of the current response passivation over six consecutive scans, fouling at the CoTSPc-fMWCNT-GCE occurred at a slower rate to that of the BGCE and CoTSPc-GCE as a gradual decrease in current response over the scan number was observed at the CoTSPc/fMWCNT-GCE. This lower rate of fouling indicates that stability of the modified-GCE was retained for a longer period of time or after a certain number of consecutive scans.

Therefore, addition of fMWCNTs to the CoTSPc solution at the GCE surface enhanced the stability of the CoTSPc at the GCE surface when placed in an aqueous solution. This enhancement is as a result of the lowered passivation, or fouling.

5.4.3.3. Mode of transport

CVs for DA conducted at various scan rates (50, 100, 200, 300, 400 and 500 mV/s) at a BGCE (a) and CoTSPc/fMWCNT-GCE (b) are illustrated in Figure 5.7. An increase in the current response for DA was observed upon the increase of the scan rate.

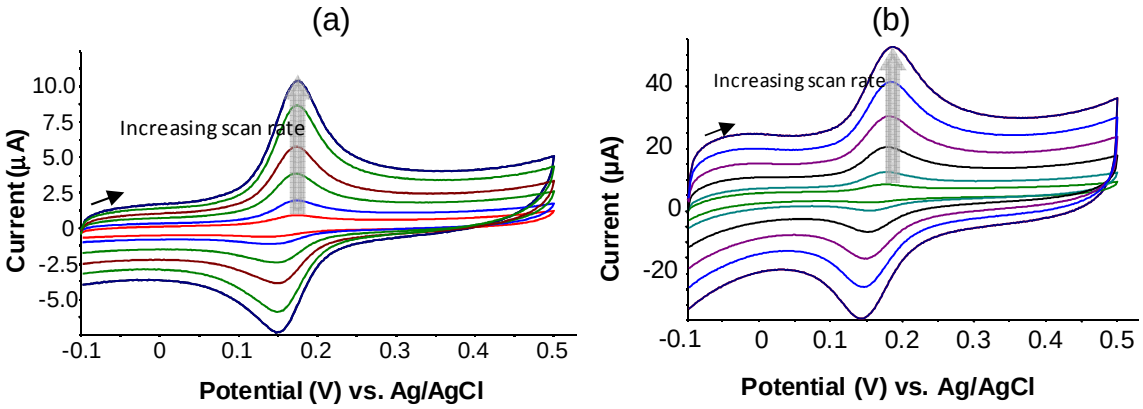

Figure 5.7: CVs of DA at the BGCE (a) and CoTSPc/fMWCNT-GCE (b) with various scan rates (pH 7.4). [DA] = 19.6 µM; Scan rates = 50, 100, 200, 300, 400 & 500 mV/s.

Analyses of the DA current responses versus the square root of the various scan rates for the different modifications were linear with a positive slope (Figure 5.8).

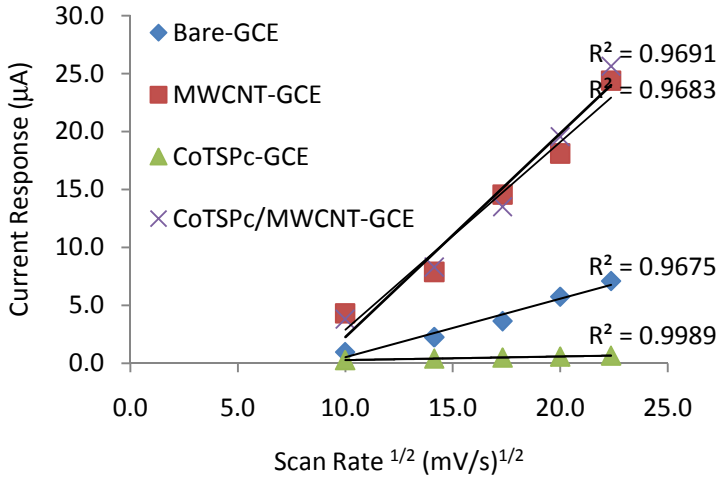

Figure 5.8: Effect of the square root of the scan rate on the current response of DA, during CV analysis, for the BGCE and modified GCEs (pH 7.4). [DA] = 19.6 µM

The linearity, illustrated in Figure 5.8, indicates that mass transport of DA towards the GCE surface is a diffusion-controlled process for all modifications (Nicholson & Shain, 1965). These results concur with previous research on DA conducted by Oni and Nyokong (2001) at a carbon paste electrode. Therefore, movement of DA towards the GCE surface occurs passively down a gradient of unoxidised molecules as an increasing number of DA molecules are oxidised at the GCE surface (Heineman & Kissinger, 1994).

5.4.4. Tryptophan analysis with the CoTSPc/fMWCNT-GCE

Figure 5.9 illustrates the observed Trp current responses at pH 3.0 (a) and pH 7.4 (b) at the CoTSPc/fMWCNT-GCE when analysed using SWV.

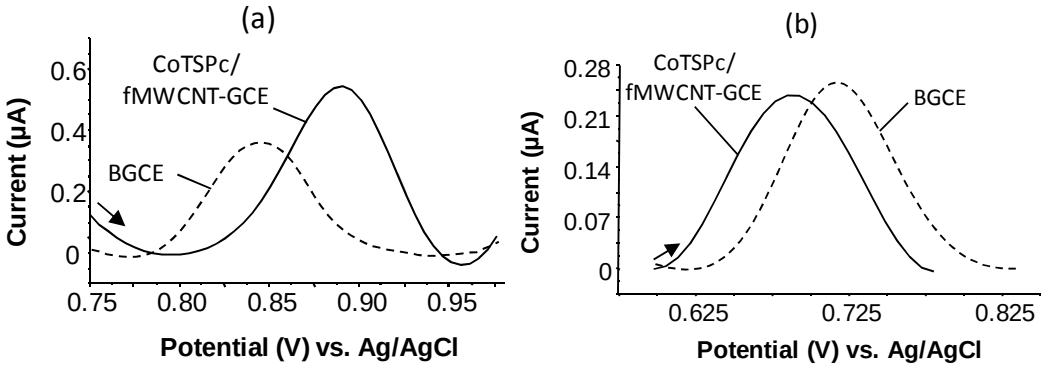

Figure 5.9: Trp anodic peaks during SWV analysis at the BGCE (dashed) and CoTSPc/fMWCNT-GCE (solid) at (a) pH 3.0 and (b) pH 7.4 (with baseline correction for better comparison of current). [Trp] = 19.6 µM.

As observed in Figure 5.9(a), an increase of 0.18 ±0.04 µA was observed for Trp at the CoTSPc/fMWCNT-GCE over that of the BGCE at pH 3.0 while no statistically significant change in current was observed between the bare and modified GCEs at pH 7.4 (Figure 5.9b). These trends in current response at the CoTSPc/fMWCNT-GCE were similar to those exhibited for Trp at the Nafion®-GCE at pH 3.0 and 7.4 (Figure 3.12). This demonstrates that the CoTSPc/fMWCNT hybrid layer exhibited cation exchange capabilities as shown for DA in Chapter 5. These cation exchange capabilities arise from the fact that, at pH 3.0, Trp becomes increasingly protonated. Due to charge interactions between Trp and the CoTSPc/fMWCNT layer, these positively charged Trp molecules accumulate at the CoTSPc/fMWCNT layer, resulting in the observed increase in current response. However, this is not the case at pH 7.4 as Trp has a net neutral charge resulting in minimal charge interaction between Trp and the negatively charged layer, leading to inconsequential changes in current response. Therefore, the observed cation exchanging properties exhibited by the CoTSPc/fMWCNT-GCE layer facilitates the sensitive detection of Trp at pH 3.0.

Characterisation studies were carried out in order to better understand the kinetics at the CoTSPc/fMWCNT-GCE for Trp.

5.4.4.1. Linearity

SWV analyses of Trp oxidation with uniform increases in concentration were performed at pH 3.0 and 7.4. The SWVs (a) and standard curve (b) for Trp at the CoTSPc/fMWCNT-GCE at pH 3.0 (Figure 5.10) and pH 7.4 (Figure 5.11) are represented.

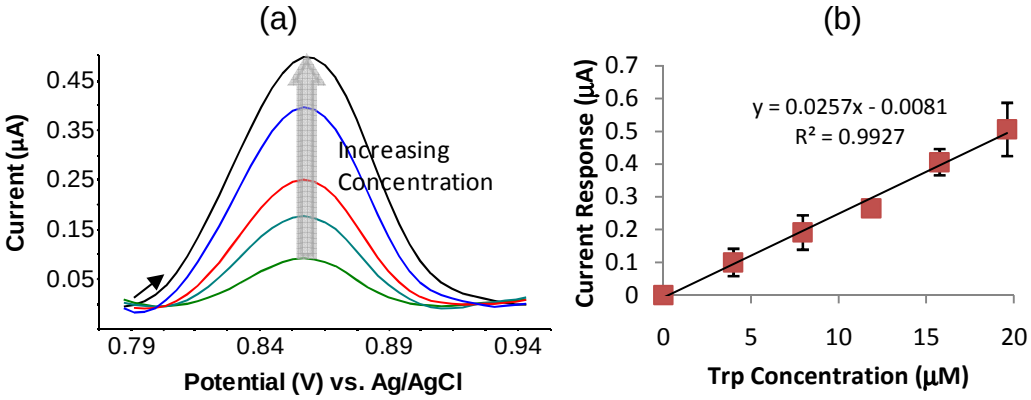

Figure 5.10: (a) SWVs of uniform increases in Trp concentration at the CoTSPc/fMWCNT-GCE at pH 3.0. (b) Standard curves ot Trp concentration versus current response at the CoTSPc/fMWCNT-GCE at pH 3.0. [Trp] = 3.9, 7.9, 11.8, 15.8 & 19.6 M.

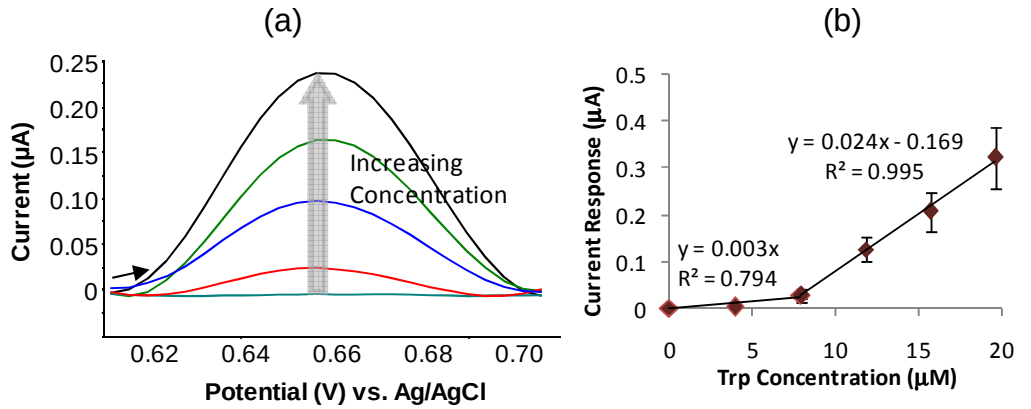

Figure 5.11: (a) SWVs of uniform increases in Trp concentration at the CoTSPc/fMWCNT-GCE at pH 7.4. (b) Standard curves ot Trp concentration versus current response at the CoTSPc/fMWCNT-GCE at pH 7.4. [Trp] = 3.9, 7.9, 11.8, 15.8 & 19.6 µM.

As observed in Figure 5.10(b), a linear trend was observed for Trp at the CoTSPc/fMWCNT-GCE at pH 3.0. However, two linear ranges were observed for Trp at pH 7.4, as illustrated in Figure 5.11(b), with one linear trend observed between 0 and 7.9 µM and the other observed between 7.9 and 19.6 µM. This non-linearity demonstrates that the CoTSPc/fMWCNT layer hampers Trp detection at lower concentrations at physiological pH. The reproducibility of the standard curves was greater at pH 3.0 (91.4 %) than at pH 7.4 (79.9 %), with the correlation co-efficients (R^2 value) at pH 7.4 for the higher concentration range nearing 1.0. Therefore, Trp detection at pH 3.0 at the CoTSPc/fMWCNT-GCE yielded an optimal response as linearity was observed over a wider concentration range. This result concurs with those for Trp at the Nafion®-GCE and Nafion®/fMWCNT-GCE as an optimal response was obtained at pH 3.0.

The LOD and LOQs for Trp at pH 3.0 and pH 7.4 are outlined in Table 5.3.

Table 5.3: The LOD and LOQs for SWV analyses of Trp at the CoTSPc/fMWCNT-GCE at pH 3.0 and 7.4.

pH	LOD (μM)	LOQ (μM)
3.0	0.179	0.543
7.4	0.749	2.270

The LODs and LOQ for Trp at the CoTSPc/fMWCNT-GCE at pH 3.0 were lower than those obtained at pH 7.4, demonstrating an enhanced sensitivity and ability to detect Trp at pH 3.0.

5.4.4.2. Passivation

The SWV scans (a) and plots of percent passivation versus the number of scans (b) illustrate the effects of fouling of Trp at the CoTSPc/fMWCNT-GCE at pH 3.0 (Figure 5.12) and pH 7.4 (Figure 5.13).

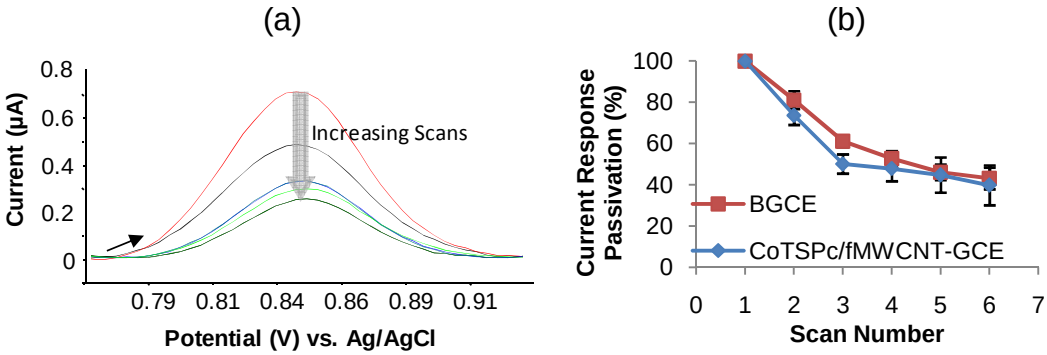

Figure 5.12: (a) SWVs of consecutive scans of Trp at the CoTSPc/fMWCNT-GCE (pH 3.0). (b) The effect of fouling, expressed as the percent of passivation, on Trp oxidation at pH 3.0. [Trp] = 19.6 μM.

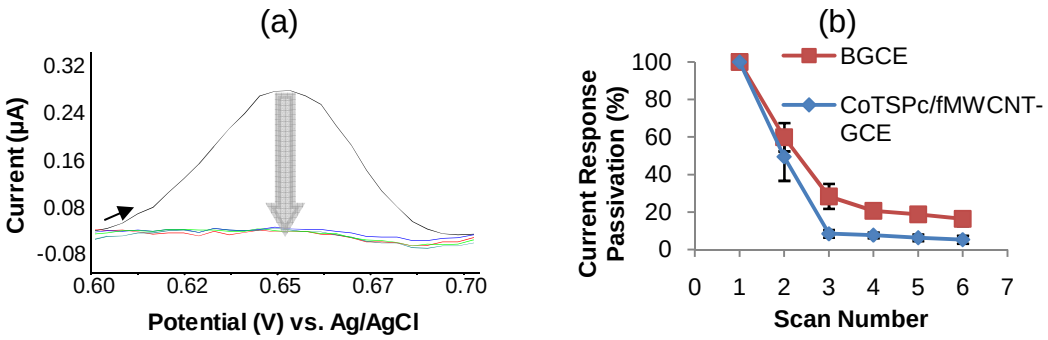

Figure 5.13: (a) SWVs of consecutive scans Trp at the CoTSPc/fMWCNT-GCE (pH 7.4). (b) The effect of fouling, expressed as the percent of passivation, on Trp oxidation at pH 7.4. [Trp] = 19.6 µM.

As observed in Figure 5.12, a decrease in the amplitude of the SWV peak, similar to the BGCE as shown in Figure 5.12(b), was observed for Trp at the CoTSPc/fMWCNT at pH 3.0. The total percent passivation for Trp after six consecutive scans at pH 3.0 (60.1 ±5.1 %) at the CoTSPc/fMWCNT-GCE was 35.6 % lower than that observed at pH 7.4 (95.7 ±1.1 %), demonstrating improved stability. The total passivation exhibited at pH 7.4 (Figure 5.13b) at the CoTSPc/fMWCNT-GCE (95.7 ±1.1 %) was, however, greater than that observed at the BGCE (83.5 ±2.4 %), demonstrating lowered stability. The high degree of passivation at the CoTSPc/fMWCNT-GCE at pH 7.4 may be attributed to the cumulative effects of fouling; and, electrostatic hindrance (scans 1 and 2) and subsequent exclusion (scans 3 to 6) of Trp.

Therefore, when analysing Trp with the CoTSPc/fMWCNT-GCE, an electrolyte solution of pH 3.0 would yield a more stable response than one at pH 7.4 when conducting repetitive scans.

5.4.4.3. Mode of transport

The effect of scan rate on the anodic oxidation peak of Trp during CV analysis at pH 3.0 is demonstrated in Figure 5.14.

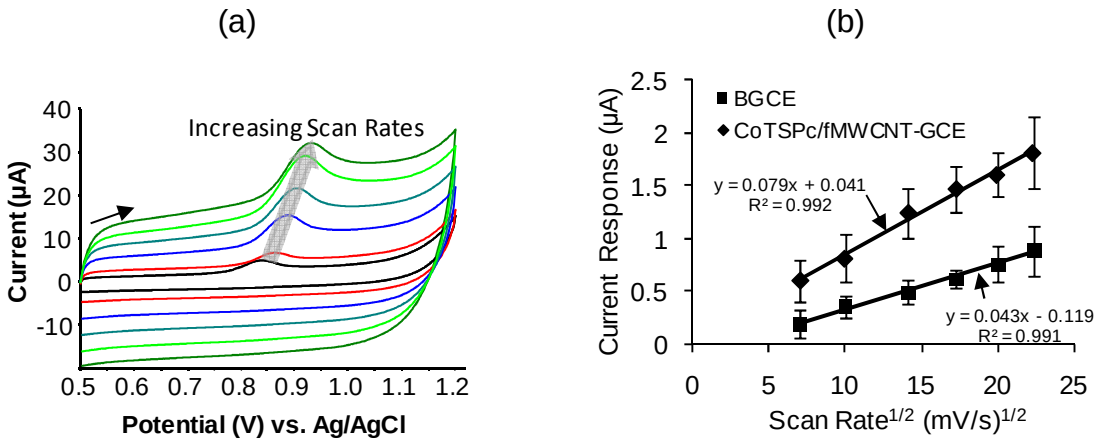

Figure 5.14: (a) CVs of Trp at the CoTSPc/fMWCNT-GCE with various scan rates (pH 3.0). (b) Plot of the square root of the scan rate on the current response of Trp at the CoTSPc/fMWCNT-GCE (pH 3.0). [Trp] = 19.6 µM; Scan rates = 50, 100, 200, 300, 400 & 500 mV/s.

A progressive change in the shape of the voltammogram was noted with increasing scan rates as the baseline current between the positive and negative scans of the CV increased with increasing scan rates (Figure 5.14a). A linear increase in the anodic current response for Trp was observed with an increase in scan rate, as observed in the plot of current response versus the square root of the scan rate (Figure 5.14b). The observed linear relation between the current response and square root of the scan rate indicates that oxidation of Trp is a diffusion controlled process at the CoTSPc/fMWCNT-GCE, similar to the BGCE.

5.4.5. Melatonin analysis with the CoTSPc/fMWCNT-GCE

Figure 5.15 illustrates Mel detection at pH 3.0 (a) and pH 7.4 (b) at the CoTSPc/fMWCNT-GCE when analysed using SWV.

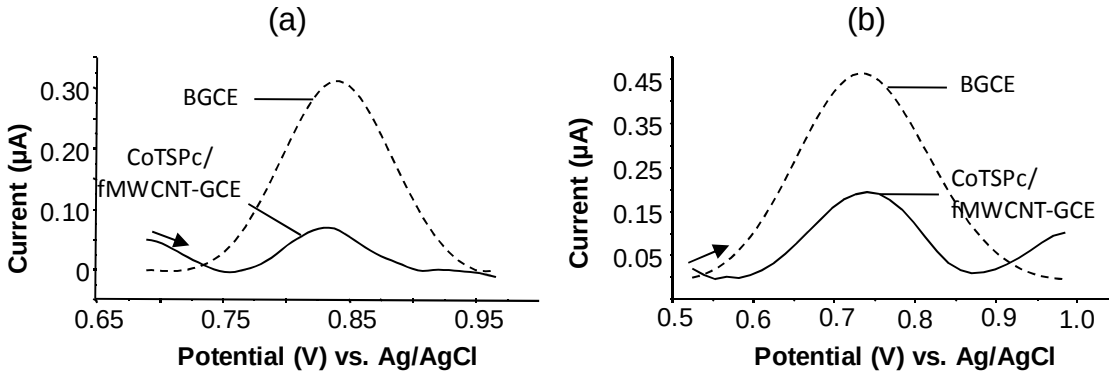

Figure 5.15: Mel anodic peaks during SWV analysis at the BGCE (dashed) and CoTSPc/fMWCNT-GCE (soldi) at (a) pH 3.0 and (b) pH 7.4 (with baseline correction). [Trp] = 19.6 µM; [Mel] = 19.6 µM.

As illustrated in Figure 5.15(a), the CoTSPc/fMWCNT-GCE (0.05 ±0.03 µA) exhibited a Mel response that was 0.26 µA lower than that of the BGCE (0.31 ±0.07 µA). When compared to the BGCE (0.45 ±0.01 µA), a decrease of 0.23 µA in the Mel current response at the CoTSPc/fMWCNT-GCE (0.22 ±0.04 µA) was observed at pH 7.4, as illustrated in Figure 5.15(b). This is dissimilar to the current responses observed at the Nafion®-GCE (Chapter 3.4.7.). The observed decrease in the Mel current response at pH 3.0 and 7.4 may be attributed to the electrostatic interactions, or hindrance, observed between the functional groups on both the CoTSPc ($-SO^{2-}_4$) and the fMWCNTs (-COOH) and the Mel species (neutral). Specifically, this repulsion is due to electronegativity of the neutral Mel molecule, which is brought about by the electron configuration of the lone pairs in the oxygen and nitrogen atoms and the π-electrons in the aromatic indole ring. Pauling's definition of electronegativity is the ability of an atom to attract electrons to itself; thereby, gaining negative charges. Therefore, these atoms/structures result in the overall repulsion of the Mel molecule by the CoTSPc/fMWCNT-GCE.

5.4.5.1. Linearity

SWV analyses of Mel oxidation with uniform increases in concentration were performed at pH 3.0 and 7.4. The SWVs (a) and standard curve (b) for Mel at the CoTSPc/fMWCNT-GCE at pH 3.0 (Figure 5.16) and pH 7.4 (Figure 5.17) are represented.

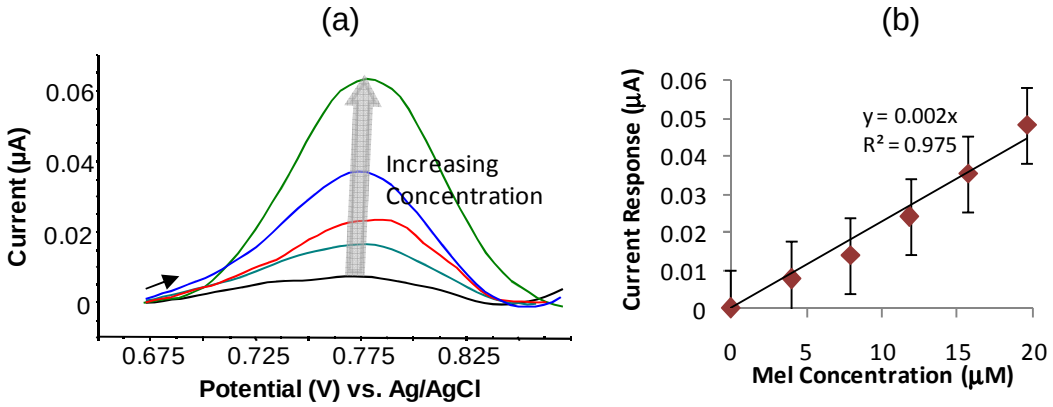

Figure 5.16: (a) SWVs of uniform increases in Mel concentration at the CoTSPc/fMWCNT-GCE at pH 3.0. (b) Standard curves of Mel concentration versus current response at the CoTSPc/fMWCNT-GCE at pH 3.0. [Mel] = 3.9, 7.9, 11.8, 15.8 & 19.6 M.

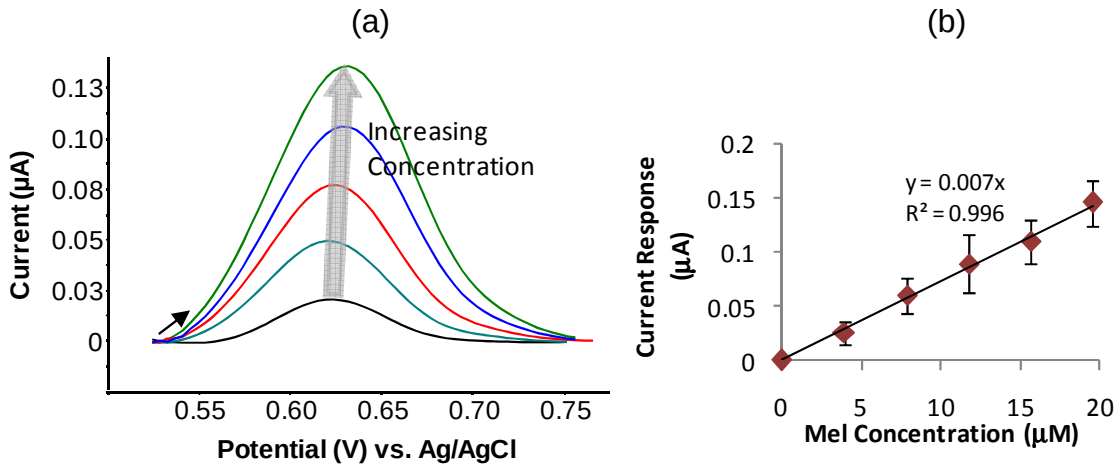

Figure 5.17: (a) SWVs of uniform increases in Mel concentration at the CoTSPc/fMWCNT-GCE at pH 7.4. (b) Standard curves of Mel concentration versus current response at the CoTSPc/fMWCNT-GCE at pH 7.4. [Mel] = 3.9, 7.9, 11.8, 15.8 & 19.6 M.

Linear trends were observed for Mel over the studied concentration range (0 to 19.6 µM) at the CoTSPc/fMWCNT-GCE at both pH 3.0 (Figure 5.16) and 7.4 (Figure 5.17). The reproducibility of the standard curves for Mel was greater at pH 7.4 (86.9 %) than at pH 3.0 (77.2 %). Moreover, the correlation co-efficient for the linear range at pH 3.0 (0.996) was nearer to 1.0 than that obtained at pH 7.4 (0.975), demonstrating improved linearity at pH 3.0. The LOD and LOQs for Mel at pH 3.0 and pH 7.4 are outlined in Table 5.4.

Table 5.4: The LOD and LOQs for SWV analyses of Mel at the CoTSPc/fMWCNT-GCE at pH 3.0 and 7.4.

pH	LOD (µM)	LOQ (µM)
3.0	1.28	3.88
7.4	0.45	1.35

The LODs and LOQ for Mel at the CoTSPc/fMWCNT-GCE at pH 7.4 were lower than those obtained at pH 3.0, demonstrating that a lower concentration of Mel can be detected at pH 7.4 at the CoTSPc/fMWCNT-GCE. This would aid in the sensitive detection of Mel at physiological pH.

5.4.5.2. Passivation

SWV scans (a) and plots of percent passivation versus the number of scans (b) illustrate the effects of fouling of Mel at the CoTSPc/fMWCNT-GCE at pH 3.0 (Figure 5.18) and pH 7.4 (Figure 5.19).

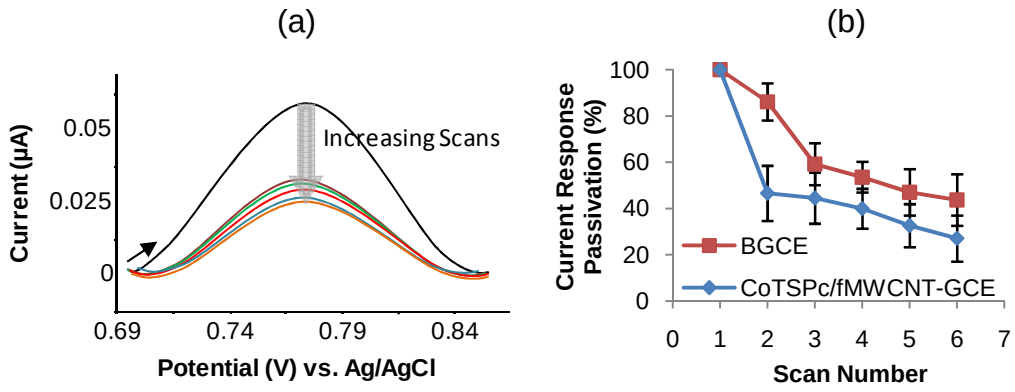

Figure 5.18: (a) SWVs of consecutive scans Mel at the CoTSPc/fMWCNT-GCE (pH 3.0). (b) The effect of fouling, expressed as the percent of passivation, on Mel oxidation at pH 3.0. [Mel] = 19.6 µM

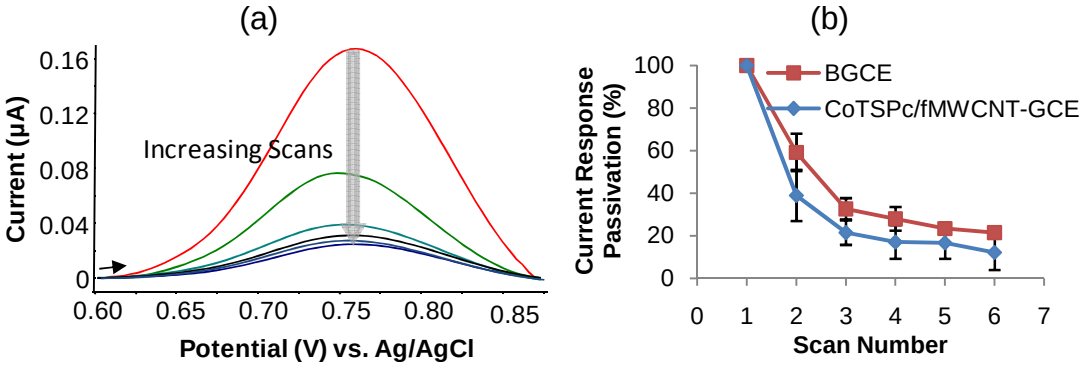

Figure 5.19: (a) SWVs of consecutive scans Mel at the CoTSPc/fMWCNT-GCE (pH 7.4). (b) The effect of fouling, expressed as the percent of passivation, on Mel oxidation at pH 7.4. [Mel] = 19.6 µM

Decreases in the peak amplitude of the SWV scans of Mel was observed at both pH 3.0 (Figure 5.18a) and 7.4 (Figure 5.19a), demonstrating passivation of the electrode. These responses were similar to those observed at the BGCE as shown in Figure 5.18(b) and Figure 5.19(b) with a higher degree of passivation occurring at the CoTSPc/fMWCNT-GCE than the BGCE throughout the fouling analyses at both pH 3.0 and 7.4. The total percent passivation after six consecutive scans at the CoTSPc/fMWCNT-GCE at pH 3.0 (73.8 ±6.2 %) was 14.1 % lower than that observed at pH 7.4, demonstrating improved stability at pH 3.0. This fouling stability at pH 3.0 at the CoTSPc/fMWCNT-GCE may be reached early during the fouling analyses as a more stable response is observed from scan 2 compared to the CoTSPc/fMWCNT-GCE at pH 7.4, in which further decreases in current response are observed following the second scan. Therefore, Mel analysis at the CoTSPc/fMWCNT-GCE was less susceptible to the effects of fouling at acidic pH (pH 3.0) than at physiological pH (pH 7.4).

5.4.5.3. Mode of transport

The effect of scan rate on the anodic oxidation peak of Mel during CV analysis at pH 3.0 at the CoTSPc/fMWCNT-GCE is demonstrated in Figure 5.20.

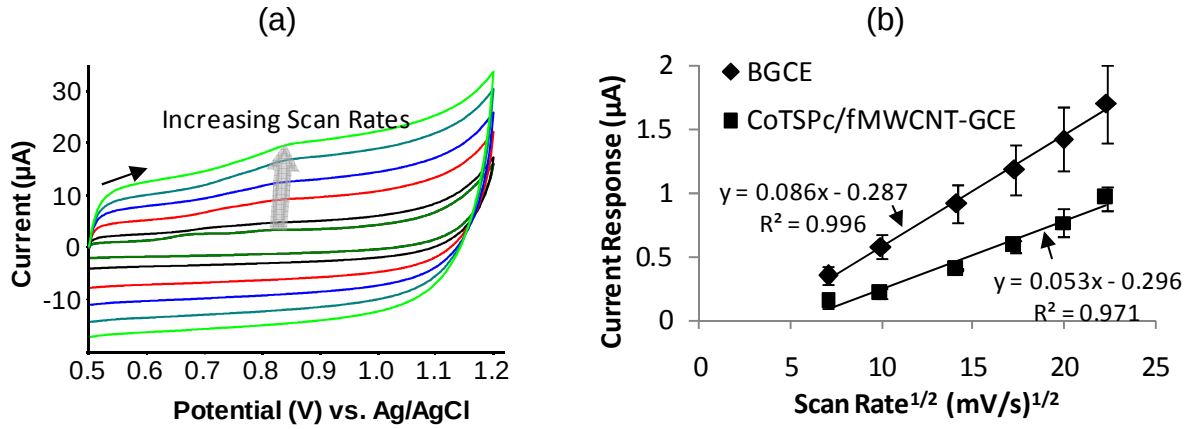

Figure 5.20: (a) CVs of Mel at the CoTSPc/fMWCNT-GCE with various scan rates (pH 3.0). (b) Plot of the square root of the scan rate on the current response of Mel at the CoTSPc/fMWCNT-GCE (pH 3.0). [Mel] = 19.6 µM; Scan rates = 50, 100, 200, 300, 400 & 500 mV/s.

As revealed in Figure 5.20b, a linear trend in the current response versus the square root of the scan rate was observed for Mel, demonstrating a diffusion-controlled movement of Mel molecules towards the CoTSPc/fMWCNT-GCE (Nicholson & Shain, 1965). This diffusion process can be explained by the depletion of oxidised molecules and buffering ions down their respective concentration gradients at the GCE surface (Heineman & Kissinger, 1994).

5.4.6. Comparative analysis of tryptophan and melatonin

Figure 5.21 demonstrates the differences in the current responses exhibited for Trp and Mel during SWV analysis at the BGCE and CoTSPc/fMWCNT-GCE at pH 3.0 and 7.4.

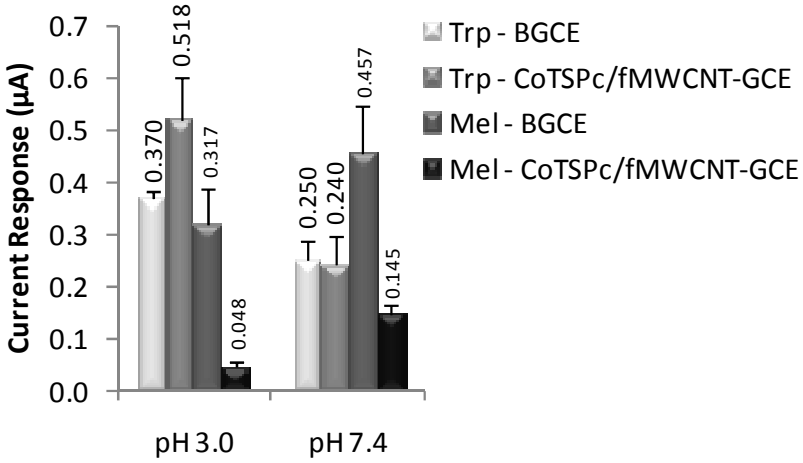

Figure 5.21: A comparison of the various current responses (µA) obtained during SWV analysis of Trp and Mel at the BGCE and CoTSPc/fMWCNT-GCE at pH 3.0 and pH 7.4.

As demonstrated in Figure 5.21, the CoTSPc/fMWCNT-GCE did exhibit cation exchange properties at pH 3.0 as the Trp current response is higher at the modified GCE than at the bare GCE. Moreover, the current response for Trp at both the BGCE and CoTSPc/fMWCNT-GCE at pH 3.0 is higher than that at pH 7.4. There was, however, no enhancing effect brought about by this cation exchange nanocomposite layer on Mel as the current responses at both pH 3.0 and 7.4 at the CoTSPc/fMWCNT-GCE remained lower than that of the BGCE. The increases in the Mel current response at pH 7.4 over that observed at pH 3.0 for the BGCE and CoTSPc/fMWCNT-GCE was previously observed for the Nafion®-GCE (Chapter 3). This can be attributed to the effect of pH on Mel oxidation as Mel is more prone to oxidation at physiological pH owing to its antioxidant activities in the body. A decrease in Mel current response at the CoTSPc/fMWCNT-GCE was attributed to repulsion between the charged sulphonate groups and the electronegative moieties on the Mel molecule.

5.5. Conclusion

This study examined the effectiveness of a (TS)MPc/fMWCNT hybrid layer for DA, Trp and Mel detection. Addition of fMWCNTs to the CoTSPc solution at the GCE surface enhanced the stability of the CoTSPc at the GCE surface when placed in an aqueous solution. This stability is as a result of the hybridisation through π-π interactions between the CoTSPc and the fMWCNTs (Schulte *et al*., 2008). Therefore, these structures support a hybrid approach to coupling the catalytic

properties of MPc complexes with that of the electron conducting and stabilising properties afforded by fMWCNTs. Moreover, trapping of CoTSPc complexes by the fMWCNTs at the GCE surface may be aided by the non-oriented conformation of the fMWCNTs at the GCE surface and bonding interactions between CoTSPc and fMWCNTs. Therefore, this method of immobilisation proves to be promising for the stabilisation of TSPcs, MPcs and other electrocatalysts that tend to leach into solution.

Addition of fMWCNTs to CoPc, CuTSPc and CoTSPc enhanced the current response for DA. While these enhancements in current response at the MPc/fMWCNT-GCEs were lower than that at the fMWCNT-GCE, the synergistic effects of CoTSPc and fMWCNTs showed a lowering of the anodic peak potential (vs. Ag/AgCl) for DA compared to the fMWCNT-GCE and CoTSPc-GCE. Furthermore, addition of fMWCNTs to the TSPc resulted in a lowering of the rate of fouling.

Cation exchange properties towards Trp were exhibited at the CoTSPc/fMWCNT-GCE as, at pH 3.0, an increase in Trp current response was observed over that of the BGCE. Evidence of cation exchange properties is given by the ability of the layer to attract or accumulate an analyte with the opposite charge as in the case of Trp and the CoTSPc/fMWCNT layer. In this case, the increased number of positively charged Trp molecules at pH 3.0 are attracted to the negatively charged moieties or functional groups on CoTSPc ($-SO_4^{2-}$) and fMWCNTs ($-COO^-$). These functional groups remain in their ionised form owing to their highly acidic pKa values (ranging from 0.2 to 2.3). Further evidence of the cation exchange property was given by the insignificant change in Trp current response between the BGCE and CoTSPc/fMWCNT-GCE at pH 7.4, in which the influence of charge is evidently lacking.

Cation exchange capabilities were not demonstrated for Mel at the CoTSPc/fMWCNT-GCE at either pH, unlike that of the Nafion®-GCE, demonstrating the influence of electrostatic repulsion and electronegativity. During Mel analysis, a significant decrease in current response was observed at the CoTSPc/fMWCNT-GCE demonstrating the near exclusion of Mel.

The large decrease in the Mel response at pH 3.0 and increase in the Trp current response, aided by the shift in the Trp peak potential, at the CoTSPc/fMWCNT-GCE has potential to aid the separation of Trp and Mel, thus facilitating the selective detection of Trp in a mixed solution containing Mel at pH 3.0. Therefore, it would be of interest to ascertain the effectiveness of the CoTSPc/fMWCNT-GCE during separation of Trp in a mixed solution containing Mel, such as a dietary supplement. In terms of sensitivity, this electrode modification does not, however, offer any advantages over the Nafion®-GCE during the sensitive detection of Trp and, therefore, practical application remains questionable.

Therefore, the CoTSPc/fMWCNT-GCE aids in the sensitive detection of DA and selective detection of Trp over Mel. As a result, it would be of interest to ascertain the effect that the CoTSPc/fMWCNT-GCE has on ascorbic acid detection. The following chapter examines the ability of the CoTSPc/fMWCNT-GCE to exclude the interferent, ascorbic acid.

Chapter 6

Exclusion of ascorbic acid using the CoTSPc/fMWCNT hybrid sensor

6.1. Introduction

To recap, ascorbic acid (AA) is a common interferent in the electrochemical detection of dopamine (DA) in biological fluids (Ewing *et al*., 1982). At physiological pH, DA and AA have different charges owing to their own unique properties and pKa values. Therefore, at pH 7.4, DA (pKa = 8.87) exists as a cation (positively charged) and AA (pKa = 4.10) is present as an anion (negatively charged). This difference in properties allows for the electrochemical elimination of the interfering AA oxidation peak through utilisation of a cation exchange polymer or resin at the GCE surface. The negatively charged Teflon polymer, Nafion®, is a cation exchanger and, therefore, has the potential to exclude negatively charged analytes/interferents. Nafion® is commonly used to exclude AA during the electrochemical detection of DA as an electrode can easily be modified with this cation exchange resin/polymer.

Studies with MWCNTs have shown promise in enhancing the detection of DA over AA through separation of the peak potentials for DA and AA or elimination of AA (Schenk *et al.*, 1983). Furthermore, Oni and Nyokong (2001) show that CoTSPc lowers the current response of AA in excess of 99.0 %. Studies in Chapter 5 for DA show the enhancement of DA detection at a CoTSPc/fMWCNT composite electrode. Therefore, examination of the effect of the CoTSPc/fMWCNT layer on AA is of immediate interest.

6.2. Aim/s

The aim of this study was to examine the effect of a Nafion®/fMWCNT and CoTSPc/fMWCNT hybrid layer at the GCE surface on the detection of AA. Furthermore, detection of AA would be carried out in order to ascertain the feasibility of each hybrid sensor on the selective detection of DA. The specific aims include:

1) Determination of the optimal combination of MPcs and fMWCNTs for AA exclusion;
2) Assessment of the characteristics for AA detection at the hybrid sensors, with

focus on the:

a. Establishment of linear concentration ranges;
b. Effects of electrode passivation;
c. Determination of diffusion characteristics; and,
d. Determination of the LOD and LOQ for DA; and,

3) Determination of the effect that the presence of AA exhibits towards the detection of DA when analysed simultaneously at the Nafion®/fMWCNT-GCE and CoTSPc/fMWCNT-GCE.

6.3. Experimental Procedure

6.3.1. Chemicals and reagents

AA (Sigma) was prepared as previously mentioned (Chapter 4.3.1.). The MWCNTs were functionalised as described in Chapter 2.3.3.1. The fMWCNT, CoPc, CoTSPc and mixed MPc/fMWCNT suspensions were prepared as previously described (Chapter 5.3.3.). The electrolyte solution used was a 0.2 M potassium phosphate buffer, pH 7.4. The pH measurements were conducted on a WTW pH 330i pH meter, coupled to a Sentix 41 pH electrode.

6.3.2. Preparation of electrodes

The Nafion®/fMWCNT-GCE was modified as described in Chapter 4.3.3. and the CoTSPc/fMWCNT-GCE was modified as described in Chapter 5.3.4.

6.3.3. Electrochemical apparatus and electrode pretreatment

The electrochemical cell and pretreatment was carried out as described in Chapter 2.3.2. The CV and SWV scans were carried out as described in Chapter 5.3.5.

6.3.4. Analyte characterisation and electrode kinetics

Standard curves, fouling analyses and mode of transport were determined as described in Chapter 3.3.4. The LOD and LOQ were calculated as described in Chapter 2.3.2.5.

6.3.5. Statistics

All studies were conducted in triplicate. Results are presented as the mean

±standard deviation.

6.4. Results and Discussion

6.4.1. Ascorbic acid detection with fMWCNTs and MPcs

Figure 6.1 shows the CV analyses that demonstrate the effects of fMWCNT, CoTSPc and CoTSPc/fMWCNT layers on AA detection.

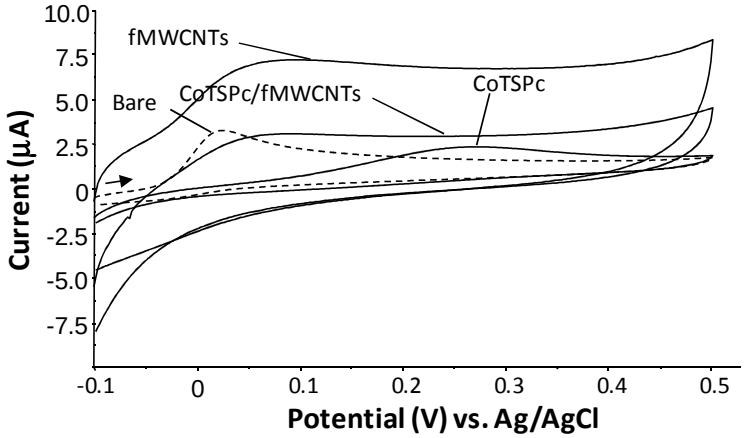

Figure 6.1: CV of AA at bare-GCE, fMWCNT-GCE, CoTSPc-GCE and CoTSPc/fMWCNT-GCE at pH 7.4. [AA] = 150 µM; scan rate = 50 mV/s

Table 6.1 shows the current responses and anodic peak potentials that arose from CVs of AA (Figure 6.1) at the BGCE, fMWCNT-GCE, CoTSPc-GCE and CoTSPc/fMWCNT-GCE.

Table 6.1: The current responses and peak potentials (vs. Ag/AgCl) for AA at the BGCE, fMWCNT-GCE, CoTSPc-GCE and CoTSPc/fMWCNT-GCE during CV analysis with AA exclusion (%) and shift in potential versus the BGCE

Modification	Current (µA)	AA Exclusion vs. BGCE (%)	Potential (V)	Potential shift (vs. BGCE)
BGCE	3.34 (±0.033)	0	0.00 (±0.013)	-
fMWCNT-GCE	1.92 (±0.142)	42.52	0.04 (±0.001)	+ 0.04
CoTSPc-GCE	1.22 (±0.021)	63.47	0.25 (±0.010)	+ 0.25
CoTSPc/fMWCNT-GCE	0.81 (±0.103)	75.75	0.12 (±0.016)	+ 0.12

A decrease in the AA current response was observed at the fMWCNT-GCE and CoTSPc-GCE compared to the BGCE in keeping with earlier studies. A broadening

of the oxidation peak was also observed for these layers when compared to the AA current response at the BGCE. This broadening demonstrates a change in the diffusional kinetics of the unoxidised/oxidised analyte towards/away from the GCE surface and the aqueous environment around the GCE surface (Takeda *et al*., 2001). By manipulating and combining the catalytic responses at the fMWCNT-GCE and CoTSPc-GCE for AA (150.0 µM), a further decrease in the current response was obtained, as illustrated for the CoTSPc/fMWCNT-GCE in Figure 6.1 and tabulated in Table 6.1.

As illustrated in Figure 6.1, a more positive anodic peak shift was observed for AA when analysed with the modified GCEs with the greatest shift observed at the CoTSPc-GCE. When compared to the AA peak potential obtained at the BGCE, a positive shift of 0.04 ±0.001 V and 0.25 ±0.010 V (vs. Ag/AgCl) was observed for the fMWCNT-GCE and CoTSPc-GCE, respectively. This shift demonstrates that AA oxidation became increasingly laboured upon modification of the GCE. Although not clearly visible in Figure 6.1, a shift of 0.12 ±0.016 V (vs. Ag/AgCl) towards a more positive potential was also observed for the AA oxidation peak at the CoTSPc/fMWCNT-GCE. Therefore, the modification of the GCE with fMWCNTs and/or CoTSPcs, affects the electrode kinetics and ease of oxidation at the GCE surface.

AA was excluded up to a concentration of 130.0 µM at the CoTSPc/fMWCNT-GCE using SWV analyses, as shown in Figure 6.2, which illustrates SWVs of an increasing AA concentration at a CoTSPc/fMWCNT-GCE.

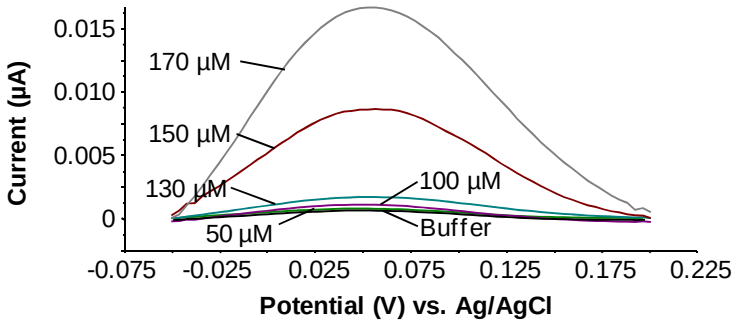

Figure 6.2: SWVs of varying concentrations (50.0, 100.0, 130.0, 150.0 & 170.0 µM) of AA at the CoTSPc/fMWCNT-GCE versus 0.2 M potassium phosphate buffer, pH 7.4 (Note: baseline correction used in order to better compare peak amplitudes).

AA has previously been excluded up to 150.0 µM using FeTSPcs at a carbon paste electrode by Oni and Nyokong (2001). An AA concentration (150.0 µM) that was higher than the detection limit (130.0 µM) was, therefore, used for all analyses at the CoTSPc/fMWCNT-GCE in order to better assess the electrochemical response.

6.4.2. Sulphonated vs. non-sulphonated CoPcs

Figure 6.3 illustrates the anodic peaks that were obtained during SWV analysis of AA at the BGCE, fMWCNT-GCE, CoPc/fMWCNT-GCE and CoTSPc/fMWCNT-GCE.

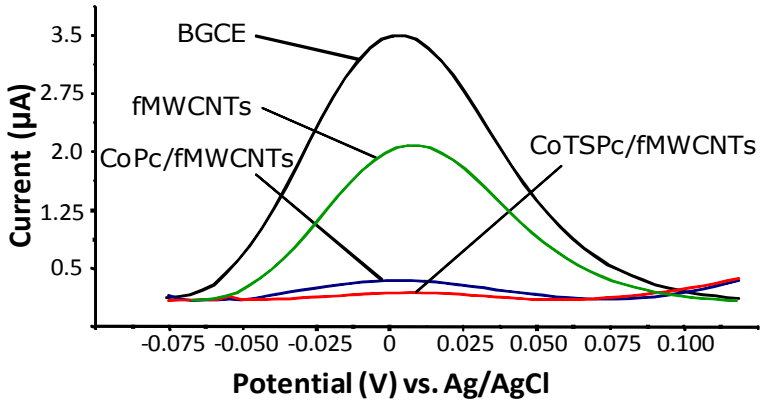

Figure 6.3: SW voltammograms of the AA anodic peaks at (a) bare-GCE; (b) fMWCNT-GCE; (c) CoPc/fMWCNT-GCE; and (d) CoTSPc/fMWCNT-GCE (pH 7.4) (with baseline correction for ease of response comparison). [AA] = 150 µM

Table 6.2 shows the current responses and peak potentials (vs. Ag/AgCl) for SWV analyses (Figure 6.3) obtained during AA analysis at the BGCE, fMWCNT-GCE, CoPc/fMWCNT-GCE and CoTSPc/fMWCNT-GCE.

Table 6.2: The current responses and peak potentials (vs. Ag/AgCl) for 150 µM AA at the BGCE, fMWCNT-GCE, CoPc/fMWCNT-GCE and CoTSPc/fMWCNT-GCE during SWV analysis with AA exclusion (%) and shift in potential versus the BGCE

Modification	Current (µA)	AA Exclusion vs. BGCE (%)	Potential (V)	Potential shift (vs. BGCE)
BGCE	3.49 (±0.035)	0	0.00 (±0.003)	-
fMWCNT-GCE	2.09 (±0.079)	40.12	0.02 (±0.003)	+ 0.02
CoPc/fMWCNT-GCE	0.22 (±0.027)	93.70	0.01 (±0.002)	+ 0.01
CoTSPc/fMWCNT-GCE	0.09 (±0.011)	97.42	0.02 (±0.001)	+ 0.02

As previously observed in Figure 6.1, a decrease of 1.4 µA in the AA current response was observed upon addition of fMWCNTs to the GCE surface (2.09 ±0.079 µA) compared to the unmodified GCE (3.49 ±0.035 µA). This was due to the negatively charged carboxyl groups on the fMWCNTs, formed as a result of the CNT functionalisation, repelling the negatively charged AA molecules at pH 7.4 (Zhang *et al*., 2005; Yin *et al*., 2006). Upon addition of CoPc to the fMWCNT mixture at the GCE surface (0.22 ±0.027 µA), a further decrease of 1.87 µA was observed for AA. This decrease shows that the cobalt metal centre interacts unfavourably with AA causing the observed decrease. This response that the cobalt metal centre exhibits towards AA has been shown in previous work (Girenko *et al.*, 2002). Alternatively, the CoPc may be forming an insulating layer (refer to Chapter 3.4.5.) that would inhibit or hinder movement of the analyte towards the GCE surface. The insulating layer would be formed as a result of the complete coverage of the GCE surface with the CoPc complexes, immobilised at the GCE surface due to π-π interactions with the fMWCNT walls.

Addition of sulphonate groups to the CoPc/fMWCNT mixture, thereby forming the CoTSPc/fMWCNT mixture, exhibited a further decrease of 0.13 µA in the AA response (0.09 ±0.011 µA) compared to the CoPc/fMWCNT-GCE. This resulted in a 97.42 % decrease in the response obtained with 150.0 µM AA at the CoTSPc/fMWCNT-GCE over that of the BGCE. Oni & Nyokong (2001) described how the observed exclusion, or deactivation, in AA current response at a MTSPc is due to negative interactions between the AA and negatively charged sulphonate groups on the MPc ring at physiological pH. This is simply described as the repulsion of the negative, or like, charges on the AA molecules and the sulphonate groups. Therefore, by combining the exhibited effects of CoTSPc with those of the fMWCNTs, exclusion of AA can be achieved up to a concentration of 130.0 µM AA.

6.4.3. Electrode kinetics for ascorbic acid at the BGCE and modified-GCEs

6.4.3.1. Passivation

A decrease in the current response after six consecutive scans without stirring is indicative of electrode passivation or fouling, as illustrated in Figure 6.4, for the BGCE (a) and CoTSPc/fMWCNT-GCE (b). A plot of current response passivation,

expressed as a percentage of the initial scan, versus the number of scans for the BGCE and all other GCE modifications is illustrated in Figure 6.5.

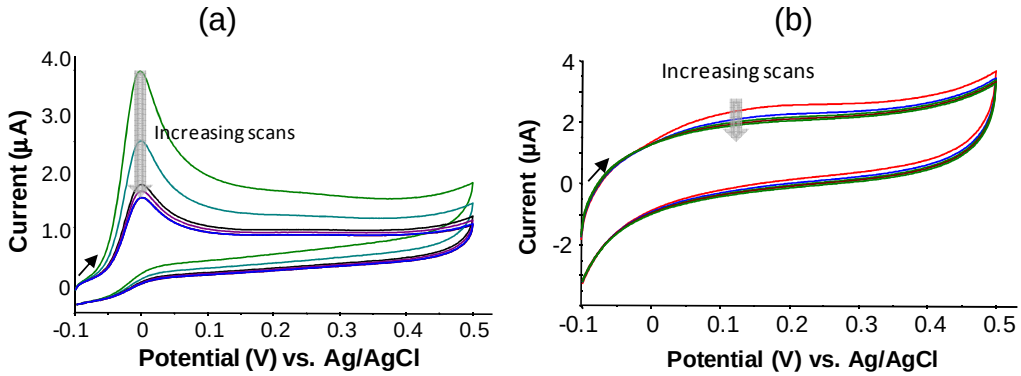

Figure 6.4: CVs of AA fouling at the BGCE (a) and CoTSPcfMWCNT-GCE (b) pH 7.4). [AA] = 150 µM; Scan rate = 50 mV/s

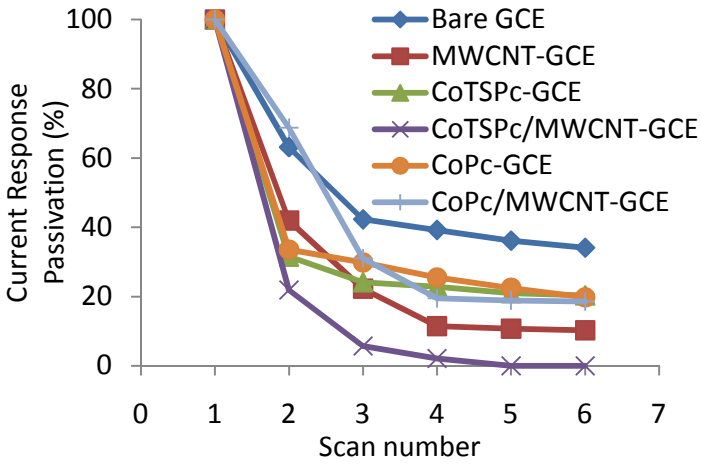

Figure 6.5: Comparisons in fouling, or loss in percentage current response, between the BGCE, CoTSPc/fMWCNT-GCE and other modified GCEs (pH 7.4). [AA] = 150 µM

A total percentage current response decrease of 65.0 % was observed for the BGCE after six consecutive scans, as demonstrated in Figure 6.4(a) and Figure 6.5. Complete passivation of the GCE occurred when modified with the CoTSPc/fMWCNT layer after five consecutive scans (Figure 6.4b and Figure 6.5). The remaining modified layers exhibited an almost complete passivation of the GCE for AA, which ranges between 80 and 90 %, after six consecutive CV scans (Figure 6.5). A greater reduction in the current responses during the fouling studies demonstrates that the modified layers are more effective at excluding AA upon consecutive scans due to accumulation of the oxidised products of AA. While passivation due to fouling has not been utilised as a means of enhancing selectivity,

it is of interest that the CoTSPc/fMWCNT layer slows the rate of passivation for DA detection compared to the BGCE (Figure 5.6), aiding in selectivity of DA.

6.4.3.2. Mode of transport

CVs for AA conducted at various scan rates (50, 100, 200, 300, 400 and 500 mV/s) at a BGCE (a) and CoTSPc/fMWCNT-GCE (b) are illustrated in Figure 6.6. The plot of current response versus the square root of the scan rate is demonstrated in Figure 6.7.

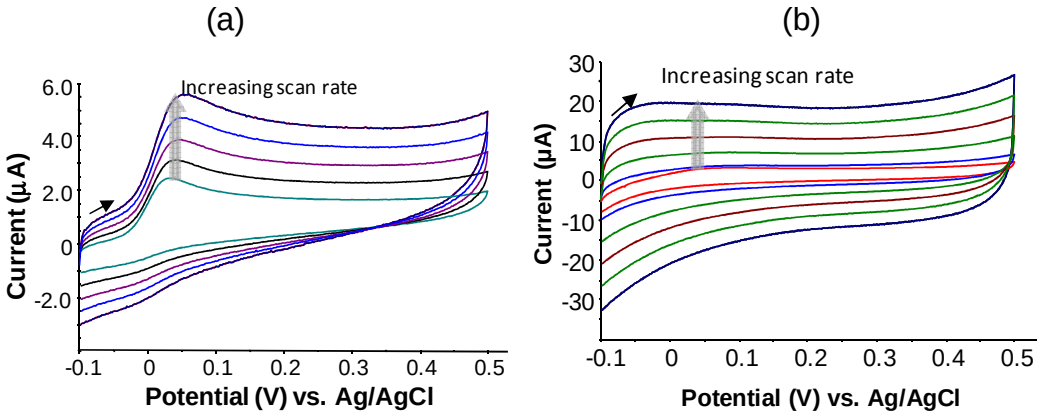

Figure 6.6: CVs of AA at the BGCE (a) and CoTSPc/fMWCNT-GCE (b) with the following scan rates: 50, 100, 200, 300, 400 & 500 mV/s. [AA] = 150 µM

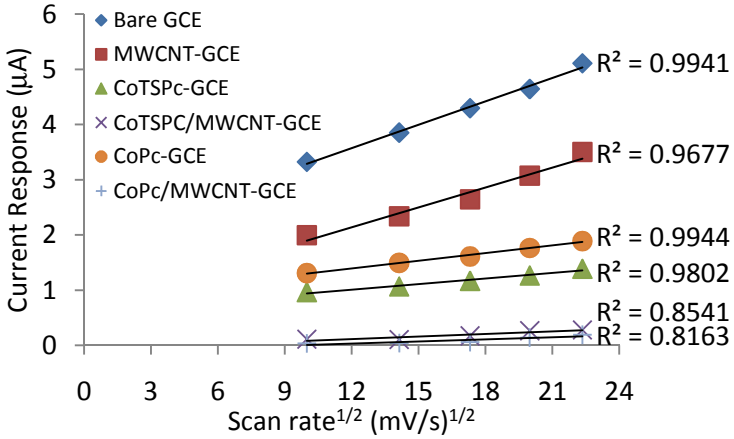

Figure 6.7: Effect of the square root of the scan rate on the current response of AA at the BGCE and CoTSPc/fMWCNT-GCE compared with other modified GCEs (c) (pH 7.4). [AA] = 150 µM

A proportional increase in the current response for AA was observed at the BGCE upon the increase in scan rate. Analyses of the AA current responses versus the square root of the various scan rates for the BGCE and various modified GCEs were linear with a positive slope (Figure 6.7). This indicates that transport of AA towards the oxidising GCE surface, in presence and absence of a modifying layer, is diffusion controlled. Increases in the scan rate for AA at the CoTSPc/fMWCNT-GCE did not

result in an increase in the anodic peak amplitude, demonstrating that AA exclusion is not linked to limitations in the transport of AA to the GCE surface.

6.4.3.3. LOD & LOQ

Table 6.3 shows the LOD and LOQ for the CV analysis of AA compared to DA at the BGCE and CoTSPc/fMWCNT-GCE with the concentration expressed as micromolar (µM) and nanomolar (nM) for AA and DA, respectively. Two GCEs were used to determine the LOD and LOQ in order to ascertain inter-electrode reproducibility. The variation between the two GCEs for AA was, on average, 2.1 ±0.09 % with 92.0 ±0.20 % intra-electrode reproducibility.

Table 6.3: The LOD and LOQ, in µM, for AA compared to DA at the BGCE and CoTSPc/fMWCNT-GCEs obtained during SWV analysis.

	AA		DA	
Modification	LOD (µM)	LOQ (µM)	LOD (µM)	LOQ (µM)
BGCE	0.539	1.633	6.13	18.57
CoTSPc/fMWCNT-GCE	130.0	433.3	0.0143	0.0433

The LODs and LOQs for AA at both the BGCE and CoTSPc/fMWCNT-GCE were higher than those obtained for DA, demonstrating a substantially lowered sensitivity for AA. Oni & Nyokong (2001) reported an LOD for DA that was in the micromolar range, which was substantially less sensitive than the LOD reported at the CoTSPc/fMWCNT-GCE (14.3 nM) presented here.

6.4.4. Detection of dopamine in presence of ascorbic acid at the CoTSPc/fMWCNT-GCE

Figure 6.8 demonstrates the effect that an increased ionic concentration of AA has on the DA peak amplitude when AA was excluded.

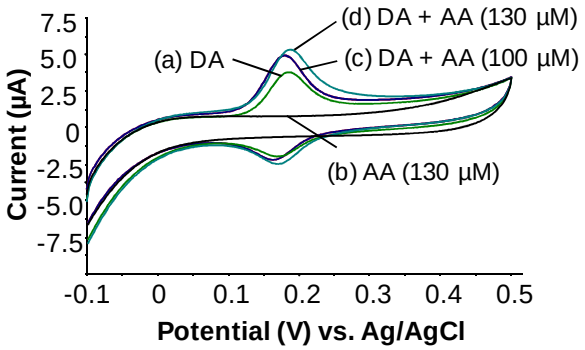

Figure 6.8: CVs of (a) DA; (b) AA (130.0 µM); (c) DA with AA (100.0 µM); and, (d) DA with AA (130.0 µM) at the CoTSPc/fMWCNT-GCE. [DA] = 19.6 µM; Scan rate = 50 mV/s.

An increase in the current response for DA was observed upon further addition of AA to the DA and AA (100 µM) mixture, resulting in a final AA concentration of 130.0 µM. However, the AA peak was not observed at its potential of 0.0 V (vs. Ag/AgCl) indicating exclusion of AA. Therefore, when analysing DA in presence of AA, the increased current response at the CoTSPc/fMWCNT-GCE can be attributed to an increase in the ionic strength particularly at the CoTSPc/fMWCNT-GCE.

The SWVs and plots thereof that demonstrate the linearity for DA in the absence of AA at the BGCE and CoTSPc/fMWCNT-GCE are illustrated in Figure 5.4 in Chapter 5.4.3.1. The SWVs that illustrate the linearity of DA in the presence of AA at the BGCE and CoTSPc/fMWCNT-GCE are shown in Figure 6.9 and Figure 6.10, respectively.

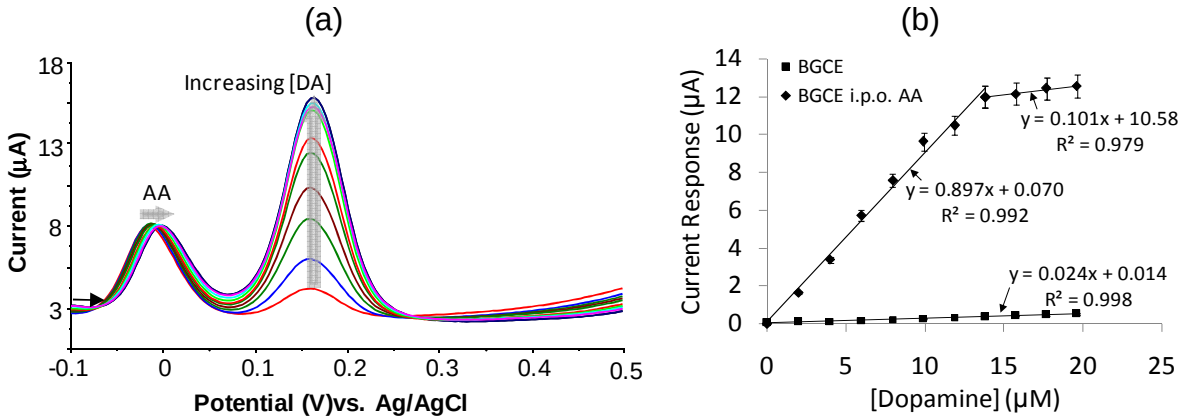

Figure 6.9: (a) SWVs of the uniform increase in the concentration of DA (0 to 19.6 µM) in the presence of a constant concentration of AA at the BGCE at pH 7.4. [AA] = 130 µM. (b) Standard curve plots of DA concentration, in absence and presence of AA, versus the current response at BGCE. (*n* = 3)

The observed AA peak potential was 0.16 V (vs. Ag/AgCl) less positive than the DA peak potential at the BGCE in phosphate buffer, pH 7.4. This is similar to previous reports on the oxidation potentials of these analytes at gold electrodes (Giz *et al.*, 1999), graphite electrodes (Duong *et al*., 1998), carbon fibre electrodes (Gonon *et al*., 1981) and GCEs (Adams, 1976). However, further studies are required in order to determine the influence that different buffer systems have on AA exclusion and DA detection at the CoTSPc/fMWCNT-GCE. Upon the increase in the concentration of DA at the BGCE, a shift in the AA oxidation peak towards more positive potentials indicates an increase in the difficulty of AA oxidation (Figure 6.9). Two linear trends were observed upon the increase in the DA concentration with one linear trend observed between 0 and 13.72 µM and the other between 13.72 and 19.6 µM. Therefore, a limit in linearity was reached in DA detection towards the higher concentrations due to saturation of the GCE and co-adsorption effects.

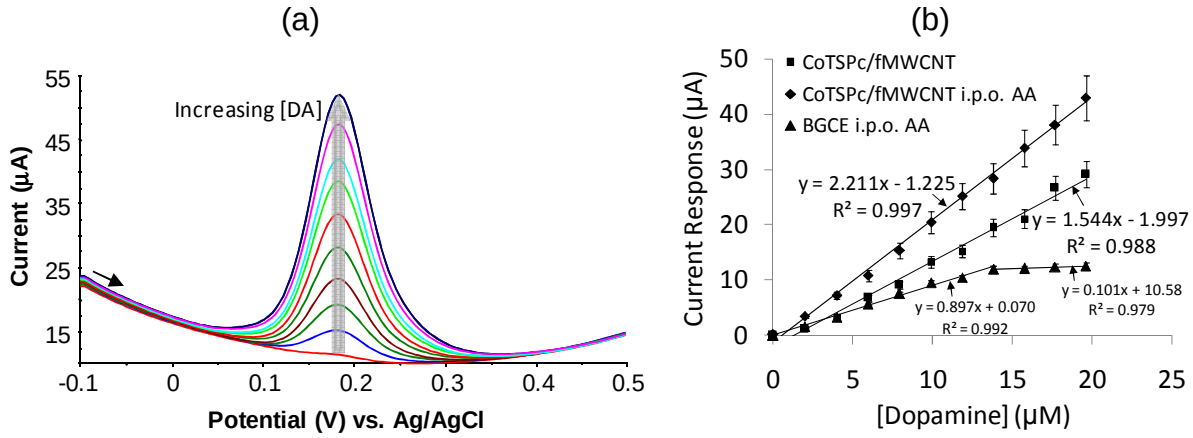

Figure 6.10: (a) SWVs of the uniform increase in the concentration of DA (0 to 19.6 µM) in the presence of a constant AA concentration at the CoTSPc/fMWCNT-GCE. [AA] = 130 µM. (b) Standard curve plots of DA concentration, in presence and absence of AA, versus the current response at CoTSPc/fMWCNT-GCE versus the BGCE in presence of AA. (*n* = 3)

Upon the increase of DA at the CoTSPc/fMWCNT-GCE, a linear response was obtained for DA with an R^2 value of 0.996 and a variation in the current response between 6.4 and 10.1 %. This indicates that the DA can be accurately measured throughout the concentration range measured. The sensitivity for DA remains similar to that observed at the CoTSPc/fMWCNT-GCE in the absence of AA (Figure 5.4). AA did not influence DA linearity as AA was excluded during oxidation analysis. Similar findings were reported for DA in the presence of AA at a FeTSPc-CPE (Oni & Nyokong, 2001).

A comparative illustration of DA responses during the above SWV analyses in the presence and absence of AA was compiled in order to better compare the exhibited DA responses. Figure 6.11 illustrates the SWV comparisons between DA detection in the presence and absence of AA at the BGCE and CoTSPc/fMWCNT-GCE.

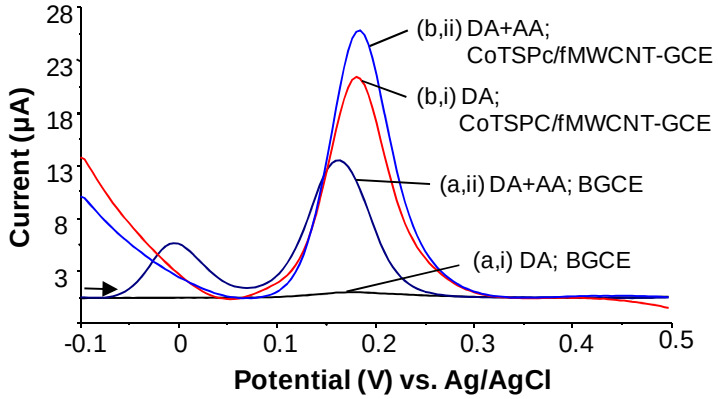

Figure 6.11: SWVs of (i) DA alone and (ii) in the presence of AA at (a) BGCE and (b) CoTSPc/fMWCNT-GCE. [DA] = 19.6 μM, [AA] = 130 μM.

As illustrated, AA did indeed affect the DA current response in that an increase in the current response for DA at the BGCE was observed in the presence of AA compared to in the absence of AA. This was, however, indeed due to an increase in the ionic strength of the solution at the BGCE and CoTSPc/fMWCNT-GCE and not an increase in response due to the presence of AA as AA was excluded.

6.5. Conclusion

Following the studies of DA at the CoTSPc/fMWCNT-GCE, analysis of the effect of AA on DA detection at this electrode surface modification was of interest. The CoTSPc/fMWCNT-GCE resulted in the reproducible decrease and exclusion of AA up to a concentration of 130.0 μM, seven fold greater than the studied DA concentration (Figure 6.3). This electrode modification, therefore, shows exceptional promise for the exclusion of physiological concentrations of AA present in blood serum, ranging from 34.0 to 85.0 μM, which is far greater than that of DA (1.0 μM) (Da Silva *et al*., 2008). As a result, it would be of interest to determine DA levels in blood serum in the presence of AA and other interferents present in the biological

matrix. It must be, hence, noted that AA had little effect on DA response and linearity when DA was analysed in the presence of AA at the CoTSPc/fMWCNT-GCE.

Exclusion of AA (150.0 µM) was, indeed, observed at both the Nafion®/fMWCNT-GCE (100.0 % exclusion) and the CoTSPc/fMWCNT-GCE (97.4 ±0.08 % exclusion). However, when analysing AA exclusion, the effect that the electrode modification has on the analyte of interest, which in this case is DA, is of the utmost importance. The Nafion®/fMWCNT-GCE and CoTSPc/fMWCNT-GCE exhibited increases in the DA current response versus the BGCE; however, the greatest LOD for DA was observed at the CoTSPc/fMWCNT-GCE (14.3 nM) compared to the BGCE (613.0 nM) and Nafion®/fMWCNT-GCE (133.9 nM). Furthermore, position and shifts in peak potential demonstrated that DA was more easily oxidised at the CoTSPc/fMWCNT-GCE (0.17 V vs. Ag/AgCl) than at the Nafion®/fMWCNT-GCE (0.24 V vs. Ag/AgCl), resulting in improved kinetics at the CoTSPc/fMWCNT-GCE. Therefore, the CoTSPc/fMWCNT-GCE was the electrode of choice for DA detection and offered a novel method, unlike the more traditional method of Nafion® modification, with which to achieve increased sensitivity towards DA whilst excluding AA at a higher concentration.

Therefore, in short, this work utilising the CoTSPc/fMWCNT hybrid sensor represents the most viable solution for selective DA detection in the presence of AA, well within physiological concentrations reported in literature to date.

Chapter 7

Surface topography and electron transfer characteristics

7.1. Introduction

Analysis of the surface layering in terms of impedance, as well as direct imaging, may provide further insights into the observed effects in analyte detection at the various layer modifications. For these purposes, Atomic Force Microscopy (AFM) provides images with nanoscale resolution of surfaces whilst impedance spectroscopy provides insights into electron flow at the modified electrodes.

7.2. Aim

Impedance spectroscopy and surface imaging were performed in order to assess electron flow and diffusion characteristics at the unmodified GCE, fMWCNT-GCE, CoTSPc-GCE and CoTSPc/fMWCNT-GCE.

7.3. Experimental procedure

7.3.1. Chemicals and reagents for impedance spectroscopy

A working solution of 5.0 mM potassium hexacyanoferrate (Merck, Germany) was prepared in 0.2 M potassium phosphate buffer, pH 7.4.

7.3.2. Preparation of electrodes

The GCEs were modified as described in Chapter 5.3.4.

7.3.3. Electrochemical apparatus and electrode pretreatment

The electrochemical cell was set up and pretreatment carried out as described in Chapter 2.3.2.1. and 2.3.2.2., respectively. The preliminary CV scans were carried out as described in Chapter 3.3.5.

7.3.4. Impedance spectroscopy

The set up that was used for the impedance spectroscopy involved the three electrode system, as described in Chapter 2.3.2.1.; however, a working solution of

5.0 mM potassium hexacyanoferrate made up in 0.2 M potassium phosphate buffer, pH 7.4, was used. Impedance spectroscopy analyses were carried out as described in Chapter 3.3.5.

7.3.5. Atomic force microscopy (AFM)

Sample layers were mounted on a polished carbon disk (0.28 cm^2; BAS). The AFM images were recorded in the non-contact mode in air at 20 ±2.0 ^oC with a CP-11 Scanning Probe microscope from Veeco Instruments (Carl Zeiss, South Africa) at a scan rate of 0.8 Hz.

7.4. Results and Discussion

7.4.1. Electron characteristics using impedance spectroscopy

The Nyquist plot (Figure 7.1) demonstrates that the BGCE, fMWCNT- and CoTSPc/fMWCNT-GCE exhibited similar electron flow characteristics in that linear responses were obtained. These linear responses demonstrate that there was little to no impedance, or resistance, to the electron flow from solution to the GCE surface.

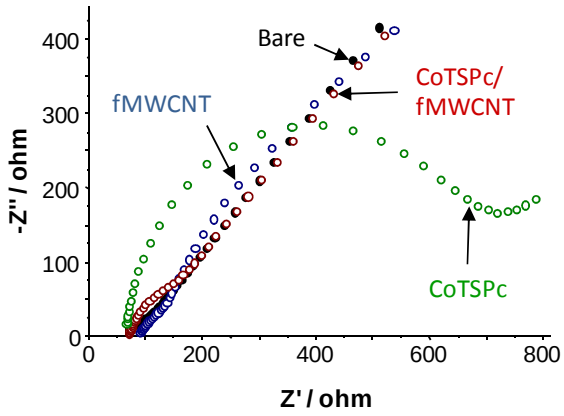

Figure 7.1: Nyquist plots of the BGCE, CoTSPc-, fMWCNT- and CoTSPc/fMWCNT-GCE using 5.0 mM potassium hexacyanoferrate in 0.2 M potassium phosphate buffer, pH 7.4.

As observed in Figure 7.1, the greatest hindrance in electron flow was observed at the CoTSPc-GCE as this modification exhibited the greatest variation in linearity, seen by the larger semi-circle, followed by a Warburg line corresponding to diffusion in the process. According to Scully *et al.* (1993), the size of this semi-circle is indicative of the degree of resistance experienced by electron flow. The increase in

the resistance is attributed to the instability of the CoTSPc in the aqueous environment. This is observed by the dispersion of the CoTSPc into solution upon immersion of the CoTSPc-GCE into the working solution, which would result in increased electrolyte resistance and an alteration in the current flow path (Scully *et al.,* 1993). This alteration would, hence, slow the movement of electrons in the solution surrounding the immediate area around the GCE surface, causing resistance and the observed effects, as seen in Chapter 3.4.5.

Upon inspection of the lower ohmic responses, differences were observed in linearity between the BGCE, fMWCNT-GCE and CoTSPc/fMWCNT-GCE (Figure 7.2). The BGCE exhibited characteristic linearity (Scully *et al.*, 1993) with slight resistance experienced at the lower ohmic values. This is due to the resistance caused by BGCE conditioning and fouling of the BGCE after the preliminary CV analysis.

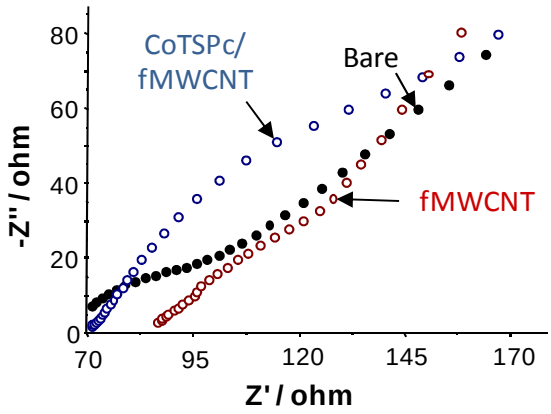

Figure 7.2: Nyquist plots of the change in linearity for the BGCE, fMWCNT-GCE and CoTSPc/fMWCNT-GCE

The fMWCNT-GCE exhibited linearity similar to that of the BGCE, as observed in Figure 7.2. However, this linearity was uneven with a broad semi-circle demonstrating a low degree of resistance. This resistance is attributed to hindrance caused by the aggregation of the fMWCNTs on the GCE surface. Greater resistance was observed for the CoTSPc/fMWCNT-GCE when compared to the BGCE and fMWCNT-GCE. This is due to leaching of the unattached CoTSPc on the CoTSPc/fMWCNT-GCE into the solution in the vicinity of the GCE surface, causing the observed resistance. However, improved electroconduction or electron flow would result upon the addition of fMWCNTs to the layer and/or electrode surface as fMWCNTs improve electron transfer towards the GCE surface, as previously

discussed. This demonstrates that fMWCNTs improve the stability and electron flow kinetics when CoTSPc is applied to the GCE surface.

The Bode plot gives an indication of the insulatory effects given by the layer on the GCE surface. The Bode plots for the BGCE, CoTSPc-GCE, fMWCNT- and CoTSPc/fMWCNT-GCE in 5.0 mM potassium hexacyanoferrate is given in Figure 7.3.

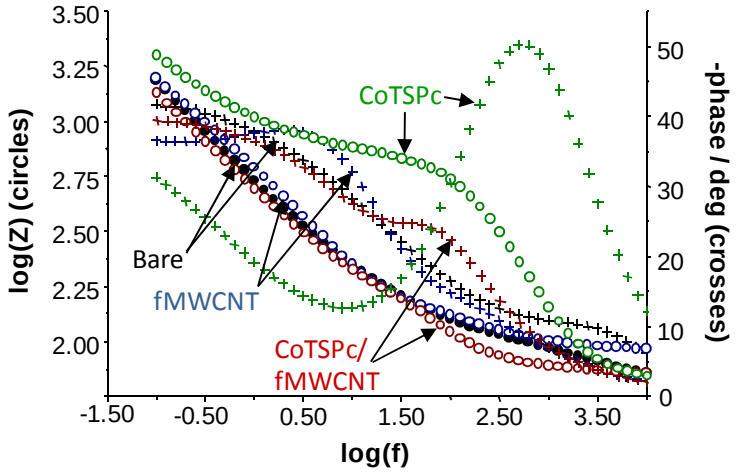

Figure 7.3: Bode plots of the BGCE (black), CoTSPc- (green), fMWCNT- (blue) and CoTSPc/fMWCNT-GCE (red) using 5.0 mM potassium hexacyanoferrate in 0.2 M potassium phosphate buffer, pH 7.4.

In Figure 7.3, a large change in the phase degree is indicative of an insulating layer or a layer more likely to act as a capacitor (Lakshminarayanan & Sur, 2003). The BGCE, fMWCNT- and CoTSPc/fMWCNT-GCEs exhibited trends that were porous or not insulating as these layers had minor changes in their phase versus log of the frequency profiles. As seen with the BGCE (black crosses (+)), a peak at approximately 0.35 $hz^{1/2}$ gives an indication of a low degree of insulation caused by fouled redox products. The fMWCNT-GCE exhibits a higher degree of capacitance, seen by the larger peak at 0.5 $hz^{1/2}$. This is due, as previously mentioned, to the aggregated fMWCNTs that would hinder electron flow. This insulatory effect is, however, reduced by the catalytic properties of the fMWCNTs and, hence, the ability to shuttle electrons. The greatest phase degree was observed with the CoTSPc-GCE. Due to resistance being affected by the solvation of CoTSPc into solution from the GCE surface, the insulatory effect or capacitance can be similarly affected. This is due to the layer of suspended CoTSPc in the aqueous environment in the direct

vicinity of the GCE surface. However, the CoTSPc-GCE did not act as a perfect insulator as the degree of capacitance would be greater, as observed at the Nafion®-GCE (Chapter 3.4.5.). A lower degree of insulation was observed at the CoTSPc/fMWCNT-GCE as the electro-conducting properties of the fMWCNTs would lower any insulatory effects caused by the CoTSPc, allowing increased electron flow (as observed above in Figure 7.1 and Figure 7.2). Moreover, a reduction in the phase degree may be attributed to improved charge distribution brought about by the synergy that exists between fMWCNTs and CoTSPc, resulting in improved electron flow and lowering of any insulatory effects.

Therefore, the CoTSPc and fMWCNTs mixture is effective at simultaneously reducing resistance and any insulatory effects when compared to CoTSPc at the GCE surface.

7.4.2. Surface topography using AFM

AFM imaging was used in order to view the bare, fMWCNT and CoTSPc/fMWCNT surfaces, as illustrated in Figure 7.4.

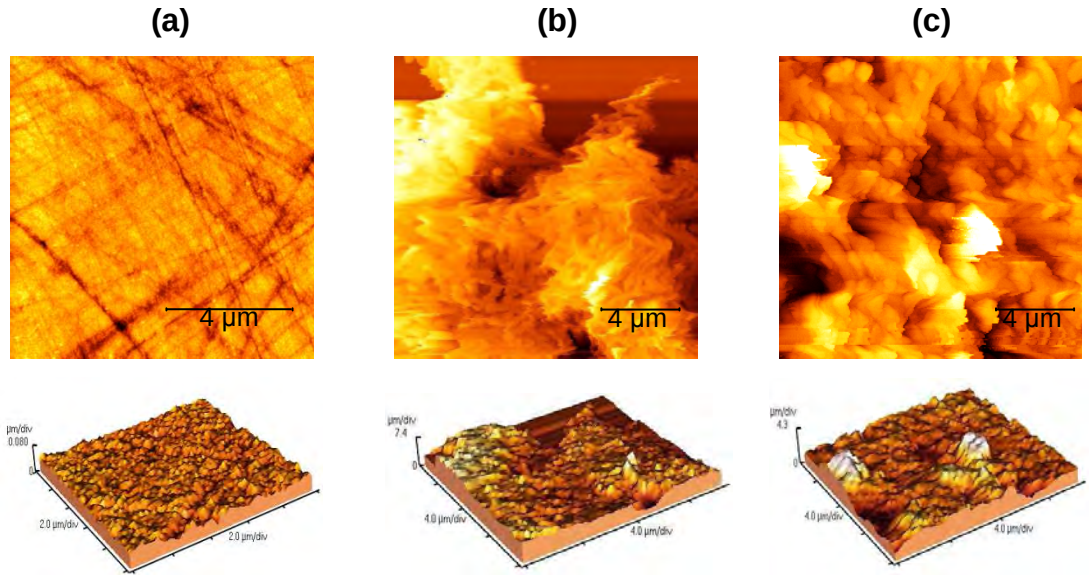

Figure 7.4: AFM images of (a) BGCE, (b) fMWCNT-GCE and (c) CoTSPc/fMWCNT-GCE. Scale bar represents 4.0 µm.

AFM imaging of the bare GCE surface (Figure 7.4a) revealed that it was relatively uneven. This surface would affect electrochemical analyses in terms of reproducibility and passivation. Since this surface cannot be used for analyses, it

remains ideal for imaging purposes as modification through the drip-dry method is not solely reliant on surface smoothness as in the case of self-assembled monolayer (SAM) formation. Aggregation of the fMWCNTs at the GCE surface is observed in Figure 7.4(b) and (c) with observable pores present in the layer. These pores may aid in the transport of analyte or electrons through to the GCE surface. The average roughness values for the BGCE, fMWCNT- and CoTSPc/fMWCNT-GCE are 5.1, 895.1 and 351.3 nm, respectively. A reduction in the average roughness of the fMWCNT layer was observed upon addition of CoTSPc into the fMWCNT mixture. The mean heights for the BGCE, fMWCNT- and CoTSPc/fMWCNT-GCE were 41.4 nm, 3.7 μm and 1.8 μm, respectively. A reduction in the average height of the fMWCNT layer was observed upon addition of CoTSPc into the fMWCNT mixture. These reductions in the roughness and height are evidence that the CoTSPc aids in the dispersion of the fMWCNTs due to electrostatic interactions. These electrostatic interactions can be described by the hybridisation (Schulte, 2008) between the cobalt metal centre with the carbon nanotube walls and resultant repelling forces between the like charges on the CoTSPc molecules and the fMWCNTs.

7.5. Conclusion

The addition of fMWCNTs to an insulating layer, such as that of an MPc, on the GCE results in an increase in the efficiency of electron flow from the working solution to the GCE surface. Therefore, sensitivity towards an analyte of interest is enhanced due to the increased flow of electrons, thus enhancing the efficacy of an analysis. Electron flow is further enhanced at the CoTSPc/fMWCNT-GCE due to the presence of pores. The pores aid movement of a desired analyte, such as DA (Chapter 5), and hinder the movement of an interfering analyte, such as AA (Chapter 6), towards the GCE surface, thereby aiding specificity. CoTSPc also aids in dispersion of fMWCNTs, which may explain the enhanced exclusion of AA at this surface when compared to the fMWCNT layer, as shown in Chapter 6.

Chapter 8

General Conclusions and Future Recommendations

8.1. General Conclusions

In this thesis, several different surface modifications were examined aimed at enhancing the selective and sensitive detection of tryptophan (Trp) in presence of melatonin (Mel), and for dopamine (DA) in the presence of ascorbic acid (AA). In the process, a greater understanding of the surface modifications examined was sought. Table 8.1 summarises the main findings in terms of sensitivity and selectivity through peak separation

Trp detection in the presence of Mel was examined with the following modifications: 1) enzymatic through biosensor development; 2) pH tuning through Nafion®; 3) a mixture of fMWCNTs in Nafion® solution; and, 4) a suspension of fMWCNTs in a solution of CoTSPc.

The biosensor, modified with Trpase, demonstrated catalysis of Trp at the surface; thus, a negative effect on sensitivity towards Trp was observed. Adsorption of Trp to the inert protein, BSA, was also demonstrated at the BSA/GA-GCE control. As a result, chemical methods of obtaining sensitivity and specificity for Trp and DA were employed with varying degrees of success. Addition of signal enhancers, such as fMWCNT, result in increases in sensitivity for Trp over the BGCE and individually modified GCEs, as summarised in Table 8.1. Increased current responses for Trp and Mel were observed in acidic solutions (pH 3.0) at the Nafion®-modified GCE over the BGCE, demonstrating improved sensitivity towards Trp and Mel, as shown in Table 8.1. Improved selectivity towards Trp in the presence of Mel and DA was achieved at pH 3.0 through separation of the respective oxidation peaks, as proven in the dietary supplement, Serene Tranquillity® Night with Tryptophan. Therefore, sensitivity and selectivity for Trp was achieved through pH manipulation and the resulting charge interactions between Trp and the Nafion® layer at the GCE surface with the presence of fMWCNTs at the Nafion®-GCE surface resulting in further signal enhancement.

When sensitivity and selectivity were determined using cation exchange electrocatalysts, namely CoTSPc, immobilised at the GCE surface using fMWCNTs (CoTSPc/fMWCNT-GCE), minimal changes in the current response were observed compared to that of the BGCE at pH 7.4, demonstrating minimal changes in cation exchange effects. However, the increase in the Trp current response at pH 3.0 over that of the BGCE demonstrated that the CoTSPc/fMWCNT-GCE did in fact exhibit cation exchange capabilities towards Trp at more acidic pH values. However, sensitivity remained lower than that exhibited for Trp at the Nafion®-GCE. This demonstrates that although the cation exchange effects exist at the CoTSPc/fMWCNT-GCE, they were not as pronounced as at the Nafion®-GCE at pH 3.0. Contrary to the observed effects on the Mel current response at the Nafion®-GCE, a decrease in current response was observed at pH 3.0 and 7.4 at the CoTSPc/fMWCNT-GCE when compared to the BGCE. This is indicative of the absence of any cation exchange effects exhibited towards Mel at this layer.

Therefore, in terms of sensitivity and selectivity for Trp in the presence of Mel, the Nafion®-GCE exhibited the optimal response as the greatest peak separation and difference in current responses was observed between Trp and Mel, as observed in Table 8.1. However, the Nafion®/fMWCNT-GCE yielded the greatest sensitivity towards Trp (LOD = 1.62 nM).

DA detection in the presence of AA was examined at the following surface modifications: 1) Nafion® with fMWCNTs; and, 2) a suspension of fMWCNTs in a solution of CoTSPc. Sensitive and selective detection of DA was achieved at both the Nafion®/fMWCNT-GCE and CoTSPc/fMWCNT-GCE at physiological pH. These modified GCEs exhibited increases in current response, and thus sensitivity, for DA over that of the BGCE, Nafion®-GCE and CoTSPc-GCE. This can be attributed to the positive influence of the electroconducting effects exhibited by the fMWCNTs. Moreover, the increase in sensitivity can be attributed to the accumulation of DA at the GCE surface brought about by charge interactions between the cationic (positively charged) DA and the anionic (negatively charged) Nafion® and CoTSPc. Complete exclusion of AA was observed under physiological conditions at the Nafion®/fMWCNT-GCE (150.0 μM) and CoTSPc/fMWCNT-GCE (130.0 μM) as a

result of the respective charge interactions between the anionic AA, ionised fMWCNTs (with COO^- groups) and anionic Nafion® and CoTSPc. Therefore, selective detection of DA was achieved through the exclusion of its common electrochemical interferent, AA. However, the system developed yielded the greatest sensitivity for DA (LOD = 14.3 nM) compared to the Nafion®/fMWCNT-GCE (LOD = 133.9 nM). AFM showed that the observed improvements are linked to an increased dispersion of fMWCNTs.

Enzyme modified sensors have distinct advantages (specificity) and disadvantages (catalysis). Specificity may be affected by the enzyme of interest having more than one substrate and by adsorption of hydrophobic molecules to the protein complexes which may cause unnecessary interference. Addition of signal enhancers, such as fMWCNT, result in increases in sensitivity for all analytes over the BGCE, as summarised in Table 8.1. The increase in sensitivity demonstrates that an increased ease in the flow of electrons towards the GCE surface occurred, confirmed by impedance spectroscopy. This effect was associated with a shift in the oxidation potential of an analyte towards a more negative potential confirming the increase in the ease of oxidation in the presence of fMWCNTs.

The Nafion®-GCE, Nafion®/fMWCNT-GCE and CoTSPc/fMWCNT-GCE exhibited excellent selectivity towards DA in presence of AA at physiological pH and towards Trp in presence of Mel at acidic pH. These layers contain negatively charged sulphonate groups that allow the cation exchange capabilities to occur; thereby, allowing selectivity of an analyte, particularly DA and Trp, to occur in presence of their respective interferents. A sensitive response towards the afore mentioned analytes was also observed at the CoTSPc/fMWCNT-GCE and Nafion®-GCE, respectively, attributable to the cation exchange and resulting accumulation effects. These layers, therefore, offer advantages over the other electrode modifications studied, which include enzymatic and electro-conducting modifiers.

Therefore, chemical methods of the electrochemical detection of an analyte can be employed to obtain both selectivity and sensitivity through pH manipulation and the resulting charge interactions between the analytes and the modified layers.

Table 8.1: The LODs (nM), LOQs (nM) and peak potentials (V vs. Ag/AgCl) for Trp, Mel, DA and AA at the various GCE modifications during SWV analysis (unless otherwise stated).

	Trp			Mel			DA			AA		
GCE Modification	LOD (nM)	LOQ (nM)	Potential (V)	LOD (nM)	LOQ (nM)	Potential (V)	LOD (nM)	LOQ (nM)	Potential (V)	LOD (µM)	LOQ (µM)	Potential (V)
BGCE	14.91	45.19	0.86	13.5	40.44	0.82	613.0	1857.0	0.17	0.539	1.633	0.00
Trpase/BSA/GA-GCE (CV; pH 8.3)	18.45	55.9	0.81	-	-	-	-	-	-	-	-	-
Nafion®-GCE*	1.62	5.40	0.86	1.60	5.33	0.66	1045.1	3167.0	0.26	118.8	360.0	0.17
Nafion®/fMWCNT-GCE (CV)*	0.59	1.79	0.86	0.80	2.42	0.69	133.9	405.7	0.24	150.0	454.5	N/A
CoTSPc/fMWCNT-GCE (pH 3.0)	179.0	543.0	0.89	1280.0	3880.0	0.84	-	-	-	-	-	-
CoTSPc/fMWCNT-GCE (pH 7.4)	749.0	2270.0	0.68	450.0	1350.0	0.74	14.3	43.3	0.18	130.0	433.3	0.02

* The LODs, LOQs and potentials at the Nafion®-GCE and Nafion®/fMWCNT-GCE are given at pH 3.0 for Trp and Mel and pH 7.4 for DA and AA.

8.2. Recommendations for future work

The CoTSPc/fMWCNT-GCE was effective in the elimination of AA during the selective determination of DA. However, there are a number of electrochemical interferents present during the detection of DA in biological fluids. These include uric acid and serotonin. The detection and analysis of serotonin in the presence of DA offers many advantages in the medical field due to the biological significance of serotonin. Therefore, it would be of interest to determine the effect that the CoTSPc/fMWCNT-GCE has on serotonin detection, as well as elimination of uric acid interference.

Following the assessment of analyte interference, detection of the biologically significant molecules, DA and serotonin, in complex biological samples, such as blood serum and urine, should be conducted. This would be carried out in order to assess the feasibility of the CoTSPc/fMWCNT-GCE for real samples and potential commercial application. However, in order for commercialisation to be feasible, the life-span or shelf-life of the CoTSPc/fMWCNT-GCE would need to be assessed under various conditions, with respect to temperature, relative humidity and exposure to oxygen and light, in order to determine optimal storage conditions. Determination of optimal storage conditions is required as it has been shown (Cook *et al*., 1995) that MPcs photooxidise when exposed to light for prolonged periods of time, affecting electrocatalysis.

Cation exchange capabilities of the CoTSPc/fMWCNT-GCE for Trp were demonstrated under acidic conditions. In order to assess the feasibility of the CoTSPc/fMWCNT layer as a cation exchange composite layer for other analytes, analysis and determination of a wider range of molecules and amino acids is required. Therefore, the CoTSPc/fMWCNT-GCE may offer advantages in the detection of other biologically relevant molecules and amino acids, such as phenylalanine or tyrosine, which have similar pKa values.

The cation exchange capabilities of the CoTSPc/fMWCNT-GCE may be further enhanced by the replacement of DMF with Nafion® as the solvent. This will provide the CoTSPc/fMWCNT with a greater number of sulphonate groups, potentially aiding

the cation exchange capabilities resulting in further enhancement of the Trp or DA current responses and exclusion of a higher concentration of AA. Conversely, addition of Nafion® to the CoTSPc/fMWCNT mixture may result in a decrease in the current responses of the desired analytes. Alternatively, it may be beneficial to ascertain the effects that a greater number of sulphonate groups have on DA and Trp detection through incorporation of a cobalt octasulphonate phthalocyanine if a decrease in current response with Nafion® is observed. Due to the fact that nanostructured materials offer distinct advantages over that of their microstructured counterparts, such as increased surface area, analysis of DA and Trp with nanoscaled CoTSPcs may of interest. Nano-scaled CoTSPcs may offer such advantages as increased current responses and improved interferent elimination.

References

1. Achtnich, U. R., Tiefenauer, L. X. & Andres, R. Y. (1992) Covalent immobilisation of avidin on glassy carbon electrodes as the basis for multivalent biosensors. *Biosensors and Bioelectronics*. **7**: 279-290.

2. Adams, R. N. (1976) Probing brain chemistry with electroanalytical techniques. *Analytical Chemistry*. **48**: 1126A-1138A.

3. Alex, K. D. & Pehek, E. A. (2007) Pharmacologic mechanisms of serotonergic regulation of dopamine neurotransmission. *Pharmacology and Therpeutics*. **113**:296-320.

4. Alexopolous, G., Meyers, B., Young, R., Mattis, S. & Kukuma, T. (1993) The course of geriatric depression with "reversible dementia": A controlled study. *American Journal of Psychiatry*. **150**: 1693-1699.

5. Alwarthan, A. A. (1993) Determination of ascorbic acid by flow injection with chemiluminescence detection. *Analyst*. **118**: 639-642.

6. Annesini, M. C., Di Carlo, C., Piemonte, V. & Turchetti, C. (2007) Bilirubin and tryptophan adsorption in albumin-containing solutions: I: Equilibrium isotherms on activated carbon. *Biochemical Engineering Journal*. **40**: 205-210.

7. Anzai, J., Shimada, M., Osa, T. & Chen, C-W. (1987) Enzyme sensors based on coated-wire electrode. Use of carboxyl substituted poly(vinyl chloride) as a support for immobilising penicillinase. *Bulletin for the Chemical society of Japan*. **60**: 4133-4137.

8. Anzai, J., & Osa, T. (1992) Langmuir-Blodgett membranes in chemical sensor applications. *Selected Electrode Reviews*. **12**: 3-34.

9. Babaei, A., Zendehde, M., Khalilzabeh, B. & Taheri, A. (2008) Simultaneous determination of tryptophan, uric acid and ascorbic acid at iron(III) doped zeolite modified carbon paste electrode. *Colloids and Surfaces B: Biointerfaces*. **66**: 226-232.

10. Banks, C. E., Moore, R. R., Davies, T. J. & Compton, R. G. (2004) Investigation of modified basal plane pyrolytic graphite electrodes: definitive evidence for the electrocatalytic properties of the ends of carbon nanotubes. *Chemistry Communications*. 1804-1805.

11. Betancor, L., López-Gallego, F., Hidalgo, A., Alonso-Morales, N., Mateo, G. D-O. C., Fernández-Lafuente, R. Guisán, J. M. (2006) Different mechanisms of protein immobilisation on glutaraldehyde activated supports: Effect of support activation and immobilisation conditions. *Enzyme and Microbial Technology*. **39**: 877-882.

12. Biggio, G., Fadda, F., Fanni, P., Tagliamonte, A. & Gessa, G. L. (1974) Rapid depletion of serum tryptophan, brain tryptophan, serotonin and 5-hydroxyindoleacetic acid by a tryptophan free diet. *Life Sciences.* **14:**1321–29.

13. Bilitewski, U. & Turner, A. P. F. (2000) In: *Biosensors for environmental monitoring*. Harwood Academic Publishers. Pp. 6-12, 137-150 & 548-270.

14. Biniak, S., Świątkowski, A. & Pakula, M. (2000) In: *Chemistry and Physics of Carbon*. Radovic, L. R. (Ed.), Vol. 27, CRC Press, New York. Pp. 154.

15. Blask, D.E., Sauer, L.A. and Dauchy, R.T. (2002) Melatonin as a chronobiotic/anti-cancer agent: cellular, biochemical and molecular mechanisms of action and their implications for circadian-based cancer therapy. *Current Topics in Medical Chemistry* **2**: 113-132.

16. Brabec, V. (1980) Electrochemical oxidation of nucleic acids and proteins at graphite electrode. Qualitative aspects. *Journal of Electroanalytical Chemistry*. **116**: 69-82.

17. Bramford, N. S., Zhang, H., Schmitz, Y., Wu, N. P., Cepeda, C., Levine, M. S., Schmauss, C., Zakharenko, S. S., Zablow, L & Sulzer, D. (2004) Heterosynaptic dopamine neurotransmission selects sets of corticostriatal terminals. *Neuron*. **42**: 653-663.

18. Brazell, M. P., Kasser, R. J., Renner, K. J., Feng, J., Moghaddam, B. & Adams, R. N. (1987) Electrocoating carbon fiber microelectrodes with Nafion improves selectivity for electroactive neurotransmitters. *Journal of Neuroscience (Methods)*. **22**: 167-172.

19. Britto, P. J., Santhanam, K. S. V. & Ajayan, P. M. (1996) Carbon nanotube electrode for oxidation of dopamine. *Bioelectrochemistry and Bioenergetics*. **41**: 121-125.

20. Britton, H. T. S. (1955) In: *Hydrogen Ions: Their determination and importance in pure and industrial chemistry*. Vol. 1 (4th Ed.) Chapman and Hall, London. Pp. 352-376.

21. Brookman, P. J. and Nicholson, J. W. (1986) In *Developments in Ionic Polymers* Wilson, A. D. & Prosser, H. J. (Eds.) Vol. 2. Elsevier Applied Science Publishers, London. pp. 269-283.

22. Brosseau, C.L., St. Maurice, M., Bearne, S.L. & Roscoe S.G. (2005) Electrochemical quartz crystal nanobalance (EQCN) studies of the adsorption behaviour of an enzyme, mandelate racemase, and its substrate, mandelic acid, on Pt. *Electrochim. Acta*. **50**: 1289-1297.

23. Cai, H., Cao, X, Jiang, Y., He, P. & Fang, Y. (2003). Carbon nanotube-enhanced electrochemical DNA biosensor for DNA hybridization detection. *Analytical and Bioanalytical Chemistry*. **375**: 287-293.

24. Capella, P., Ghasemzadeh, B., Mitchell, K. & Adams, R. N. (1990) Nafion-coated carbon fibre electrodes for neurochemical studies in brain tissue. *Electroanalysis*. **2**: 175-182.

25. Carlsson, A. & Lindqvist, M. (1957) 3,4-Dihydroxyphenylalanine and 5-hydroxytryptophan as reserpine antagonists. *Nature*. **180**: 1200.

26. Carlsson, A. & Lindqvist, M. (1963) Effect of chlorpromazine or haloperidol on formation of 3-methoxytyramine and normetanephrine in mouse brain. *Acta Pharmacology and Toxicology*. **20**: 140-144.

27. Chaubey, A. & Malhotra, B. D. (2002) Mediated Biosensors. *Biosensors and Electronics*. **17**: 451-456.

28. Chen, J., Hamon, M. A., Hu, H., Chen, Y., Rao, A. M., Eklund, P. C. & Haddon, R. C. (1998). Solution properties of single-walled carbon nanotubes. *Science*. **282**: 95-98.

29. Chen, Z., Okamura, K., Nanaki, M. & Nagaoka, T. (2002) Selective determination of tryptophan using a carbon paste electrode modified with an overoxidised polypyrrole film. *Analytical Sciences*. **18**: 417-421.

30. Chen, G. N., Zhao, Z. F., Wang, X. L., Duan, J. P. & Chen, H. Q. (2002a) Electrochemical behaviour of tryptophan and its derivatives at a glassy carbon electrode modified with hemin. *Analytica Chimica Acta*. **452**: 245-254.

31. Cook, , M. J., Chambrier, I., Cracknell, S. J., Mayes, D. A. & Russell, D. A. (1995) Octa-alkyl zinc phthalocyanines: Potential photosensitizers for use in the photodynamic therapy of cancer. *Photochemistry and Photobiology*. **62**: 542-545.

32. Cotzias, G. C., Van Woert, M. H. & Schiffer, L. M. (1967) Aromatic amino acids and modification of Parkinsonism. *North England Journal of Medicine*. **276**: 374-379.

33. Da Silva, R. P., Lima, A. W. O. & Serrano, S. H. P. (2008) Simultaneous voltammetric detection of ascorbic acid, dopamine and uric acid using a pyrolytic graphite electrode modified into dopamine solution. *Analytica Chimica Acta*. **612**: 89-98.

34. Day, T. M., Wilson, N. & Macpherson, J. V. (2004) Electrochemical and conductivity measurements of single-wall carbon nanotube network electrodes. *Journal of the American Chemical Society*. **126**: 16724-16725.

35. Deakin, M. R., Kovach, P. M., Stutts, K. J. & Wightman, R. M. (1986) Heterogenous mechanisms of the oxidation of catechols and ascorbic acid at carbon electrodes. *Analytical Chemistry*. **58**: 1474-1480.

36. de la Torre, G., Vázquez, P., Agullo-Lopez, F., & Tórres, T. (1998) Phthalocyanines and related compounds: organic targets for nonlinear optical applications. *Journal of Material Chemistry.* **8**: 1671-1683.

37. Dent, C. E., Linstead, R. P. & Lowe, A. R. (1934) 217. Phthalocyanines. Part VI: The Structure of the Phthalocyaines. *Journal of the Chemical Society*. 1033-1039.

38. Devanand, D., Sano, M., Tang, M-X., Taylor, S., Gurland, B., Wilder, D., Stern, Y. & Mayneux, R. (1996) Depressed mood and the incidence of Alzheimer's disease in the elderly living in the community. *Archives of General Psychiatry*. **53**: 174-182.

39. Dubocovich, M. L., Mansana, M. I. and Benloucif, S. (1999) Molecular pharmacology and function of melatonin receptor subtypes. *Advances in Experimental and Medical Biology.* **460**: 181-190.

40. Duong, B., Arechabaleta, R. & Tao, N. J. (1998) In situ AFM/STM characterization of porphyrin electrode films for electrochemical detection of neurotransmitters. *Journal of Electroanalytical Chemistry*. **447**: 63-69.

41. Ebbesen, T. W., Lezec, H. J., Hiura, H., Bennet, J. W., Ghaemi, H. F. & Thio, T. (1996) Electrical conductivity of individual carbon nanotubes. *Nature*. **382**: 54.

42. Emanuele, J. J., Heasley, C. J. & Fitzpatrick, P. F. (1995) Purification and charachterisation of the flavoprotein tryptophan-2-monooygenase expressed at high levels in *E. coli. Archives of Biochemistry and Biophysics*. **316**: 241-248.

43. Ensafi, A. A. & Hajian, R. (2006) Determination of tryptophan and histidine by adsorptive cathodic stripping voltammetry using H-point standar addition method. *Analytica Chimica Acta*. **580**: 236-243.

44. Ewing, A. G., Wightman, R. M. & Dayton, M. A. (1982) *In vivo* voltammetry with electrodes that discriminate between dopamine and ascorbate. *Brain Research*. **249**: 361-370.

45. Fahn, S. & Cohen, G. (1992) The oxidant stress hypothesis in Parkinson's disease. *Annals of Neurology*. **32:** 804–812.

46. Fang, B., Wei, Y., Li, M., Wang, G. & Zhang, W. (2007) Study on electrochemical behavior of tryptophan at a glassy carbon electrode modified with multi-walled carbon nanotubes embedded cerium hexacyanoferrate. *Talanta*. **72**: 1302-1306.

47. Fernstrom, J. D. & Wurtman R. J. (1971) Brain serotonin content: physiological dependence on plasma tryptophan levels. *Science.* **173:**149–52.

48. Fernstrom, M. H., Massoudi, M. S. & Fernstrom, J. D. (1990) Effect of 8-hydroxy-2-(di-n-propylamino)-tetralin on the tryptophan-induced increase in 5-hydroxytryptophan accumulation in rat brain. *Life Sciences*. **47**: 283-289.

49. Ferry, G., Ubeaud, C., Lambert, P., Bertin, S., Cogé, F., Chomarat, P., Delagrange, P., Serkiz, B., Bouchet, J., Truscott, R. J. W. and Boutin, J. A. (2005) Molecular evidence that melatonin is enzymatically oxidized in a different manner than tryptophan: investigations with both indoleamine 2,3-dioxygenase and myeloperoxidase. *Journal of Biochemistry*. **388:** 205-215.

50. Fischer, A., Simanyi, M. & Danielczyk, W. (1990) Depression in dementia of the Alzheimer type and in multi-farct dementia. *American Journal of Psychiatry*. **42**: 186-191.

51. Fogel, R., Mashazi, P., Nyokong, T. & Limson, J. (2007) Critical assessment of the Quartz Crystal Microbalance with Dissipation as an analytical tool for biosensor development and fundamental studies: Metallophtalocyanines-glucose oxidase biocomposite sensors. *Biosensors and Bioelectronics*. **23**: 95-101.

52. Francisco Silva, J., Griveau, S., Richard, C., Zagal, J. H. & Bedioui, F. (2007) Glassy carbon electrodes modified with single-walled carbon nanotubes and cobalt phthalocyanine and nickel tetrasulphonated phthalocyanine: Highly stable new hybrids with enhanced electrocatalytic performances. *Electrochemistry Communications*. **9**: 1629-1634.

53. Frith, K-A & Limson, J. L. (2009) pH tuning of Nafion® for selective detection of tryptophan. *Electrochimica Acta*. **54**: 3600-3605.

54. Frolich, L., and Rierder, P. (1995) Free radical mechanisms in dementia of Alzheimer type and the potential for antioxidative treatment. *Arzneimittelforschcung.* **45:**443–446.

55. Gerhardt, G. A., Oke, A. F., Nagy, G., Moghaddam, B. & Adams, R. N. (1984) Nafion-coated electrodes with high selectivity for CNS electrochemistry. *Brain Research.* **290**: 390-395.

56. Giles, J. (2004) Growing nanotech trade hit by questions over quality. *Nature*. **432**: 791-791.

57. Gilman, A. G., Goodman, L. S. & Gilman, A. (1980) In: The pharmacological basis of therapeutics. (6th Ed.) Macmillan Publishing Co., Inc., New York. pp. 154.

58. Girenko, E. G., Borisenkova, S. A. & Kaliya, O. L. (2002) Oxidation of ascorbic acid in the presence of phthalocyanine metal complexes. Chemical aspects of catalytic anticancer therapy. 1. Catalysis of oxidation by cobalt octacarboxyphthalocyanine. *Russian Chemical Bulletin*. **51**: 1231-1236.

59. Giz, M. J., Duong, B. & Tao, N. J. (1999) In situ STM study of self-assembled mercaptopropionic acid monolayers fro electrochemical detection of dopamine. *Journal of Electroanalytical Chemistry*. **465**: 72-79.

60. Gogol, E. V., Evtugyn, G. A., Marty, J.-L., Budnikov, H. C. & Winter, V. G. (2000) Amperometric biosensors based on Nafion®-coated screen-printed electrode for the determination of cholinesterase inhibitors. *Talanta*. **53**: 379-389.

61. Gogoleva, O. I., Zakomirdina, L. N., Demidkina, T. Y., Phillips, R. S. & Faleev, N. G. (2003) Tryptophanase in aqueous methanol: the solvent effects and a probable mechanism of the hydrophobic control of substrate specificity. *Enzyme and Microbial Technology*. **32**: 843-850.

62. Gonon, F. G., Fombarlet, C. M., Buda, M. J. & Pujol, J. F. (1981) Electrochemical treatment of pyrolytic carbon fibre electrodes. *Analytical Chemistry.* **53**: 1386-1389.

63. Griveau, S., Gulppi, M., Pavez, J., Zagal, J. H. & Bedioui, F. (2003) Cobalt phthalocyanine-based molecular materials for the electrocatalysis and electroanalysis of 2-mercaptoethanol, 2-mercaptoethanesulphonic acid, reduced glutathione and L-cysteine. *Electroanalysis*. **15**: 77-786.

64. Guan, C. L., Oujang, J., Li, Q. L., Liu, B. H. & Baeyens, W. R. G. (2000) Simultaneous determination of catecholamines by ion chromatography with direct conductivity detection. *Talanta*. **50**: 1197-1203.

65. Guerrero, J.M. and Reiter, R.J. (2002) Melatonin-immune system relationships. *Current Topics in Medical Chemistry*. **2**: 167-180.

66. Guo, J., Goasguen, S., Lundstrom, M. & Datta, S. (2002) Metal-insulator-semiconductor electrostatics of carbon nanotubes. *Applied Physics Letters.* **81**: 1486-1499.

67. Hawley, M. D., Tatawawadi, S. V., Piekarski, S. & Adams, R. N. (1967) Electrochemical studies of the oxidation pathways of catecholamines. *Journal of the American Chemical Society*. **89**: 447-450.

68. Hegyi, J., Schwartz, R. & Hegyi, V. (2004). Pellagra: dermatitis, dementia, and diarrhea. *International Journal of Dermatology.* **43:** 1-5.

69. Heineman, W. R. & Kissinger, P. T. (1996) In: *Laboratory Techniques in Electroanalytical Chemistry*. Kissinger, P. T. & Heineman, W. R. (Eds.) 2nd Ed. Marcel Dekker, New York. Pp. 51-123.

70. Heitner-Wirguin, C. (1996) Recent advances in perfluorinated ionomer membranes: structure, properties and applications. *Journal of Membrane Science*. **120**: 1-33.

71. Hopkins, F. G. & Cole, S. W, (1901) A contribution to the chemistry of proteids. Part 1: A preliminary study of a hitherto undescribed product of tryptic digestion. *The Journal of Physiology*. **27**: 419-428.

72. Horwitt, K., Harvey, C. C., Rothwell, W. S., Cutler, J. L. & Haffron, D. (1965) Tryptohan-niacin relationships in man. Studies with diets deficient in riboflavin and niacin together with observation on the excretion of nitrogen and niacin metabolites. *Journal of Nutrition*. **60** (Suppl): 1-43.

73. Hu, I-F. & Kuwana, T. (1986) Oxidative mechanism of ascorbic acid at glassy carbon electrodes. *Analytical Chemistry*. **58**: 3235-3239.

74. Hu, C., Yuan, S. & Hu, S. (2006) Studies on electrochemical properties of MWCNTs-Nafion composite films based on the redox behaviour of incorporated Eu^{3+} by voltammetry and electrochemical impedance spectroscopy. *Electrochimica Acta*. **51**: 3013-3021.

75. Hu, G-Z., Zhang, D-P., Wu, W-L, & Yang, Z-S. (2008) Selective determination of dopamine in the presence of high concentration of ascorbic acid using nano-Au self-assembly glassy carbon electrode. *Colloids and Surface B: Biointerfaces*. **62**: 199-205.

76. Huang, W., Mai, G., Liu, Y., Yang, C. & Qu, W. (2004) Voltammetric determination of tryptophan at a single-wall carbon nanotube modified electrode. *Journal of Nanoscience and Nanotechnology*. **4**: 423-427.

77. Huang, K-J., Luo, D-F., Xie, W-Z. & Yu, Y-S. (2008) Sensitive voltammetric determination of tyrosine using multi-walled carbon nanotubes/4-aminobenzenesulphonic acid film-coated glassy carbon electrode. *Colloids and Surfaces B: Interfaces*. **61**: 176-181.

78. Hughes, D. E. (1982) Titrimetric determination of ascorbic acid with 2,6-dichlorophenol indophenols in commercial liquid diets. *Journal of Pharmaceutical Sciences*. **72**: 126-129.

79. Ikeda, S-I. & Fukui, S. (1973) Preparation of pyridoxal 5'-phosphate-bound sepharose and its use for immobilization of tryptophanase. *Biochemical and Biophysical Research Communications*. **52**: 482-488.

80. Ikeda, S-I., Sumi, Y. & Fukui, S. (1975) Kinetic studies on coenzyme binding and coenzyme dissociation in Tryptophanase immobilized on sepharose. *Biochemistry*. **14**: 1464-1470.

81. Isupov, M. N., Antson, A. A., Dodson, E. J., Dodson, G. G., Dementieva, I. S. & Zakomirdina, L. N. (1998) Crystal structure of tryptophanase. *Journal of Molecular Biology*. **276**: 603–23.

82. Jin, G-P. & Lin, X-Q. (2004) The electrochemical behaviour and amperometric determination of tyrosine and tryptophan at a glassy carbon electrode modified with butyrylcholine. *Electrochemistry Communications*. **6**: 454-460.

83. Jin, G-P., Lin, X-Q. & Gong, J-M. (2004) Novel choline and acetylcholine modified glassy carbon electrodes for simultaneous determination of dopamine, serotonin and ascorbic acid. *Journal of Electroanalytical Chemistry*. **569**: 135-142.

84. Jin, G., Zhang, Y. & Cheng, W. (2005) Poly(p-aminobenzene sulphonic acid)-modified glassy carbon electrode for simultaneous detection of dopamine and ascorbic acid. *Sensors and Actuators B: Chemical*. **107**: 528-534.

85. Joshi, K. A., Tang, J., Haddon, R., Wang, J., Chen, W. & Mulchandani, A. (2005) A disposable biosensor for organophosphorus nerve agents based on carbon nanotubes modified thick film strip electrode *Electroanalysis.* **17**: 54-58.

86. Jung, D. H., Kim, B. H., Ko, Y. K., Jung, M. S., Jung, S., Lee, S. Y. & Jung, H. T. (2004) In situ observation of the stability of anatase nanoparticles and their transformation to rutile in an acidic solution. *Langmuir*. **20**: 8886-8891.

87. Kang, T-F., Shen, G-L. & Yu, R-Q. (1997) Voltammetric behaviour of dopamine at nickel phthalocyanine polymer modified electrodes and analytical applications. *Analytica Chimica Acta*. **356**: 245-251.

88. Kim, O. K., Je, J., Baldwin, J. W., Kooi, S., Pehrsson, P. E. & Buckley, L. J. (2003) Solubilisation of single-wall carbon nanotubes by supramolecular encapsulation of helical amylose. *Journal of the American Chemical Society*. **125**: 4426-4427.

89. Kim, H-J. & Kim, Y-K. (2006) Analysis of ascorbic acid by ion exchange chromatography with electrochemical detection. *Journal of Food Science*. **53**: 1525-1527.

90. Klein, D. C., Coon, S. L., Roseboom, P. H., Weller, J. L., Bernard, M., Gastel, J. A., Zats, M., Iubone, M., Rodriguez, I. R., Begay, V., Falcon, J., Cahill, G., Cassone, V. M. & Baler, R. (1997) The melatonin rhythm generating enzyme: molecular regulation of serotonin N-acetyl-transferase in the pineal gland. *Recent Progress in Hormone Research.* **52**: 307-358.

91. Kounaves, S. P. (1997) In: *Handbook of Instrumental Techniques for Analytical Chemistry.* Settle, F. A. (Ed.) Prentice Hall, New Jersey. Pp. 709-725.

92. Kreuer, K. D., Ise, M., Fuchs, A. & Maier, J. (2000) Proton and water transport in Nano-separated polymer membranes. *Journal de Physique IV: JP*. **10**: 279-281.

93. Krstulovic, A. M., Friedman, M. J., Colin, H., Guiochon, G. & Pajer, K. (1984) Analytical methodology for assays of serum tryptophan metabolites in control subjects and newly abstinent alcoholics: preliminary investigation by liquid chromatography with amperometric detection. *Journal of Chromatography*. **142**: 271-281.

94. Kulikova, V. V., Zakomirdina, L. N., Dementieva, I. S., Phillips, R. S., Gollnick, P. D., Demidkina, T. & Faleev, N. G. (2006) Tryptophanase from *Proteus vulgaris*: The conformational rearrangement in the active site, induced by the mutation of Tyrosine 72 to Phenylalanine, and its mechanistic consequences. *Biochemica et Biophysica Acta*. **1764**: 750-757.

95. Lakshminarayanan, V. & Sur, U. K. (2003) Hydrophobicity-induced drying transition in alkanethiol self-assembled monolayer-water interface. *Pramana*. **61**: 361-371**.**

96. Langlois, R., Ali, H., Brasseur, N., Wagner, J. R. & van Lier, J. E. (1986) Biological activities of phthalocyanines – IV. Type II sensitized phootooxidation of L-Tryptophan and cholesterol by sulphonated metallophthalocyanines. *Photochemistry and Photobiology*. **44**: 117-123.

97. Lee, K. & Hong, J. (1992) Electrokinetic transport of amino acids through a cation exchange membrane. *Journal of Membrane Science*. **75**: 107-120.

98. Lever, A. B. P., Pickens, S. R., Minor, P. C., Licoccia, S., Ramaswamy, B. S. & Magnell, K. (1981) Charge-transfer spectra of metallophthalocyanines: Correlation with electrode potentials. *Journal of the American Chemical Society*. **103:** 6800-6806.

99. Li, Y-G., Zhou, Y-X., Feng, J-L., Jiang, Z-H. & Ma, L-R. (1999) Immobilisation of enzyme on screen-printed electrode by exposure to gluteraldehyde vapour for the construction of amperometric acetylcholinesterase electrodes. *Analytica Chimica Acta*. **382**: 277-282.

100. Li, X., Zhang, S. & Sun, C. (2003) Fabrication of a covalently attached multilayer film electrode containing cobalt phthalocyanine and its electrocatalytic oxidation of hydrazine. *Journal of Electroanalytical Chemistry*. **553**: 139-145.

101. Li, J. & Lin, X. (2007) Simultaneous determination of dopamine and serotonin on gold nanocluster/overoxidised-polypyrrole composite modified glassy carbon electrode. *Sensors and Actuators B*. **124**: 486-493.

102. Limson, J., Nyokong, T. & Daya, S. (1998) The interaction of melatonin, and its precursors, with aluminium, cadmium, copper, lead and zinc: An adsorptive voltammetric study. *Journal of Pineal Research*. **24**: 15-21.

103. Lin Ling, B., Baeyens, W. R. G., van Acker, P. & Dewaele, C. (1992) Determination of ascorbic acid and isoascorbic acid by capillary zone electrophoresis: Application to fruit juices and to a pharmaceutical formulation. *Journal of Pharmaceutical and Biomedical Analysis*. **10**: 717-721.

104. Liu, J., Rinzler, A. G., Dai, H., Hafner, J. H., Bradley, R. K., Boul, P. J., Lu, A., Iverson, T., Shelimov, K., Huffman, C. B., Rodriguez-Macias, F., Shon, Y-S., Lee, T. R., Colbert, D. T. & Smalley, R. E. (1998) Fullerene pipes. *Science*. **280**: 1253-1256.

105. Luo, H. X., Shi, Z. J., Li, N. Q., Gu, Z. N. & Zhuang, Q. K. (2001) Investigation of the electrochemical and electrocatalytic behavior of single-wall carbon nanotube film on a glassy carbon electrode. *Analytical Chemistry*. **73**: 915-920.

106. Luque, G. L., Ferreyra, N. F. & Rivas, G. A. (2007) Electrochemical sensor for amino acids and albumin based on composites containing carbon nanotubes and copper microparticles. *Talanta*. **71**: 1282-1287.

107. Luz, R. C. S., Moreira, A. B., Damos, F. S., Tanaka, A. A. & Kubota, L. T. (2006) Cobalt tetrasulphonated phthalocyanine immobilized on poly-L-lysine film onto glassy carbon electrode as amperometric sensor for cysteine. *Journal of Pharmaceutical and Biomedical Analysis*. **42**: 184-191.

108. Macchi, M. M. & Bruce, J. N. (2004) Human pineal physiology and functional significance of melatonin. *Frontiers in Neuroendocrinology*. **25**: 177-195.

109. Malpaux, B., Migaud, M., Tricoire, H. and Chemineau, P. (2001). Biology of mammalian photoperiodism and the critical role of the pineal gland and melatonin. *Journal of Biological Rhythms*. **16**:336-346

110. Martin, A. & Frei, B. (1997) Both intracellular and extracellular vitamin C inhibit atherogenic modification of LDL by human vascular endothelial cells. *Arteriosclerosis, Thrombosis, and Vascular Biology*. **17**: 1583-1590.

111. Martin, M., Macias, M., Escames, G., Leon, J. & Acuna-Castroviejo, D. (2000) Melatonin but not Vitamin C and E Maintains Glutathione Homeostasis in t-Butyl Hydroperoxide-induced Mitochondrial Oxidative Stress. *FASEB Journal*.**14**: 1677-1679.

112. Mashazi, P. N., Ozoemena, K. I. & Nyokong, T. (2006) Tetracarboxylic acid cobalt phthalocyanine SAM on gold: Potential applications as amperometric sensor for H_2O_2 and fabrication of glucose biosensor. *Electrochimica Acta*. **52**: 177-186.

113. McCreery, L. (1991) In: *Electroanalytical Chemistry*. Bard, A. J. (Ed.) Vol. 17. Marcel Dekker, New York. Pp. 221.

114. McGeer, P. L., McGeer, M. G. & Susuki, J. S. (1977) Aging and extrapyramidal function. *Archives of Neurology*. **34**: 33-35.

115. McMenamy, R. H. & Oncley, J. L. (1958) The specific binding of L-tryptophan to serum albumin. *Journal of Biological Chemistry*. **233**: 1436-1447.

116. Mendels, J., Stinnet, J. L., Burns, D & Frazer, A. (1975) Amine precursors and depression. *Archives of General Psychiatry*. **32**: 22.

117. Meltzer, C. C., Smith, G., DeKosky, S. T., Pollock, B. G., Mathis, C. A., Moore, R. Y., Kupfer, D. J. & Reynolds, C. F. (1998) Serotonin in aging, late-life depression, and Alzheimer's disease: The emerging role of functional imaging. *Neuropsychopharmacology*. **18**: 407-430.

118. Merkoçi, A., Pumera, M., Llopis, X., Pérez, B., del Valle, M. & Aleget, S. (2005) New materials for electrochemical sensing VI: Carbon nanotubes. *Trends in Analytical Chemistry*. **24**: 826-838.

119. Millar, J., Stamford, J. A., Kruk, Z. L. & Wightman, R. M. (1985) Electrochemical, pharmacological and electrophysiological evidence of rapid dopamine release and removal in the rat caudate nucleus following electrical stimulation of the median forebrain bundle. *European Journal of Pharmacology*. **109**: 341-348.

120. Moore, R. R., Banks, C. E. & Compton, R. G. (2004) Basal plane pyrolytic graphite modified electrodes: Comparison of carbon nanotubes and graphite powder as electrocatalysts. *Analytical Chemistry*. **76**: 2677-2682.

121. Moreno, L., Merkoçi, A., Alegret, S., Hernández-Cassou, S. & Saurina, J. (2004) Analysis of amino acids in complex samples by using voltammetry and multivariate calibration methods. *Analytica Chimica Acta*. **507**: 247-253.

122. Morino, Y. & Snell, E. E. (1967) The subunit structure of Tryptophanase. I. The effect of pyridoxal phosphate on the subunit structure and physical properties of Tryptophanase. *Journal of Biological Chemistry*. **242**: 5591-5601.

123. Mulchandani, A., Kaneva, I. & Chen, W. (1998) Microbial biosensor for direct determination of organophosphate nerve agents using recombinant *Escherichia coli* with surface - expressed organophosphorus hydrolase-2. Fiber-optic microbial biosensor. *Analytical Chemistry.* **70**: 5042.

124. Musameh, M., Wang, J., Merkoçi, A. & Lin, Y. (2002) Low-potential stable NADH detection at carbon-nanotube-modified glassy carbon electrodes. *Electrochemistry Communications*. **4**: 743-746.

125. Nagy, G., Gerhardt, G. A., Oke, A. F., Rice, M. E., Adams, R. N., Moore, R. B., Szentirmy, M. N. & Martin, C. R. (1985) Ion exchange and transport of neurotransmitters in Nafion films on conventional and microelectrode surfaces. *Journal of Electroanalytical Chemistry*. **188**: 85-94.

126. Narasaiah, D. (1994) An enzyme electrode for hydrogen peroxide detection based on peroxidise immobilised on a glassy carbon electrode. *Biosensors and Bioelectronics*. **9**: 415-422.

127. Newton, W. A. & Snell, E. E. (1964) Catalytic properties of Tryptophanase, a multi-functional pyridoxal phosphate enzyme. *Proceedings of the National Academy of Science.* **51**: 382-389.

128. Newton, W. A., Morino, Y. & Snell, E. E. (1965) Properties of crystalline Tryptophanase. *Journal of Biological Chemistry.* **240**: 1211-1218.

129. Nicholson & Schain (1965)

130. Nguyen, N. T., Wrona, M. Z. & Dryhurst, G. (1985) Electrochemcal oxidation of tryptophan. *Journal of Electroanalytical Chemistry*. **199**: 101-126.

131. Oni, J. & Nyokong, T. (2001) Simultaneous voltammetric determination of dopamine and serotonin on carbon paste electrodes modified with iron(II) phthalocyanine complexes. *Analytica Chimica Acta*. **434**: 9-21.

132. Ozoemena, K. I., Pillay, J. & Nyokong, T. (2006) Preferential electrosorption of cobalt (II) tetra-aminophthalocyanine at single-wall carbon nanotubes immobilized on a basal plane pyrolytic graphite electrode. *Electrochemistry Communications*. **8**: 1391-1396.

133. Padayatty, S., Katz, A., Wang, Y., Eck, P., Kwon, O., Lee, J., Chen, S., Corpe, C., Dutta, A., Dutta, S. & Levine, M. (2003) Vitamin C as an antioxidant: Evaluation of its role in disease prevention. *Journal of the American College of Nutrition*. **22**: 18-35.

134. Parmar, P., Limson, J., Daya, S. and Nyokong, T. (2002) Melatonin protects against copper-induced free radical damage. *Journal of Pineal Research*. **32**: 237-242.

135. Peigney, A., Laurent, Ch., Flahaut, E., Bacsa, R. R. & Rousset, A. (2001) Specific surface area of carbon nanotubes and bundles of carbon nanotubes. *Carbon*. **39**: 507-517.

136. Poeggeler, B., Saarela, S., Reiter, R. J., Tan, D. X., Chen, L. K., Manchester, L. C. & Barlow-Walden, L. R. (1994) Melatonin – A highly potent endogenous radical scavenger and electron donor: New aspects of the oxidation chemistry of his indole assessed *in vivo*. *Annals of the New York Academy of Sciences*. **738**: 419-420.

137. Pumera, M., Sánchez, S., Ichinose, I. & Tang, J. (2007) Electrochemical nanobiosensors. *Sensors and Actuators B*. **123**: 1195-1205.

138. Radi, A. & Bekhiet, G. E. (1998) Voltammetry of melatonin at carbon electrodes and determination in capsules. *Bioelectrochemistry and Bioenergetics*. **45**: 275-279.

139. Ramesh, S., Ericson, L. M., Davis, V. A., Saini, R. K., Kittrell, C., Pasquali, M., Billups, W. E., Adams, W., Hauge, R. H. & Smalley, R. E. (2004) dissolution of pristine single walled carbon nanotubes in superacids by direct protonation. *Journal of Physical Chemistry B*. **108**: 8794-8798.

140. Rao, C. N. R., Satishkumar, B. C., Govindaraj, A. & Nath, M. (2001) Nanotubes. *Chemphyschem*. **2**: 78-105.

141. Rasooly, L. & Rasooly, A. (1999) Real time biosensor analysis of Staphylococcal enterotoxin A in food. *International Journal of Food Microbiology*. **49**: 119-127.

142. Reiter, R. J. (1991) Pineal Gland: Interface between the photoperiodic environment and the endocrine system. *Trends in Endocrinology and Metabolism*. **2**: 13-19.

143. Reiter, R. J. (1993) The melatonin rhythm: both a clock and a calendar. *Experientia.* **49**: 654-664.

144. Reiter, R. J. (1995) The pineal gland and melatonin in relation to aging: A summary of the theories and the data. *Experimental Gerontology*. **50**: 199-212.

145. Reiter, R. J. (1997) Antioxidant actions of melatonin. *Advances in Pharmacology*. **38**: 103-117.

146. Ren, G. Xu, X., Liu, Q., Cheng, J., Yuan, X., Wu, L. & Wan, Y. (2006) Electrospun poly(vinyl alcohol)/glucose oxidase biocomposite membranes for biosensor application. *Reactive & Functional Polymers*. **66**: 1559-1564.

147. Rivas, G. A., Miscoria, S. A., Desbrieres, J. & Barrera, G. D. (2007) New biosensing platforms based on the layer-by-layer self-assembling of polyelectrolytes on Nafion/carbon nanotubes-coated glassy carbon electrodes. *Talanta*. **71**: 270-275.

148. Rivot, J-P., Cespuglio, R., Puig, S., Jouvet, M. & Besson, J-M. (1995) *In vivo* electrochemical monitoring of serotonin in spinal dorsal horn with Nafion-coated multi-carbon electrodes. *Journal of Neurochemistry*. **65**: 1257-1263.

149. Rocha, L.S. & Carapuça, H. M. (2006) Ion-exchange voltammetry of dopamine at Nafion®-coated glassy carbon electrodes: Quantitative features of ion-exchange partition and reassessment of the oxidation mechanism of dopamine in the presence of excess ascorbic acid. *Bioelectrochemistry*. **69**: 258-266.

150. Rubianes, M. D. & Rivas, G. A. (2001) Highly selective dopamine quantification using a glassy carbon electrode modified with a melanin-type polymer. *Analytica Chimica Acta*. **440**: 99-108.

151. Salem, F. B. (1987) Spectrophotometric and titrimetric determination of catecholamines. *Talanta*. **34**: 810-812.

152. Sangur, S., Emregul, E., Gunendi, G. & Numanoglu, Y. (2004) New Glucose Biosensor Based on Glucose Oxidase-immobilized Gelatin Film Coated Electrodes. *Journal of Biomaterial Applications*. **18:** 264-277.

153. Sarre, S., Michotte, Y., Herregodts, P., Deleu, D., Klippel, N. D. & Ebinger, G. J. (1992) High-performance liquid chromatography with electrochemical detection for the determination of levodopa, catecholamines and their metabolites in rat brain dialysates. *Chromatography*. **75**: 207-212.

154. Schenk, J. O., Miller, E., Rice, M. E. & Adams, R. N. (1983) Chronoamperometry in brain slices: Quantitative evaluations of *in vivo* electrochemistry. *Brain Research.***277**: 1-8.

155. Schulte, K., Yan, C., Ahola-Tuomi, M., Stróżecka, A., Moriarty, P. J. & Khlobystov, A. N. (2008) Encapsulation of cobalt phthalocyanine molecules in carbon nanotubes. *Journal of Physics: Conference Series*.**100**: 012017.

156. Scully, J. R., Silverman, D. C. & Kendig, M. W. (1993) In: *Electrochemical Impedance: Analysis and Interpretation*. Scully, J. R. (Ed.) ASTM international, USA.

157. Selvaraju, T. & Ramaraj, R. (2003) Simultaneous determination of ascorbic acid, dopamine and serotonin at poly(phenosafranine) modified electrode. *Electrochemistry Communications*. **5**: 667-672.

158. Shahrokhian, S. & Fotouhi, L. (2007) Carbon paste electrode incorporating multi-walled carbon nanotube/cobalt salophen for sensitive voltammetric determination of tryptophan. *Sensors and Actuators B*. **123**: 942-949.

159. Shahrokhian, S. & Zare-Mehrjardi, H. R. (2007) Application of thionine-nafion supported on multi-walled carbon nanotube for preparation of a modified electrode in simultaneous voltammetric detection of dopamine and ascorbic acid. *Electrochimica Acta*. **52**: 6310-6317.

160. Shen, Z., Sun, Z., Wu, L., Wu, K., Sun, S. & Huang, Z. (2002) Rapid method for the determination of amino acids in serum by capillary electrophoresis. *Journal of Chromatography*. **979**: 227-232.

161. Simonian, A. L., Rainina, E. I., Fitzpatrick, P. F. & Wild, J. (1999) Enhancement of the specificity of an enzyme-based biosensor for L-tryptophan. *Advances in Experimental Medical Biology.* **106**: 833-840.

162. Siswana, M. P., Ozoemena, K. I. & Nyokong, T. (2006) Electrocatalysis of asulam on cobalt phthalocyanine modified multi-walled carbon nanotubes immobilizsed on a basal plane pyrolytic graphite electrode. *Electrochimica Acta*. **52**: 114-122.

163. Skene, D. J. (1996) The Miracle of Melatonin: fact, fancy and future. *Chemistry and Industry*. **9**: 637-640.

164. Skinner, D. C. & Malpaux, B. (1999) High Melatonin Concentrations in Third Ventricular Cerebrospinal Fluid Are not due to Galen Vein Blood Re-circulating through the Choroid Plexus. *Endocrinology. **140***: 4399-4405.

165. Smith, S. E., Pihl, R. O., Young, S. N. & Ervin, F. (1987) A test of possible cognitive and environmental influences on the mood lowering effect of tryptophan depletion in normal males. *Psychopharmacology*. **91**: 451–457.

166. Smith, K. A., Fairburn, C. G. & Cowen, P. J. (1997) Relapse of depression after rapid depletion of tryptophan. *The Lancet*. **349**: 915-919.

167. Snell, E. E. (1975) Tryptophanase: structure, catalytic activities, and mechanism of action. *Advances in Enzymology*. **42**: 287–333.

168. Su, P-G., Sun, Y-L. & Lin, C-C. (2006) A low humidity sensor made of quartz crystal microbalance coated with multi-walled carbon nanotubes/Nafion composite material films. *Sensors and Actuators B*. **115**: 338-343.

169. Sun, Y., Ye, B., Zhang, W. & Zhou, X. (1998) Simultaneous determination of dopamine and ascorbic acid at poly (neutral red) modified electrodes. *Analytica Chimica Acta*. **363**: 75-80.

170. Szepesi, G. (1947) New method for the spectrophotometric determinations of ascorbic acid and dehydroascorbic acid. *Fresenius' Journal of Analytical Chemistry*. **265**: 334-336.

171. Tagliamonte, A., Tagliamonte, P., Perez-Cruet, J. & Gessa, G. L. (1971) increase of brain tryptophan caused by drugs which stimulate serotonin synthesis. *Nature New Biology*. **229**: 125-126.

172. Takeda, N., Stawasz, M. E. & Parkinson, B. A. (2001) Electrochemical oxidation and ex-situ STM observation of bis(4-dimethylamino-2-dihydroxyphenyl)squaraine dye layers in HOPG electrodes. *Journal of Electroanalytical Chemistry*. **498**: 19-33.

173. Tan, D.X., Manchester, L.C., Reiter, R.J., Qi. W., Hanes, M.A. & Farley, N.J. (1999) High Physiological Levels of Melatonin in the Bile of Mammals. *Life Sciences*. **65:** 2523-2529.

174. Tans, S. J. (1997) Individual single-wall carbon nanotubes as quantum wires. *Nature*. **386**: 474-477.

175. Tasis, D., Tagmatarchis, N., Georgakilas, V. & Prato, M. (2003) Soluble carbon nanotubes. *Chemistry- A European Journal.* **9**: 4001-4008.

176. Tonelli, D., Gattavecchia, E. & Gandolfi, M. (1982) Thin-layer chromatographic determination of indolic tryptophan metabolites in human urine using Sep-Pak C18 extraction. *Journal of Chromatography*. **231**: 283-289.

177. Treacy, M. M., Ebbesen, T. W. & Gibson, J. M. (1996) Exceptionally high Young's modulus observed for individual carbon nanotubes. *Nature*. 381: 678-680.

178. Tsai, Y-C. & Chui, C-C. (2007) Amperometric biosensors based on multiwalled carbon nanotube-Nafion-tyrosinase nanobiocomposites for the determination of phenolic compounds. *Sensors and Actuators*. **125**: 10-16.

179. Valentini, F., Amine, A., Orlanducci, S., Terranova, M. L. & Palleschi, G. (2003) Carbon nanotube purification: Preparation and characterization of carbon nanotube paste electrodes. *Analytical Chemistry*. **75**: 5413-5421.

180. Valentini, F., Orlanducci, S., Tamburri, E., Terranova, M. L., Curulli, A. & Palleschi, G. (2005) Single-walled carbon nanotubes on tungsten wires: A new class of microelectrochemical sensors. *Electroanalysis*. **17**: 28-37.

181. Vincke, B. J., Vire, J. C. & Patriarche, G. J. (1986) In *Electrochemistry: Sensors and Analysis*. Smyth, M. R. & Vos, J. G. (Eds.) Elsevier Science Publishers, Amsterdam. pp. 147-154

182. Wang, J. (1994) In: *Analytical Chemistry*. VCH, New York. Pp. 15-42.

183. Wang, J., Musemah, M. & Lin, Y. (2003) Solubilisation of carbon nanotubes by Nafion® toward the preparation of amperometric biosensors. *Journal of the American Chemical Society*. **125**: 2408-2409.

184. Wang, J., Deo, R. P. & Musemah, M. (2003a) Stable and sensitive electrochemical detection of phenolic compounds at carbon nanotube modified glassy carbon electrodes. E*lectroanalysis*. **15**: 1830-1834.

185. Wang, H-S., Li, T-H., Jia, W-L. & Xu, H-Y. (2006) Highly selective and sensitive determination of dopamine using Nafion/carbon nanotubes coated poly(3-methylthiophene) modified electrode. *Biosensots and Bioelectronics*. **22**: 664-669.

186. Wang, K., Xu, J-J. & Chen, H-Y. (2006a) Biocomposite of cobalt phthalocyanine and lactate oxidase for lactate biosensing with MnO_2 nanoparticles as an eliminator of ascorbic acid interference. *Sensors and Actuators B: Chemical*. **114**: 1052-1058.

187. Wegmann, H., Curtius, H-C. & Redweik, U. (1978) Selective ion monitoring of tryptophan, N-acetyltryptophan and kynurenine in human serum. Application to the in vivo measurement of tryptophan pyrrolase activity. *Journal of Chromatography*. **158:** 305-312.

188. Wightman, M., May, L. J. & Michael, A. C. (1988) Detection of dopamine dynamics in the brain. *Analytical Chemistry*. **60**: 769A-779A.

189. Williams, C. D. (1935) Kwashiorkor: A nutritional disease of children associated with a maize diet. *Lancet.* **229**:1151-1152.

190. Withey, G. D., Lazareck, A. D., Tzolov, M. B., Yin, A., Aich, P., Yeh, J. I. & Xu, J. M. (2006) Ultra-high redox enzyme signal transduction using highly ordered carbon nanotube array electrodes. *Biosensors and Bioelectronics*. **21**: 1560-1565.

191. Wohlstadter, J. N., Wilbur, J. L., Sigal, G. B., Biebuyck, H. A., Billadeau, M. A., Dong, L. W., Fischer, A. B., Gudibande, S. R., Jamieson, S. H., Kenten, J. H., Leginus, J., Leland, J. K., Massey, R. J. & Wohlstadter, S. J. (2003) Carbon nanotube-based biosensor *Advanced Materials.* **15**: 1184-1186.

192. Wolowacz, S. E., Yon Hin, B. F. Y. & Lowe, C. R. (1992) Covalent electropolymerisation of glucose oxidase in polypyrrole. *Analytical Chemistry*. **64**: 1541-1545.

193. Wopschall, R. H. & Shain, I. (1967) Adsorption effects in stationary electrode polarography with a chemical reaction following charge transfer. *Analytical Chemistry*. **39**: 1535-1542.

194. Wu, X., Diao, Y., Sun, C., Yang, J., Wang, Y. & Sun, S. (2002) Fluormetric determination of ascorbic acid with o-phenylenediamine. *Talanta*. **59**: 95-99.

195. Wu, K., Fei, J. & Hu, S. (2003) Simultaneous determination of dopamine and serotonin on a glassy carbon electrode coated with a film of carbon naotubes. *Analytical Biochemistry*. **318**: 100-106.

196. Yilmaz, I., Arslan, S., Guney, S. & Becerik, I. (2007) Synthesis, electro-spectroelectrochemical characterisation and electrocatalytic behaviour towards dioxygen reduction of a new water-soluble cobalt phthalocyanine containing naphthoxy-4-sulphonic acid sodium salt. *Electrochimica Acta*. **52**: 6611-6621.

197. Yin, T., Wei, W. & Zeng, J. (2006) Selective detection of dopamine in the presence of ascorbic acid by use of glassy-carbon electrodes modified with both polyaniline film and multi-walled carbon nanotubes with incorporated β-cyclodextrin. *Analytical and Bioanalytical Chemistry*. **386**: 2087-2094.

198. Yogeswaran, U. & Chen, S. M. (2008) Multi-walled carbon nanotubes with poly(methylene blue) composite film for the enhancement and separation of electroanalytical responses of catecholamine and ascorbic acid. *Sensors and Actuators B: Chemical*. **130**: 739-749.

199. Young, T. E. & Babbitt, B. W. (1983) Electrochemical study of the oxidation of α-methyldopamine, α-methylnoradrenaline and dopamine. *Journal of Organic Chemistry*. **48:** 562-566.

200. Young, S. N., Smith, S. E., Pihl, R. O. & Ervin, F. R. (1987) Tryptophan depletion causes a rapid lowering of mood in normal males. *Psychopharmacology*. **87**: 173–177.

201. Young, S. N., Ervin, F. R., Phil, R. O., & Finn P. (1989) Biochemical aspects of tryptophan depletion in primates. *Psychopharmacology.* **98:** 508–11.

202. Zagal, J. H. (1992) Metallophthalocyanines as catalysts in electrochemical reactions. *Coordination Chemistry Reviews*. **119**: 89-136.

203. Zagal, J., Páez, M., Tanaka, A. A., dos Santos, J. R. & Linkous, C. A. (1992) Electrocatalytic activity of metal phthalocyanines for oxygen reduction. *Journal of Electroanalytical Chemistry*. **339**: 13-30.

204. Zecevic, S., Simic-Glavaski, B., Yeager, E., Lever, A. B. P. & Minor, P. C. (1985) Spectroscopic and electrochemical studies of transition-metal tetrasulphonate phthalocyanines. 5. Voltammetry studies of adsorbed tetrasulphonated phthacyanines (MTSPc) in aqueous-solutions. *Journal of Electroanalytical Chemistry*. **196**: 339-358.

205. Zen, J-M., Wang, W-M. & Ilangovan, G. (1998) Adsorptive potentiometric stripping analysis of dopamine on clay-modified electrode. *Analytica Chimica Acta*. **372**: 315-321.

206. Zhang, H-M., Li, N-Q. & Zhu, Z-W. (2000) Electrocatalytic response of dopamine at a *DL*-homocysteine self-assembled monolayer. *Microchemical Journal*. **64**: 277-282.

207. Zhang, F-F., Wan, Q., Li, C-X., Wang, X-L., Zhu, Z-Q., Xian, Y-Z., Jin, L-T. & Yamamoto, K. (2005) Simultaneous monitoring of glucose, lactate, L-glutamate and hypoxanthine levels in rat striatum by a flow-injection enzyme electrode array system with *in vivo* microdialysis sampling. *Journal of Electroanalytical Electrochemistry*. **575**: 1-7.

208. Zhang, P., Wu, F-H., Zhao, G-C. & Wei, X-W. (2005) Selective response of dopamine in the presence of ascorbic acid at multi-walled carbon nanotube modified gold electrode. *Bioelectrochemistry*. **67**: 109-114.

209. Zhao, Y., Gao, Y., Zhan, D., Liu, H., Zhao, Q., Kou, Y., Shao, Y., Li, M., Zhuang, Q. & Zhu, Z. (2005) Selective detection of dopamine in the presence of ascorbic acid and uric acid by a carbon nanotubes-ionic liquid gel modified electrode. *Talanta*. **66**: 51-57.

210. Zhao, G-H., Li, M-F. & Li, M-L. (2007) Differential pulse voltammetric determination of dopamine with the coexistence of ascorbic acid on boron-doped diamond surface. *Central European Journal of Chemistry*. **5**: 1114-1123.

211. Zoulis, N. E., Nikolelis, D. P. & Efstathiou, C. E. (1990) Pre-concnetration of indolic compounds at a carbon paste electrode and direct determination of L-tryptophan in serum by adsorptive stripping voltammetry. *Analyst*. **115**: 291-295.

Additional References:

212. U. S. Food and Drug Administration © 2005 Validation of analytical procedures for type C medicated feeds. Guideline No. 136. (http://www.fda.gov/cvm/Guidance/guide135.htm#6.3) Accessed December, 2008.

213. Perma Pure LLC. © 2004. Nafion® Physical Properties.*Technical Notes and Articles*. (http://www.permapure.com/TechNotes/Nafion%20physical%20&%20chemical.htm). Accessed June, 2006